U.S. Department
of Commerce

Volume 123
Number 2
April 2025

Fishery Bulletin

U.S. Department of Commerce

Howard Lutnick
Secretary

National Oceanic and Atmospheric Administration

Vice Admiral Nancy Hann
Performing the duties of Administrator

National Marine Fisheries Service

Emily Menashes
Acting Assistant Administrator for Fisheries

Fishery Bulletin

Scientific Editor
José I. Castro
National Marine Fisheries Service, NOAA
263 13th Avenue South
Saint Petersburg, Florida 33701

Managing Editor
Kathryn Dennis
Scientific Publications Office
National Marine Fisheries Service, NOAA
1845 Wasp Boulevard, Building 176
Honolulu, Hawaii 96818

Associate Editor
Cara Mayo
Scientific Publications Office
National Marine Fisheries Service, NOAA
7600 Sand Point Way NE
Seattle, Washington 98115-0070

Editorial Board

Henry L. Bart Jr.	Tulane University, New Orleans, Louisiana
Katherine E. Bemis	National Systematics Laboratory, Washington, DC
Matthew D. Campbell	National Marine Fisheries Service, Pascagoula, Mississippi
William B. Driggers III	National Marine Fisheries Service, Pascagoula, Mississippi
Gretchen L. Grammer	South Australian Research and Development Institute, Adelaide, Australia
Eric R. Hoffmayer	National Marine Fisheries Service, Pascagoula, Mississippi
Richard Langton	National Marine Fisheries Service, Walpole, Maine (retired)
J. Fernando Márquez-Farías	Universidad Autónoma de Sinaloa, Mazatlán, México
Richard S. McBride	National Marine Fisheries Service, Woods Hole, Massachusetts
Richard L. Merrick	National Marine Fisheries Service, Falmouth, Massachusetts (retired)
Richard D. Methot	National Marine Fisheries Service, Seattle, Washington
Lisa J. Natanson	National Marine Fisheries Service, Narragansett, Rhode Island (retired)
Mark S. Peterson	University of Southern Mississippi, Ocean Springs, Mississippi
André E. Punt	University of Washington, Seattle, Washington
Joseph M. Quattro	University of South Carolina, Columbia, South Carolina
John F. Walter III	National Marine Fisheries Service, Miami, Florida

***Fishery Bulletin* website: https://spo.nmfs.noaa.gov/fb.htm**

Fishery Bulletin (ISSN 0090-0656) is published quarterly by the Scientific Publications Office, National Marine Fisheries Service, NOAA, 7600 Sand Point Way NE, Seattle, WA 98115-0070.

Although the contents of this publication have not been copyrighted and may be reprinted entirely, reference to source is appreciated.

The Secretary of Commerce has determined that the publication of this periodical is necessary according to law for the transaction of public business of this Department. Use of funds for printing of this periodical has been approved by the Director of the Office of Management and Budget.

For Sale by the Superintendent of Documents, U.S. Government Publishing Office, Washington, DC 20401. Subscription price per year: $32.00 domestic and $44.80 foreign. Cost per single issue: $19.00 domestic and $26.60 foreign. **See back for order form.**

Fishery Bulletin carries original research reports on investigations in fishery science, engineering, and economics. It began as the Bulletin of the United States Fish Commission in 1881; it became the Bulletin of the Bureau of Fisheries in 1904 and the *Fishery Bulletin* of the U.S. Fish and Wildlife Service in 1941. Separates were issued as documents through volume 46; the last document was no. 1103. Beginning with volume 47 in 1931 and continuing through volume 62 in 1963, each separate appeared as a numbered bulletin. A new system began in 1963, with volume 63, in which papers are bound together in a single issue. Beginning with volume 70, number 1, January 1972, *Fishery Bulletin* became a periodical, issued quarterly. In this form, it is available by subscription from the Superintendent of Documents, U.S. Government Publishing Office, Washington, DC 20401. It is also available free in limited numbers to libraries, research institutions, and state and federal agencies and in exchange for other scientific publications.

U.S. Department of Commerce
Seattle, Washington

Volume 123
Number 2
April 2025

Fishery Bulletin

Contents

Articles

75–87 **Tomoki Kanna, Sayaka Takahashi, Eundeok Byun, Atsushi Yamashiro, Rui Matsumoto, Shinsuke Torisawa, and Yasushi Mitsunaga**

Seasonal behavioral changes of a captive whale shark (*Rhincodon typus*) under variable temperature and light conditions

88–104 **Jon Brodziak, Matthew Supernaw, Bai Li, Christine Stawitz, Haley Oleynik, and Teresa A'mar**

Engineering a prototype for a next-generation stock assessment modeling platform

105–118 **Paul Geoghegan, Michael D. Murphy, Maureen Madray, M. Conor McManus, Eric Nestler, and Ann E. Pembroke**

The structure of the larval fish assemblage of Massachusetts Bay in 2008–2012 and 2015–2022

119–126 **Ruairi MacNamara, Michael Shane, Victor Bach Muñoz, and Mark Drawbridge**

Assessing postrelease mortality in hook-and-line fishing of a large coastal sciaenid, the white seabass (*Atractoscion nobilis*)

127–142 **Kelli C. Mosca, Thomas F. Savoy, Jacqueline B. Roberts, Evan C. Ingram, Eric T. Schultz, and Hannes Baumann**

Age structure and seasonal movement of Atlantic sturgeon (*Acipenser oxyrinchus*) aggregating in eastern Long Island Sound and the Connecticut River

143–146 **Guidelines for authors**

The National Marine Fisheries Service (NMFS) does not approve, recommend, or endorse any proprietary product or proprietary material mentioned in this publication. No reference shall be made to NMFS, or to this publication furnished by NMFS, in any advertising or sales promotion that would indicate or imply that NMFS approves, recommends, or endorses any proprietary product or proprietary material mentioned herein or that has as its purpose an intent to cause directly or indirectly the advertised product to be used or purchased because of this NMFS publication.

The NMFS Scientific Publications Office is not responsible for the contents of the articles.

National Marine Fisheries Service
NOAA

Fishery Bulletin
established in 1881

Spencer F. Baird
First U.S. Commissioner of Fisheries and founder of *Fishery Bulletin*

Seasonal behavioral changes of a captive whale shark (*Rhincodon typus*) under variable temperature and light conditions

Tomoki Kanna[1]
Sayaka Takahashi[2]
Eundeok Byun[2]
Atsushi Yamashiro[2]
Rui Matsumoto[2,3]
Shinsuke Torisawa (contact author)[1]
Yasushi Mitsunaga[1]

Email address for contact author: ns_torisawa@nara.kindai.ac.jp

[1] Graduate School of Agriculture
Kindai University
Nakamachi 3327-204
Nara City, Nara 631-8505, Japan

[2] Okinawa Churaumi Aquarium
Ishikawa 424
Motobu, Okinawa 905-0206, Japan

[3] Okinawa Churashima Research Institute
Okinawa Churashima Foundation
Ishikawa 888
Motobu, Okinawa 905-0206, Japan

Abstract—Long-term quantitative observations are essential for the conservation of the whale shark (*Rhincodon typus*), which requires a long time to grow and mature. In this study, a data logger was attached to a mature male whale shark that had been maintained in captivity for over 29 years at the Okinawa Churaumi Aquarium in Japan. Because long-term rearing of whale sharks in captivity is desirable, the effects of water temperature and light on the swimming behavior of the captive whale shark were investigated. Tail-beat frequencies (TBFs), activity levels, and frequencies of clasper crosses, which are thought to be a mating-like behavior, were calculated from the swimming data. In all seasons, TBF, swimming speed, and activity level of the shark were 4%–20% less during the nighttime than during the daytime, particularly at cool water temperatures (≤23.6°C). Furthermore, approximately 90% of the clasper crosses occurred during the daytime. These results indicate that the shark is active during the daytime, engaging in activities such as mating behavior. In contrast, during the nighttime, it rests while swimming, slowing down the beat of its caudal fin and lowering swimming speed to conserve energy. Therefore, we conclude that this individual has adopted this diurnal rhythm to adapt to its current rearing environment.

Manuscript submitted 25 June 2024.
Manuscript accepted 10 January 2025.
Fish. Bull. 123:75–87 (2025).
Online publication date: 3 February 2025.
doi: 10.7755/FB.123.2.1

The views and opinions expressed or implied in this article are those of the author (or authors) and do not necessarily reflect the position of the National Marine Fisheries Service, NOAA.

The whale shark (*Rhincodon typus*) is a species within the order Orectolobiformes. Species of this order are predominantly benthic in nature; however, the whale shark is the only pelagic species within this order and, therefore, the only one that makes movements at the scale of an ocean basin. This species has become popular as an attraction for ecotourism activities, such as leisure diving (e.g., Gallagher and Hammerschlag, 2011; Legaspi et al., 2020; Reynolds et al., 2024). It is listed as endangered on the IUCN Red List of Threatened Species (Pierce and Norman, 2016); therefore, this species requires active protection and conservation. Long-term and wide-ranging tracking and other research are essential for improving understanding of the behavioral traits and ecology of the whale shark. Such knowledge can aid the conservation of this species, which migrates across long distances in the ocean, grows slowly, and takes a long time to reach maturity.

In cases where long-term and detailed observations in the field are difficult to collect, behavioral observations in captivity can help advance understanding of the swimming performance and reproductive ecology of a species, while also serving as a useful reference for interpreting the experimental observations of behavior gathered in field studies. The whale shark is difficult to keep in captivity; however, multiple individuals have been reared at the Okinawa Churaumi Aquarium (OCA). In particular, a male whale shark has been kept in the aquarium for more than 29 years, setting the world record for the longest period of captivity for this species. This individual is also the first in the world for which the sexual maturation process of a male whale shark was successfully observed (Matsumoto et al., 2019).

This species mainly occurs in waters with sea-surface temperatures ranging between 23°C and 30°C across the world's oceans (Hearn et al., 2021). Researchers have speculated that whale sharks may avoid prolonged exposure to excessively cool and warm water temperatures through vertical or extensive horizontal migration. This species is ectothermic and has the stability of its body temperature being derived from a

large body that allows it to tolerate ambient water temperatures below 20°C for short periods of time (Nakamura et al., 2020); however, its long-term temperature tolerance has not been examined. Although water temperature is thought to significantly influence the behavior of this species, the range of suitable water temperatures for the whale shark still needs to be determined. Understanding how water temperature affects the swimming behavior of this ectothermic species is particularly important in the finite space of captivity, where deep diving and large-scale horizontal movements are not possible, and estimation of the range of suitable water temperatures is necessary to optimize the conditions of their captive environment.

Gleiss et al. (2013) found that this species increases its activity around sunrise and sunset in the wild, and its crepuscular pattern of locomotor activity is becoming better understood in Australia. However, the observed diel behavioral patterns of this species vary by region and location (Rohner et al., 2020), with some populations spending more time in shallow areas during the day and staying in deeper areas at night (Robinson et al., 2017; Araujo et al., 2018) and vice versa (Ramírez-Macías et al., 2017). However, the diel patterns of the whale shark's swimming behavior in captivity have only recently been explored (Gallimore et al., 2024).

One particularly unexplored aspect of the ecology of this species is its reproduction. Whale sharks are ovoviviparous, but only one case of a gravid female has been found in Taiwan (Joung et al., 1996), and other aspects, such as mating behavior, remain unclear. Since April 2012, the male whale shark at the OCA has been observed to perform one of its courtship behaviors, namely a large body rotation along with the crossing of both claspers (called a *clasper cross*), and because sperm release was also observed, it was reported that the individual reached sexual maturity in the same year (Sato et al., 2016; Matsumoto et al., 2019). During mating, male elasmobranchs usually maintain their position by biting the pectoral fins and trunk of the female and inserting their crossed claspers into the cloaca of females (Pratt and Carrier, 2001). This behavior is considered one of the reproductive behaviors of this species. Although such behavior, including the clasper cross, has been recorded by surveillance cameras, quantitative analysis of visual observations is needed for further evaluation.

To solve these problems, we used biologging to study the swimming behavior of whale sharks in captivity. The tools have been expanded to study various shark behaviors and to analyze activity patterns and energy use (Andrzejaczek et al., 2019).

Overall dynamic body acceleration (ODBA), a metric that Wilson et al. (2006) proposed as a substitute for rate of energy expenditure, has been found to be a useful measure of animal activity (Halsey et al., 2011), and results of experiments with 3 shark species indicate that ODBA was significantly correlated with energy consumption (Lear et al., 2017). More recently, measures of such activity levels have been quantified to indicate animal welfare in ecotourism and aquariums (Lauderdale et al., 2021; Barry et al., 2023).

We used relative entropy (RE) to detect specific behaviors like the clasper cross. When applied to animal behavior, higher RE values indicate that the target behavior is more specific than normal behavior (Kadota et al., 2011).

The objectives of this study were 1) to quantitatively evaluate the swimming characteristics of this species in captivity, 2) to obtain understanding of the effects of illumination and water temperature on the long-term swimming behavior of an individual, and 3) to contribute to the interpretation of the behaviors of this species. More specifically, the aims of this project were to examine the swimming behavior of an individual that has adapted to a captive environment (that has successfully been kept for the longest period of time in the world) and to evaluate the current rearing environment of the OCA. The results of this study will contribute to the development of captive conservation techniques by clarifying the rearing environment conditions that are appropriate for the whale shark, knowledge that is essential for the long-term rearing of this species.

Materials and methods

Experiment site, duration, specimens, and captivity conditions

An adult male whale shark, which had been kept in the tank at the OCA since 1995 and had a total length of 8.8 m and a body weight of approximately 6000 kg, was used in this study. The length was measured in 2020, and the weight was estimated on the basis of the regression equation of total length and weight used by Matsumoto et al. (2017). Data were collected in the Kuroshio Tank (width: 35 m; length: 27 m; depth: 10 m; and capacity: 7500 metric tons) at the OCA over 4 periods: 16–19 September 2020, 13–17 December 2020, 11–22 March 2021, and 6–9 June 2021.

During these periods, the Kuroshio Tank contained natural sea water pumped directly from the open sea; therefore, the temperature of the tank water was completely dependent on that of open sea water. The sea water in the tank was constantly circulated and replaced within approximately 2 h. Lighting was installed in the tanks and was turned on and off at predetermined times (0800 and 1850, respectively). Although sunlight shone through the top of the tank, light intensity measurements inside the tank, taken by using an illuminance logger, revealed an illuminance range of approximately 30–5000 lx during the daytime (when the lights were on) and 1–30 lx during the nighttime (when the lights were off). In addition to the individual that was the focus of our experiment, the tank also contained an immature female whale shark, Alfred manta (*Mobula alfredi*), and Pacific bluefin tuna (*Thunnus orientalis*). Approximately 60 other species were maintained in the Kuroshio Tank during the experiment (Okinawa Churaumi Aquarium[1]). Whale sharks were fed 4 times a day at fixed times, at approximately 0945, 1145, 1500, and 1700. The average ambient temperature of the water in the

[1] Okinawa Churaumi Aquarium. 2021. Churaumi Fish Encyclopedia. Search by area: The Kuroshio Sea. [Available from website, accessed March 2021.]

tank was measured with a data logger during each of the 4 observation periods of this study. These temperatures are listed in Table 1 along with the date and duration of each period of the experiment.

This study was conducted as part of the monitoring of the health of captive animals at the OCA. A separate or specific approval from any association was not required for this work. Maintenance, animal handling, and all procedures associated with this study were conducted in accordance with the ethical guidelines of the Okinawa Churashima Foundation.

Tagging and deployment

A data logger (ORI400-3MPD3GT[2], Little Leonardo Co., Tokyo, Japan; diameter: 16.5 mm; length: 83.5 mm; and weight in air: 42.4 g) was used to obtain information on the swimming behavior of the male whale shark. This data logger, which was attached to the shark, was used to measure the swimming speed (in meters per second), swimming depth (in meters), ambient water temperature (in degrees Celsius), triaxial acceleration (in g, with 1 g equal to 9.8 m/s^2), and triaxial magnetism (in micro Tesla). Swimming speeds, swimming depths, and ambient water temperatures were measured at 1-Hz intervals, and triaxial accelerations and triaxial magnetism were measured at 20-Hz intervals. The duration for recording these data was approximately 95 h when measurements were taken under these settings. The logger was fixed to a base fabricated by using a 3D printer, 2 suction cups were attached to the base, and instant glue applied to these suction cups was used to attach the logger to the shark (Fig. 1). The side of the logger with the propeller in it was attached to the anterior base of the first dorsal fin of the whale shark so that the position of the logger was as parallel to the body of the shark as possible (Fig. 1). By repeatedly attaching loggers to the same location on the shark during all experimental periods, it was possible to compare activity levels. Although no particular changes were observed in the swimming behavior of this individual as a result of the attachment and removal of loggers, the periods of approximately 20 min before and after the attachment and removal of loggers were excluded from analysis to avoid such effects. During analysis, some data were deemed to be unreliable because of missing or misaligned loggers, and these data were excluded.

[2] Mention of trade names or commercial companies is for identification purposes only and does not imply endorsement by the National Marine Fisheries Service, NOAA.

Data analysis

The data were analyzed by using Igor Pro analysis software (vers. 6.12; WaveMetrics, Portland, OR) and the add-on program Ethographer (Sakamoto et al., 2009). The raw acceleration data included data on static acceleration, which has 2 components that needed to be separated prior

Table 1

Dates, duration, and average water temperatures in the Kuroshio Tank, at the Okinawa Churaumi Aquarium in Japan, for an experiment during which the behavior of a male whale shark (*Rhincodon typus*) was observed in 2020 and 2021. Mean temperatures experienced by the whale shark in the tank are provided with standard deviations in parentheses.

Dates	Duration (h)	Temperature (°C)
16–19 September 2020	73	28.5 (0.1)
13–20 December 2020	143	23.6 (0.3)
11–22 March 2021	221	22.1 (0.3)
6–9 June 2021	57	26.8 (0.0)

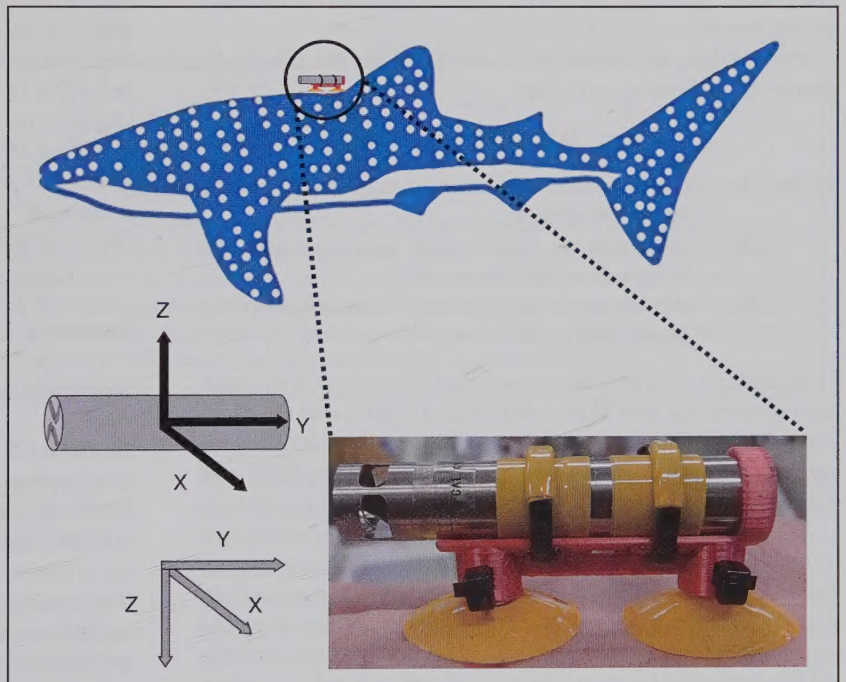

Figure 1

Diagram and photograph of the data logger attached to a male whale shark (*Rhincodon typus*) in the Kuroshio Tank at the Okinawa Churaumi Aquarium in Japan during 4 experimental periods: 16–19 September 2020, 13–17 December 2020, 11–22 March 2021, and 6–9 June 2021. The diagram shows the mounting position of the data logger and direction of the device and logger axes. The black axis represents the direction of the acceleration, and the gray axis represents the geomagnetic direction. The X, Y, and Z labels represent the lateral (sway), longitudinal (surge), and dorsoventral (heave) axes, respectively.

to behavioral analysis: gravitational acceleration, caused by changes in the animal's posture, and dynamic acceleration, caused by the animal's movement (Sakamoto et al., 2009). To visualize the periodic components of the acceleration time series, a continuous wavelet transformation (CWT) was performed on all raw acceleration data. Results from the CWT indicate that most periodic components have peaks in periods less than 10 s in all acceleration data, the components with a period shorter than 10 s were classified as acceleration derived from the whale shark's motion (i.e., dynamic acceleration), and the components with a period longer than 10 s were classified as acceleration derived from its posture or body angle (i.e., static acceleration).

Next, by using the CWT Filter function in Ethographer, the dynamic and static accelerations were separated, and a CWT was applied to the *x*-axial (lateral) dynamic acceleration data separated from the raw acceleration data. The peak tracer function was then used to extract the dominant oscillation period component, which was considered the tail-beat period, and its reciprocal was calculated as the tail-beat frequency (TBF). We employed the *k*-means algorithm to cluster the tail-beat spectra at each second, to understand the characteristics of the tail beat. *K*-means clustering is an unsupervised, interactive algorithm that minimizes the within-cluster sum of squared Euclidean distances from the cluster centroids. For a detailed description of this algorithm, see Sakamoto et al. (2009).

The ODBA, an indicator of activity, was calculated by using the following equation:

$$ODBA = |D\alpha_x| + |D\alpha_y| + |D\alpha_z|, \quad (1)$$

where $D\alpha_x$ = the dynamic acceleration component in the lateral direction;
$D\alpha_y$ = the dynamic acceleration component in the longitudinal direction; and
$D\alpha_z$ = the dynamic acceleration component in the dorsoventral direction.

Statistical analysis was conducted by using 2-way analysis of variance and Mann–Whitney *U* tests, and the Bonferroni correction was used to compare the significance among swimming variables (swimming speed, TBF, and ODBA) in each month and during daytime and nighttime.

Furthermore, RE was calculated by using the calculated *z*-axis (heave) static acceleration (rotational posture) as an indicator for detection of a clasper cross, which is a mating-like behavior not observed during normal swimming. The sampling interval of the static acceleration of the *z*-axis was 20 Hz, but only the starting value of each second was taken from the calculated values, so that the analysis was performed on 1-Hz samples of data in the time series. In this study, the amount of change in rotational posture ($C\alpha_z$) was calculated by using the following equation:

$$C\alpha_z(t) = S\alpha_z(t) - S\alpha_z(t - \Delta t), \quad (2)$$

where $S\alpha_z$ = the static acceleration of the *z*-axis (i.e., the rotational posture); and
Δt = the measurement interval (in seconds; i.e., 1 s in this study).

The data in the time series were divided into bins with intervals of 20 s (number of bins=20). At each time t_k, the probability distribution followed by $C\alpha_z$ was assumed to be a normal distribution, and the statistical parameters μ and σ of each bin were estimated by using maximum likelihood estimation. The parameter μ represents the mean, and σ represents the standard deviation. The distribution $Q(C\alpha_z)$ for the entire measurement period was defined as the distribution form representing the average swimming state. Furthermore, the probability density functions were obtained for the continuous probability distributions $P(C\alpha_z,t_k)$ and $Q(C\alpha_z)$, and the RE was calculated for the time series by using the following equation:

$$RE(t_k) = \int_{-\infty}^{\infty} P(C\alpha_z, t_k) \log\left(\frac{P(C\alpha_z, t_k)}{Q(C\alpha_z)}\right) S\alpha_z \quad (3)$$

$$= \frac{1}{2}\left[\log\left(\frac{\sigma_q}{\sigma_p(t_k)}\right)^2 + \left(\frac{\sigma_p(t_k)}{\sigma_q}\right)^2 - 1\right] + \frac{1}{2}\frac{(\mu_p(t_k) - \mu_p)^2}{\sigma_q^2}.$$

In this study, RE was high if the amount of change in rotational posture during a given 20-s period was extraordinarily active in comparison to the entire measurement period. Because the occurrence probability of such specific behavior is equivalent to the –RE power of the base *e* of the natural logarithm, it is considered to be equivalent to $P=e^{-20}=2.06\times10^{-9}$, if RE is 20. In this study, the frequency of clasper crosses was determined by checking the video images of the surveillance camera when the RE value obtained with Equation 3 was high.

Results

Swimming behavior at ambient temperatures

In Figure 2, we provide, as an example of changes in the time series, a graphic representation of raw data of *x*-axis acceleration and *x*-axis dynamic acceleration, dynamic acceleration after CWT, swimming speed, TBF, and ODBA for a period of 3 d. The period of dynamic acceleration on the *x*-axis was typically in the range of 4–10 s, with some exceptions. Swimming speeds were higher at higher TBFs and lower at lower TBFs (coefficient of correlation [*r*]=0.43, $P<0.001$). The mean values of swimming speed, TBF, and ODBA in daytime and nighttime for each temperature during the experimental period, as well as the ratios of decreases from daytime to nighttime, are listed in Table 2. Swimming speed, TBF, and ODBA values were significantly lower during the nighttime than during the daytime across all experimental periods (speed: $U>5.5\times10^9$, $P<0.001$; TBF: $U>6.5\times10^8$, $P<0.001$; ODBA: $U>9.1\times10^8$, $P<0.001$) (Table 2, Fig. 3). The analysis of variance results indicate that month, time of day (daytime or nighttime), and their interaction significantly affected speed, TBF, and

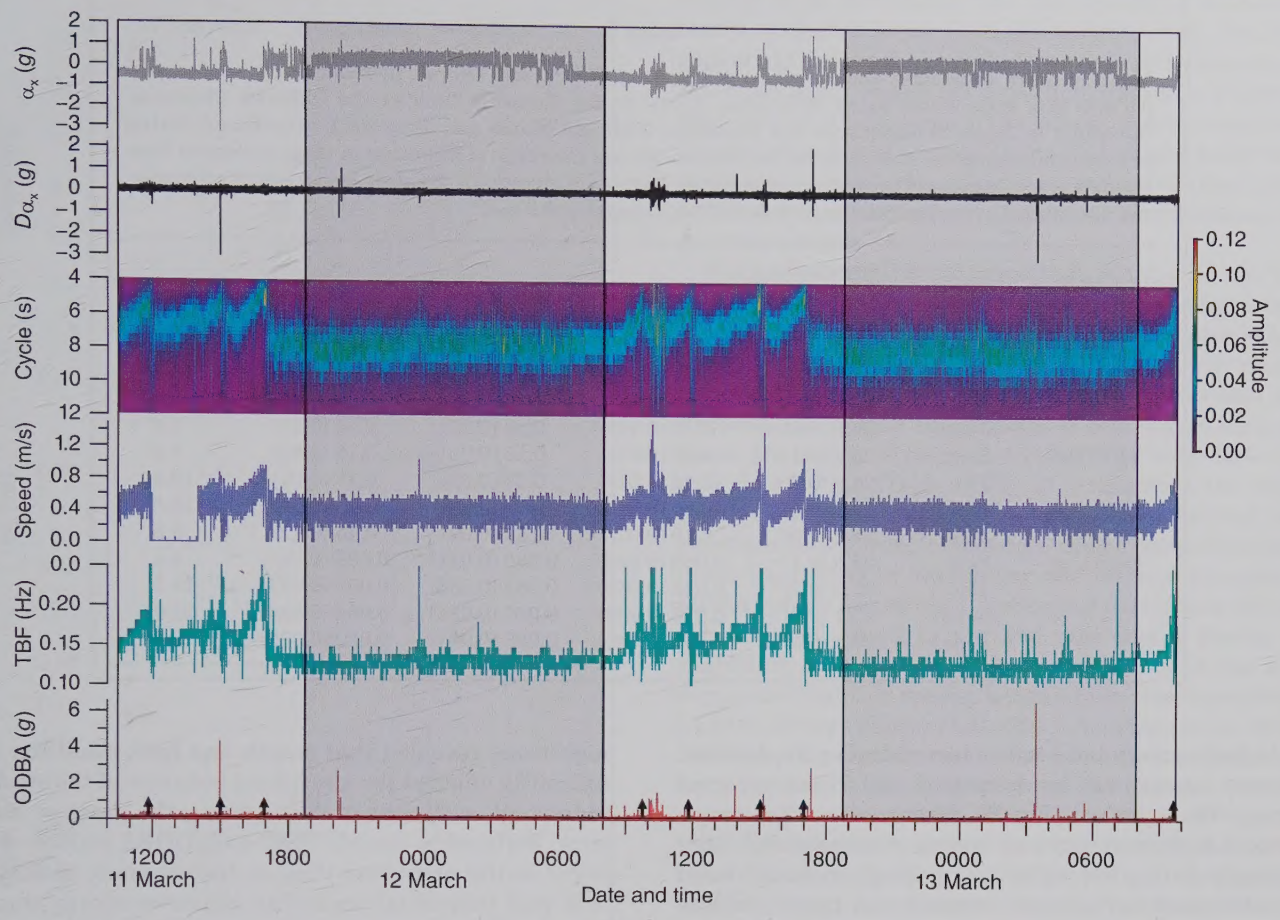

Figure 2

Movement and acceleration time series collected on 11–13 March 2021 with a data logger attached to a male whale shark (*Rhincodon typus*) in the Kuroshio Tank at the Okinawa Churaumi Aquarium in Japan. The panels show, from the top, the raw data of *x*-axis acceleration (α_x) and dynamic acceleration on the *x*-axis ($D\alpha_x$, sway), a spectrogram of dynamic acceleration after continuous wavelet transformation (cycle, sway), swimming speed, tail-beat frequency (TBF, sway), and overall dynamic body acceleration (ODBA). The white and gray areas indicate periods of daytime and nighttime, respectively. The arrows above the *x*-axis indicate the feeding times. Note that 1 *g*, the unit of measure for α_x, $D\alpha_x$, and ODBA, is equal to 9.8 m/s^2.

ODBA, with the effect of time of day being particularly dominant (speed: $F(1, 1{,}299{,}893)=85{,}305.37$, $P<0.001$; TBF: $F(1, 1{,}588{,}564)=510{,}614.11$, $P<0.001$; ODBA: $F(1, 1{,}326{,}286)=52{,}872.65$, $P<0.001$).

The seasonal data indicate that swimming speed, TBF, and ODBA values were significantly lower during the cooler months of December and March than during the warmer months of June and September (speed: $U=1.5\times10^{11}$, $P<0.001$; TBF: $U=1.3\times10^{11}$, $P<0.001$; ODBA: $U=1.1\times10^{11}$, $P<0.001$) (Fig. 3). During the periods of cool water temperatures, the ratios of the decreases in swimming speed, TBF, and ODBA between daytime and nighttime ranged from 14.9% to 19.7%, 15.5% to 15.6%, and 15.9% to 21.0%, respectively. The ratios of the decreases between daytime and nighttime for all 3 parameters were greater in the period of cool water temperatures than in the period of warm water temperatures (Table 2). Box plots of ODBA by time of day for the entire period reveal that ODBA tended to be lower during the nighttime than during the daytime and was intermittently high at 0900, 1100, 1400, and 1600, times that correspond to the times before feeding (Fig. 4).

Because it was difficult to compare the characteristics of the TBFs for each condition (water temperature and light) by using only the average values, we used the *k*-means method for cluster analysis of the *x*-axis dynamic acceleration data. In all experimental periods, there were 2 distinct patterns of TBF: high and low frequency, representing fast and slow tail-beat movements (Fig. 5, A–D). The high-frequency peak, the low-frequency peak, and the difference between the 2 frequencies were 0.16 Hz, 0.14 Hz, and 0.02 Hz in September, 0.15 Hz, 0.13 Hz, and 0.02 Hz in December, 0.17 Hz, 0.13 Hz, and 0.04 Hz in March, and 0.17 Hz, 0.15 Hz, and 0.02 Hz in June, respectively. Furthermore, the occurrence ratios of the 2 TBF components were calculated for each minute, and almost

Table 2

Monthly mean swimming speed, tail-beat frequency (TBF), and overall dynamic body acceleration (ODBA) of a male whale shark (*Rhincodon typus*) in the Kuroshio Tank at the Okinawa Churaumi Aquarium in Japan in September and December 2020 and March and June 2021, overall and during daytime and nighttime. Also provided for each month are the ratios of decreases in these measures from daytime to nighttime and the mean temperature. Means are given with standard deviations in parentheses. Note that 1 *g*, the unit of measure for ODBA, is equal to 9.8 m/s^2.

Index	Month	Temperature (°C)	Overall	Daytime	Nighttime	Ratio (%)
Speed (m/s)	Sept.	28.5 (0.1)	0.42 (0.10)	0.43 (0.12)	0.41 (0.08)	6.1
	Dec.	23.6 (0.3)	0.37 (0.11)	0.41 (0.12)	0.35 (0.08)	14.9
	March	22.1 (0.3)	0.40 (0.12)	0.46 (0.14)	0.37 (0.08)	19.7
	June	26.8 (0.0)	0.42 (0.11)	0.43 (0.13)	0.41 (0.11)	4.4
TBF (Hz)	Sept.	28.5 (0.1)	0.15 (0.02)	0.15 (0.02)	0.15 (0.01)	6.2
	Dec.	23.6 (0.3)	0.14 (0.02)	0.15 (0.02)	0.13 (0.01)	15.5
	March	22.1 (0.3)	0.14 (0.02)	0.15 (0.02)	0.13 (0.01)	15.6
	June	26.8 (0.0)	0.16 (0.02)	0.16 (0.02)	0.15 (0.02)	5.5
ODBA (*g*)	Sept.	28.5 (0.1)	0.088 (0.044)	0.090 (0.046)	0.086 (0.042)	4.4
	Dec.	23.6 (0.3)	0.075 (0.038)	0.082 (0.038)	0.069 (0.037)	15.9
	March	22.1 (0.3)	0.071 (0.036)	0.080 (0.038)	0.064 (0.034)	21.0
	June	26.8 (0.0)	0.084 (0.040)	0.088 (0.041)	0.080 (0.039)	9.1

all high-frequency tail beats occurred during the daytime, whereas almost all low-frequency tail beats occurred during the nighttime (Fig. 6). Strong pulse-like components of high-frequency tail beating were recorded intermittently during the nighttime, although most tail beats were recorded during slow swimming in periods of low-frequency tail beating (Fig. 6).

Calculation of clasper crosses

In all experimental periods, high values of RE were observed mostly during the daytime and rarely during the nighttime (Fig. 7). When the RE value was higher than 20, the behavior of the shark was checked on the video from the aquarium surveillance cameras. The shark was found to be engaged in a clasper cross in all cases during the experiment, with the exception of 4 cases when the shark was just changing direction. The counts of clasper crosses during each 24-h period indicate that 85.3% of the clasper crosses occurred during the daytime and 14.6% occurred during the nighttime (Fig. 8). The frequency of clasper crosses during each experimental period is shown in Table 3. The frequencies of clasper crosses per day were lower during periods of cool water temperatures (March and December) than during periods of warm water temperatures (June and September), and the highest frequency of clasper crosses per day was recorded in June (χ^2=10.18, P=0.00142) (Table 3).

Discussion

Comparisons of the swimming speed, TBF, and ODBA during each month and time of day (daytime and nighttime) revealed that month and light condition significantly affected the swimming behavior of the studied individual, with time of day exerting the greatest influence. Swimming speed, TBF, and ODBA values were lower in the nighttime than in the daytime, indicating that this individual tended to conserve energy during the nighttime.

During the experimental period, as mentioned previously, we recorded 2 distinct patterns of TBF, high and low frequency (i.e., fast and slow movements of the caudal fin). In the hourly ratio of these 2 frequencies, high-frequency tail beats were dominant in the daytime, and low-frequency tail beats were dominant in the nighttime. This individual used both fast and slow modes of tail beating and rested during the nighttime, when it mainly used the slow mode of tail beating. The intervals of low-frequency tail beating lasted about 50 min, and the pulse-like components of high-frequency tail beating, which indicate active, fast swimming, lasted from 1 to 5 min. This resting pattern indicates that the male whale shark has a rhythm of 50-min periods of sleep-like rest with slow swimming, interspersed with periods of 1–5 min of awake-like activity with fast swimming (Fig. 6). The metabolic rate of draughtsbroad sharks (*Cephaloscyllium isabellum*) decreases during sleep, and sleep plays a role in energy conservation (Kelly et al., 2022); however, few physiological studies have been conducted on sleep in elasmobranchs, especially by using electroencephalograms (Kelly et al., 2019). The diurnal circadian rhythm and nighttime resting of the male whale shark in our study differed from the findings of Gleiss et al. (2013), who reported that, in the wild, this species is more active around sunrise and sunset. The effects of fixed feeding times at the OCA for

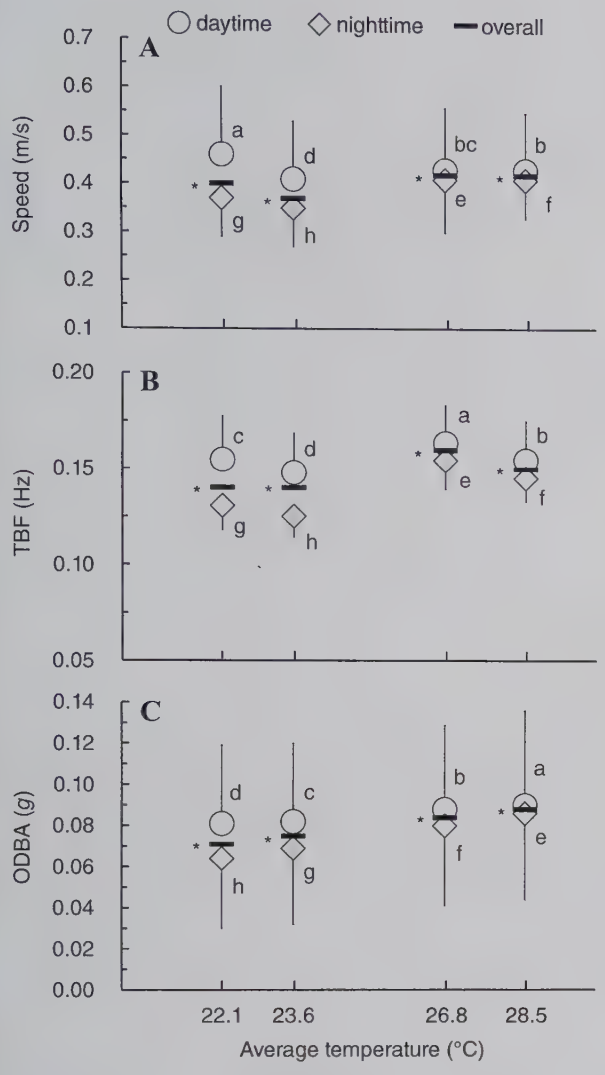

Figure 3

Relationships between average (overall) water temperature and daytime and nighttime (**A**) swimming speed, (**B**) tail-beat frequency (TBF), and (**C**) overall dynamic body acceleration (ODBA) for a male whale shark (*Rhincodon typus*) in the Kuroshio Tank at the Okinawa Churaumi Aquarium, in Japan, over 4 experimental periods: 16–19 September 2020, 13–17 December 2020, 11–22 March 2021, and 6–9 June 2021. The temperatures of 22.1°C, 23.6°C, 26.8°C, and 28.5°C represent those in March, December, June, and September, respectively. Error bars indicate the standard deviations. Asterisks indicate that there was a significant difference ($P<0.01$) between daytime and nighttime. Different letters indicate significant differences between the groups of each condition (water temperature and time of day [daytime or nighttime]). Note that 1 *g*, the unit of measure for ODBA, is equal to 9.8 m/s^2.

whale sharks during only the daytime should be investigated in a future study.

The ODBA increased during the periods of warm water temperatures, indicating that the amount of energy consumed for swimming was higher in warm water. This finding is in accordance with the results of a previous study conducted at the OCA (Matsumoto et al., 2018). In that study, during the period of warm water temperatures, the male whale shark fed more, but the ratio of girth to total length, which is one of the fatness indices, decreased. On the other hand, during the period of cool water temperatures, this ratio increased even though the food intake of this fish was not as high as that during the warm temperature period.

Nakamura et al. (2020) found that, in the wild, the TBF of this species also decreased with decreasing muscle temperature, indicating that this individual also experienced a decrease in TBF due to a reduction in muscle temperature during the period when the water was cool. Particularly, during the periods of cool water temperatures, the ratios of decreases in ODBAs were 15%–20% and clearly high (Table 2, Fig. 3C); therefore, the whale shark could easily rest in the nighttime under cool temperature conditions. In contrast, under temperatures at more than 28°C in September, the ratio of decrease in ODBA was as low as 4.4%, indicating that it was difficult for the whale shark to rest and save energy during the nighttime in warm temperature conditions. It has been suggested that this species behaviorally thermoregulates by deep diving (Thums et al., 2013; Robinson et al., 2017). However, our results were obtained in limited space and temperature ranges because deep diving is not possible under captive conditions. The aquarium staff reported that this species is prone to feeding problems during the summer, indicating that in captivity, it struggles to adapt to warm water temperatures in summer, when the in-tank water temperature can exceed 28°C, and that it adapts to low water temperatures by decreasing its activity level. Given the findings of Ryan et al. (2017), which indicate that this species spends approximately 75% of its time in water with temperatures of 22°C–26°C and tends to inhabit waters with stable temperatures averaging 25°C, we estimated the optimal range of water temperatures for this species in captivity as approximately 22°C–27°C.

The clasper cross, a mating-like behavior, tended to occur mostly during the daytime. This result indicates that this behavior is affected by illumination. It had been reported that vision of the whale shark plays an important role in short-range perception (Martin, 2007; Tomita et al., 2020). Therefore, we suggest that the male whale shark engages in clasper crosses during the daytime to make courtship visually appealing to the female whale shark.

Our results indicate that the frequency of clasper crosses was lower in the cool temperature periods than in the warm temperature periods; the highest clasper-cross frequency was observed in June (when the water temperature was around 26°C). Matsumoto et al. (2021) reported that the highest clasper-cross frequency occurred in early summer from May through July, when the water temperature in the aquarium was approximately 25°C, a finding that is quite close to the results of this study. Increased blood levels of testosterone have

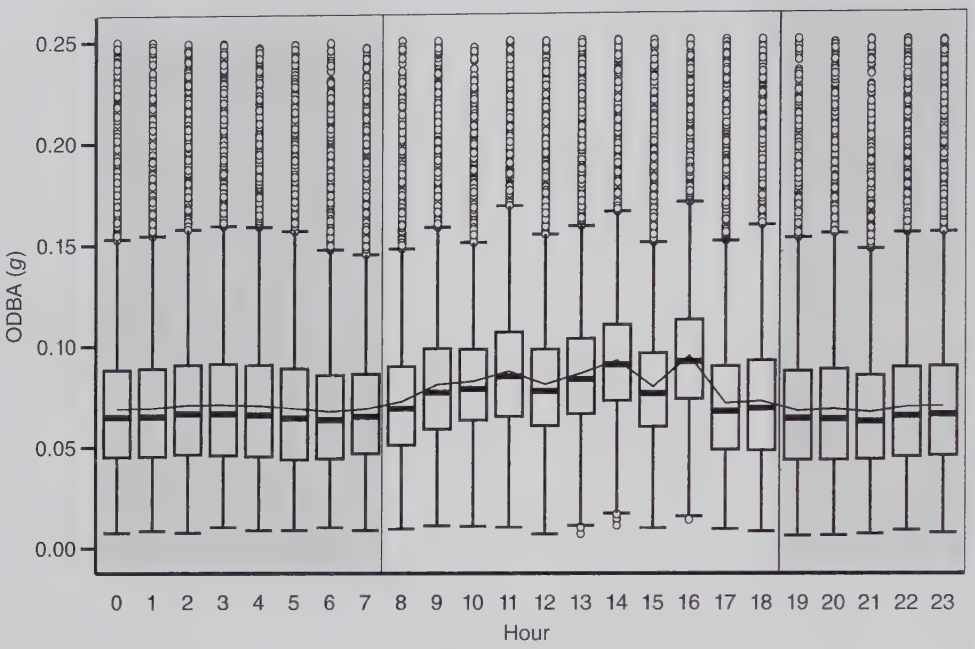

Figure 4

Box plots of overall dynamic body acceleration (ODBA) by hour of day for a male whale shark (*Rhincodon typus*) in the Kuroshio Tank at the Okinawa Churaumi Aquarium, in Japan, during an experiment conducted in September and December 2020 and March and June 2021. The trend line indicates average values. The thick line in each box indicates the median, and the ends of the box represent the upper and lower quartiles. The whiskers indicate the highest and lowest values, excluding the outliers (circles). The white and gray areas indicate periods of daytime and nighttime, respectively. Note that 1 *g*, the unit of measure for ODBA, is equal to 9.8 m/s^2.

also been observed for this individual within this water temperature range, indicating a relationship between the elevation of this hormone and the rise in the number of clasper crosses (Matsumoto et al., 2021). Therefore, we speculate that reproductive behavior is greatly affected by ambient water temperature and that the optimal reproductive water temperature for this species may be approximately 26°C.

The findings of our study indicate that the behavior of the male whale shark is significantly affected by ambient water temperature and illumination. The studied shark successfully adapted to the current rearing environment by managing swimming and resting while conserving activity and energy, a flexibility that is thought to be one of the reasons for the long-term success in rearing of this species at the OCA. In particular, a period of cool temperatures is considered more suitable for resting than a period of warm temperatures, and the frequency of clasper crosses during cool temperature periods is about half that during warm temperature periods. Therefore, there seems to be a trade-off between rest for saving energy and mating-like behaviors. All of these results indicate that, in order to promote growth, maturity, and ultimately successful breeding of this species in captivity, water temperature should be allowed to fluctuate within a range of approximately 22°C–27°C, as it is in the current rearing environment at the OCA, rather than kept at a constant level.

Conclusions

The results of this study, in which detailed data from long-term biologging were used to quantify the behavior of a whale shark successfully adapted to captive conditions, provide an important basis for developing captive conservation methods for this species. In particular, the findings of this study indicate that 2 factors are key to long-term rearing of this species: 1) active swimming during the daytime and resting at nighttime and 2) seasonal changes in the water temperature of the aquarium (i.e., allowing the fish to experience cool water conditions). In the future, staff of other aquariums should consider the nighttime resting behavior of this species and how to manage water temperature, in order to aid health management and to enable long-term rearing of this species. Long-term rearing of this species will reduce the

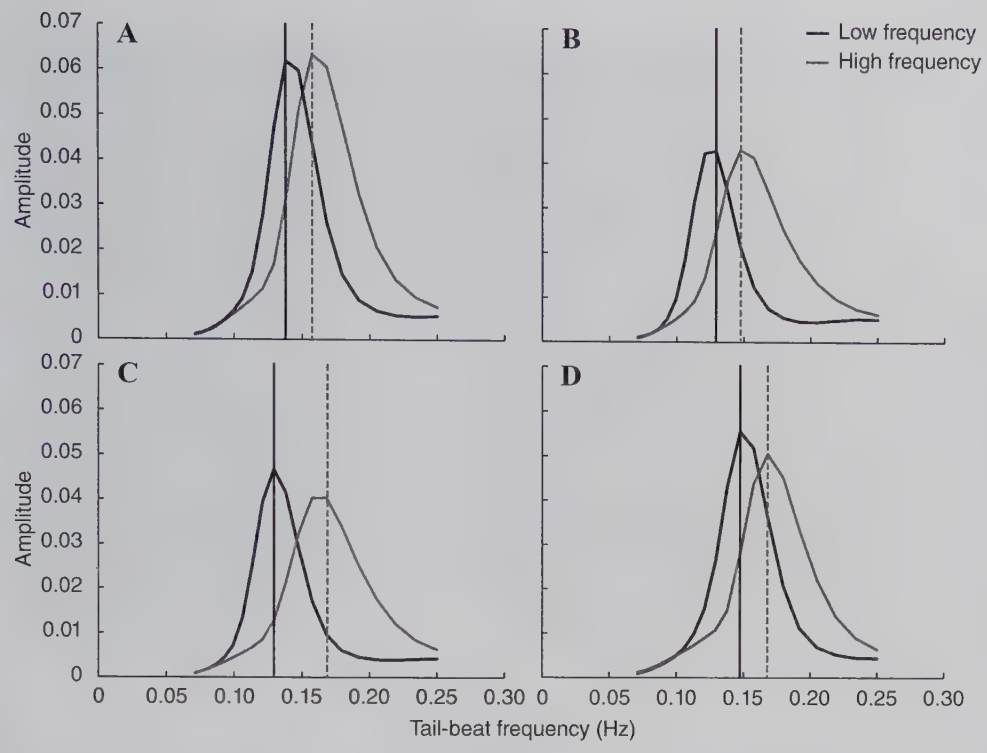

Figure 5

Results of cluster analysis, with the *k*-means method, of oscillations of the caudal fin of a male whale shark (*Rhincodon typus*) in the Kuroshio Tank at the Okinawa Churaumi Aquarium in Japan during 4 periods: (**A**) 16–19 September 2020, (**B**) 13–17 December 2020, (**C**) 11–22 March 2021, and (**D**) 6–9 June 2021. The vertical axis represents the amplitude strength, and the horizontal axis represents the tail-beat frequency. The gray and black dashed lines represent the high- and low-frequency peaks in oscillations, respectively.

need to take more individuals from the wild, leading to resource conservation.

Resumen

Las observaciones cuantitativas a largo plazo son esenciales para la conservación del tiburón ballena (*Rhincodon typus*), el cual necesita mucho tiempo para crecer y madurar. En este estudio, se colocó un dispositivo de registro de datos en un tiburón ballena macho maduro que se había mantenido en cautiverio durante más de 29 años en el Acuario Churaumi de Okinawa (Japón). Debido a que es deseable la crianza a largo plazo del tiburón ballena en cautiverio, se investigaron los efectos de la temperatura del agua y la luz sobre el comportamiento de natación del tiburón ballena en cautiverio. A partir de los datos de natación, se calcularon las frecuencias de los latidos de la cola (TBF), los niveles de actividad y la frecuencia de cruces de los claspers, que se considera un comportamiento similar al apareamiento. En todas las estaciones, la TBF, la velocidad de nado y el nivel de actividad del tiburón fueron entre un 4% y un 20% menores durante la noche que durante el día, especialmente a temperaturas de agua frías (≤23.6°C). Además, aproximadamente el 90% de los cruces del claspers se produjeron durante el día. Estos resultados indican que el tiburón está activo durante el día, realizando actividades como el apareamiento. Por el contrario, durante la noche descansa mientras nada, ralentizando el batido de su aleta caudal y reduciendo la velocidad de nado para conservar energía. Por lo tanto, concluimos que este individuo ha adoptado este ritmo diurno para adaptarse a su actual entorno de cría.

Acknowledgments

We express our gratitude to the staff of the OCA and the Okinawa Churashima Research Center of the Okinawa Churashima Foundation for giving us the opportunity to conduct this research and for their cooperation. This study was partially supported by a Grant-in-Aid for Scientific Research (C) from the Japan Society for Promotion of Science (grant number 23K03754). We would like to thank Editage for English language editing.

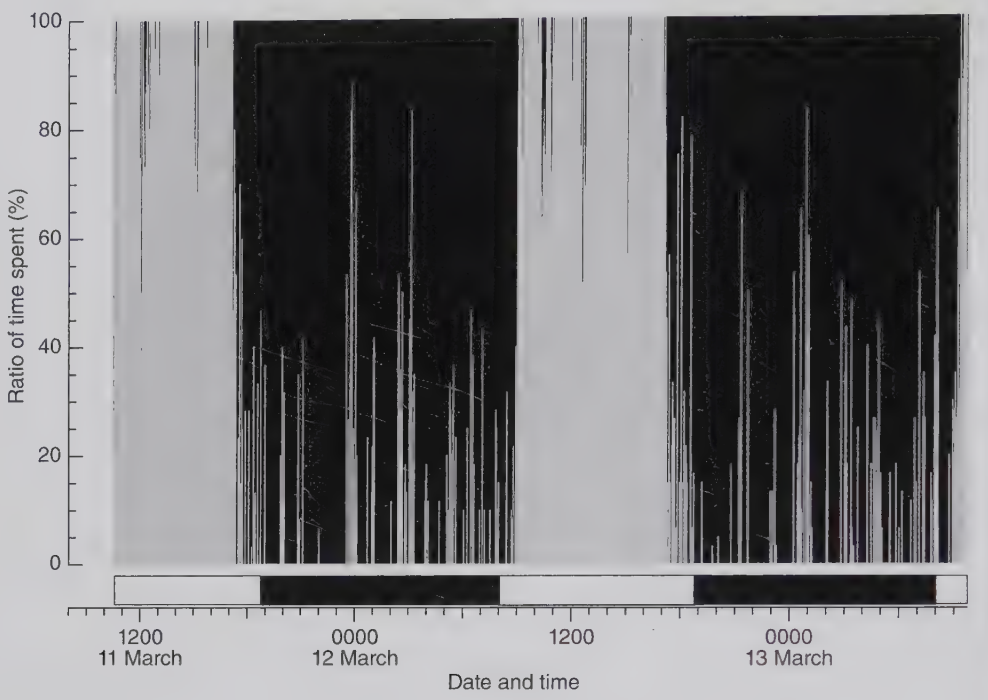

Figure 6

Ratio of time occupied by 2 types of tail-beat frequencies in 1 min of data from the data logger attached to a male whale shark (*Rhincodon typus*) in the Kuroshio Tank at the Okinawa Churaumi Aquarium, in Japan, during 11–13 March 2021. The gray part of the graph represents the time with high-frequency tail beats, classified by using the *k*-means method, and the black part represents the time with low-frequency tail beats. The white and black horizontal bars at the bottom of the graph indicate periods of daytime and nighttime, respectively.

Table 3

Frequency and duration of clasper crosses of a male whale shark (*Rhincodon typus*) in the Kuroshio Tank at the Okinawa Churaumi Aquarium in Japan during September and December 2020 and March and June 2021. Mean temperatures in the tank for each month are also provided, with standard deviations in parentheses. A clasper cross is a mating-like behavior that includes a large body rotation and a crossing of both claspers.

Month	Temperature (°C)	Duration (h)	Frequency of clasper crosses	Frequency of clasper crosses per day
Sept.	28.5 (0.1)	23.2	4	4.1
Dec.	23.6 (0.3)	119.0	10	2.0
March	22.1 (0.3)	220.2	14	1.5
June	26.8 (0.0)	56.3	13	5.5

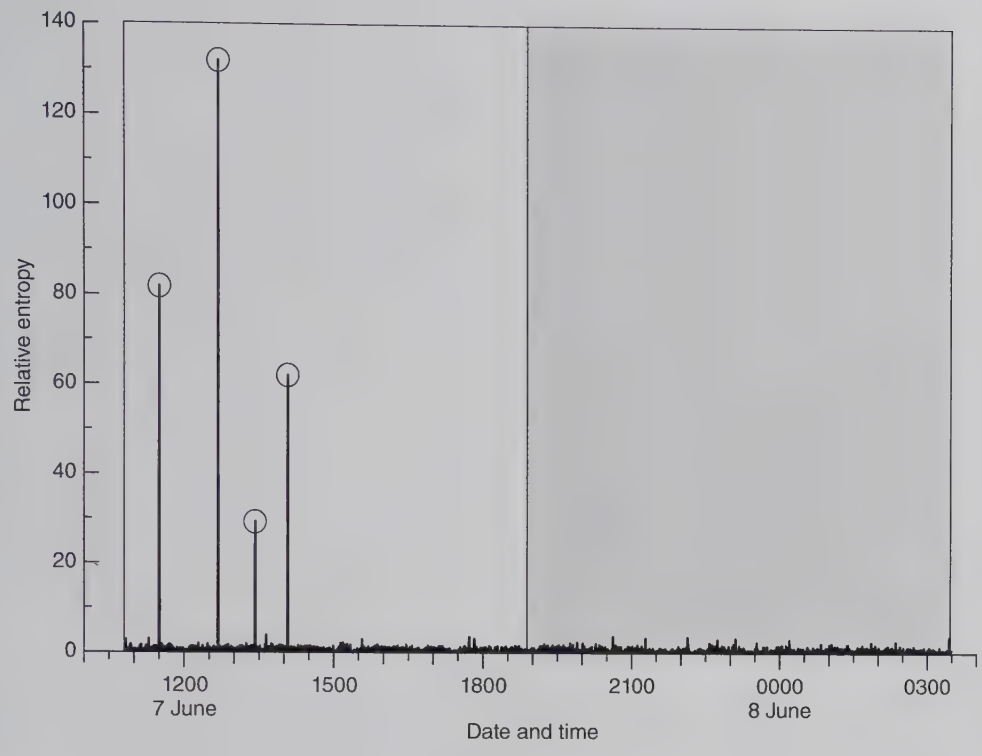

Figure 7

Variation in relative entropy values calculated from static acceleration on the *z*-axis for a male whale shark (*Rhincodon typus*) in the Kuroshio Tank at the Okinawa Churaumi Aquarium in Japan during 7–8 June 2021. The relative entropy values >20 indicate a clasper cross, a mating-like behavior that includes a large body rotation and a crossing of both claspers (white circles). Relative entropy values <4 indicate normal behavior. The white and gray areas indicate periods of daytime and nighttime, respectively.

Literature cited

Andrzejaczek, S., A. C. Gleiss, K. O. Lear, C. B. Pattiaratchi, T. K. Chapple, and M. G. Meekan.
2019. Biologging tags reveal links between fine-scale horizontal and vertical movement behaviors in tiger sharks (*Galeocerdo cuvier*). Front. Mar. Sci. 6:229.

Araujo, G., C. A. Rohner, J. Labaja, S. J. Conales, S. J. Snow, R. Murray, S. J. Pierce, and A. Ponzo.
2018. Satellite tracking of juvenile whale sharks in the Sulu and Bohol Seas, Philippines. PeerJ 6:e5231.

Barry, C., C. Legaspi, T. M. Clarke, G. Araujo, C. J. A. Bradshaw, A. C. Gleiss, L. Meyer, and C. Huveneers.
2023. Estimating the energetic cost of whale shark tourism. Biol. Conserv. 284:110164.

Gallagher, A. J., and N. Hammerschlag.
2011. Global shark currency: the distribution, frequency, and economic value of shark ecotourism. Current Issues Tour. 14:797–812.

Gallimore, C. G., C. Walton, R. Nugent, M. Fradkin, L. Poppell, C. Schreiber, C. Coco, M. Grober, B. Carlson, A. D. M. Dove, et al.
2024. A longitudinal behavioral analysis of aquarium whale sharks (*Rhincodon typus*): insights into anticipatory cues, individual variation, and social interaction. Front. Mar. Sci. 11:1418002.

Gleiss, A. C., S. Wright, N. Liebsch, R. P. Wilson, and B. Norman.
2013. Contrasting diel patterns in vertical movement and locomotor activity of whale sharks at Ningaloo Reef. Mar. Biol. 160:2981–2992.

Halsey, L. G., E. L. C. Shepard, and R. P. Wilson.
2011. Assessing the development and application of the accelerometry technique for estimating energy expenditure. Comp. Biochem. Physiol. A 158:305–314.

Hearn, A. R., J. R. Green, C. R. Peñaherrera-Palma, S. Reynolds, C. A. Rohner, M. Román, and A. M. M. Sequeira.
2021. Whale shark movements and migrations. *In* Whale sharks: biology, ecology, and conservation (A. D. M. Dove and S. J. Pierce, eds.), p. 105–128. CRC Press, Boca Raton, FL.

Joung, S.-J., C.-T. Chen, E. Clark, S. Uchida, and W. Y. P. Huang.
1996. The whale shark, *Rhincodon typus*, is a livebearer: 300 embryos found in one 'megamamma' supreme. Environ. Biol. Fishes 46:219–223.

Kadota, M., E. J. White, S. Torisawa, K. Komeyama, and T. Takagi.
2011. Employing relative entropy techniques for assessing modifications in animal behavior. PLoS ONE 6(12): e28241.

Kelly, M. L., S. P. Collin, J. M. Hemmi, and J. A. Lesku.
2019. Evidence for sleep in sharks and rays: behavioural, physiological, and evolutionary considerations. Brain Behav. Evol. 94:37–50.

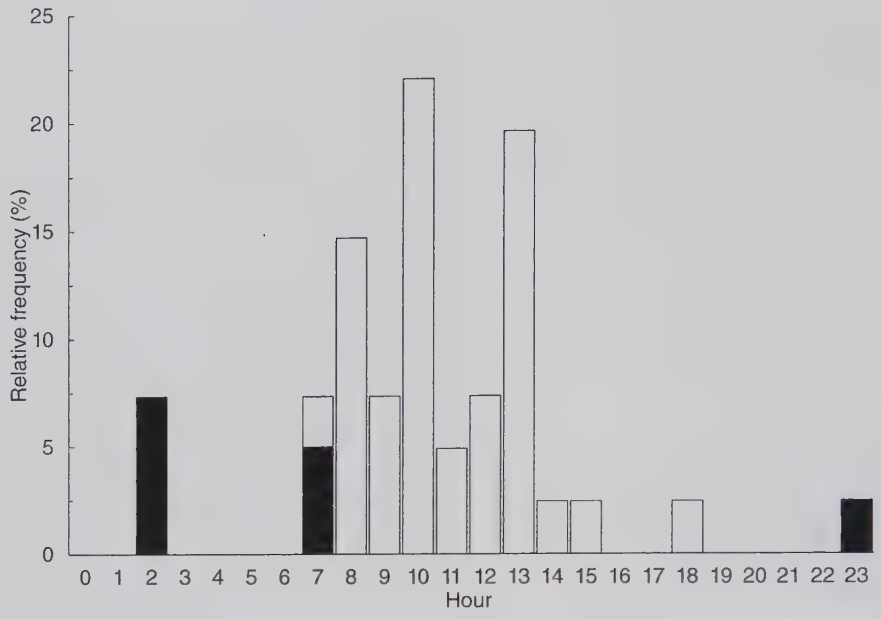

Figure 8

Relative frequency of clasper crosses (number observed=41) by hour of day for a male whale shark (*Rhincodon typus*) in the Kuroshio Tank at the Okinawa Churaumi Aquarium, in Japan, during September and December 2020 and March and June 2021. A clasper cross is a mating-like behavior that includes a large body rotation and a crossing of both claspers. The white and black bars indicate the relative frequencies of clasper crosses that occurred during daytime and nighttime, respectively.

Kelly, M. L., S. P. Collins, J. A. Lesku, J. M. Hemmi, S. P. Collin, and C. A. Radford.
2022. Energy conservation characterizes sleep in sharks. Biol. Lett. 18:20210259.

Lauderdale, L. K., K. A. Shorter, D. Zhang, J. Gabaldon, J. D. Mellen, M. T. Walsh, D. A. Granger, and L. J. Miller.
2021. Bottlenose dolphin habitat and management factors related to activity and distance traveled in zoos and aquariums. PLoS ONE 16(8):e0250687.

Lear, K. O., N. M. Whitney, L. R. Brewster, J. J. Morris, R. E. Hueter, and A. C. Gleiss.
2017. Correlations of metabolic rate and body acceleration in three species of coastal sharks under contrasting temperature regimes. J. Exp. Biol. 220:397–407.

Legaspi, C., J. Miranda, J. Labaja, S. Snow, A. Ponzo, and G. Araujo.
2020. In-water observations highlight the effects of provisioning on whale shark behaviour at the world's largest whale shark tourism destination. R. Soc. Open Sci. 7:200392.

Martin, R. A.
2007. A review of behavioural ecology of whale sharks (*Rhincodon typus*). Fish. Res. 84:10–16.

Matsumoto, R., M. Toda, Y. Matsumoto, K. Ueda, M. Nakazato, K. Sato, and S. Uchida.
2017. Notes on husbandry of whale sharks, *Rhincodon typus*. *In* Elasmobranch husbandry manual II: recent advances in the care of sharks, rays and their relatives (M. Smith, D. Warmolts, D. Thoney, R. Hueter, M. Murray, and J. Ezcurra, eds.), p. 15–22. Ohio Biol. Survey, Columbus, OH.

Matsumoto, R., K. Murakumo, R. Furuyama, and S. Matsuzaki.
2018. Effects of energy intake and water temperature on the body shape of whale sharks at the Okinawa Churaumi Aquarium. *In* Proceedings of 10th International Aquarium Congress Fukushima 2018; Fukushima, 7–10 November, p. 80–84. Int. Aquar. Congr.

Matsumoto, R., Y. Matsumoto, K. Ueda, M. Suzuki, K. Asahina, and K. Sato.
2019. Sexual maturation in a male whale shark (*Rhincodon typus*) based on observations made over 20 years of captivity. Fish. Bull. 117:78–86.

Matsumoto, R., K. Murakumo, R. Nozu, T. Tomita, and K. Sato.
2021. Observation on the reproductive behaviors of a captive male whale shark. *In* Proceedings of the Elasmobranch Symposium 2021; Chiba, 17 December, p. 8. Jpn. Soc. Elasmobranch Stud., Chiba, Japan. [In Japanese.]

Nakamura, I., R. Matsumoto, and K. Sato.
2020. Body temperature stability in the whale shark, the world's largest fish. J. Exp. Biol. 223(11):jeb210286.

Pierce, S. J., and B. Norman.
2016. *Rhincodon typus*. The IUCN Red List of Threatened Species 2016:e.T19488A2365291. [Available from website, accessed November 2021].

Pratt, H. L., Jr., and J. C. Carrier.
2001. A review of elasmobranch reproductive behavior with a case study on the nurse shark, *Ginglymostoma cirratum*. Environ. Biol. Fishes 60:157–188.

Ramírez-Macías, D., N. Queiroz, S. J. Pierce, N. E. Humphries, D. W. Sims, and J. M. Brunnschweiler.
2017. Oceanic adults, coastal juveniles: tracking the habitat use of whale sharks off the Pacific coast of Mexico. PeerJ 5:e3271.

Reynolds, S. D., J. Redcliffe, B. M. Norman, R. P. Wilson, M. Holton, C. E. Franklin, and R. G. Dwyer.
2024. Swimming with humans: biotelemetry reveals effects of "gold standard" regulated tourism on whale sharks. J. Sustain. Tour. 1–20.

Robinson, D. P., M. Y. Jaidah, S. S. Bach, C. A. Rohner, R. W. Jabado, R. Ormond, and S. J. Pierce.
2017. Some like it hot: repeat migration and residency of whale sharks within an extreme natural environment. PLoS ONE 12(9):e0185360.

Rohner, C. A., J. E. M. Cochran, E. F. Cagua, C. E. M. Prebble, S. K. Venables, M. L. Berumen, B. L. Kuguru, J. Rubens, J. M. Brunnschweiler, and S. J. Pierce.
2020. No place like home? High residency and predictable seasonal movement of whale sharks off Tanzania. Front. Mar. Sci. 7:423.

Ryan, J. P., J. R. Green, E. Espinoza, and A. R. Hearn.
2017. Association of whale sharks (*Rhincodon typus*) with thermo-biological frontal systems of the eastern tropical Pacific. PLoS ONE 12(8):e0182599.

Sakamoto, K. Q., K. Sato, M. Ishizuka, Y. Watanuki, A. Takahashi, F. Daunt, and S. Wanless.
2009. Can ethograms be automatically generated using body acceleration data from free-ranging birds? PLoS ONE 4(4):e5379.

Sato, K., R. Matsumoto, K. Murakumo, and K. Asahina.
2016. Long-term husbandry and physical observation of the whale sharks in Okinawa Churaumi Aquarium. QScience Proc. (4th International Whale Shark Conference). 2016:iwsc4.56. [Available from website.]

Thums, M., M. Meekan, J. Stevens, S. Wilson, and J. Polovina.
2013. Evidence for behavioural thermoregulation by the world's largest fish. J. R. Soc. Interface 10:20120477.

Tomita, T., K. Murakumo, S. Komoto, A. Dove, M. Kino, K. Miyamoto, and M. Toda.
2020. Armored eyes of the whale shark. PLoS ONE 15(6):e0235342.

Wilson, R. P., C. R. White, F. Quintana, L. G. Halsey, N. Liebsch, G. R. Martin, and P. J. Butler.
2006. Moving towards acceleration for estimates of activity-specific metabolic rate in free-living animals: the case of the cormorant. J. Anim. Ecol. 75:1081–1090.

National Marine
Fisheries Service
NOAA

Fishery Bulletin
established in 1881

Spencer F. Baird
First U.S. Commissioner
of Fisheries and founder
of *Fishery Bulletin*

Engineering a prototype for a next-generation stock assessment modeling platform

Jon Brodziak (contact author)[1]
Matthew Supernaw[2]
Bai Li[3]
Christine Stawitz[4]
Haley Oleynik[5]
Teresa A'mar[6]

Email address for contact author: jon.brodziak@noaa.gov

[1] Pacific Islands Fisheries Science Center
National Marine Fisheries Service, NOAA
1845 Wasp Boulevard
Honolulu, Hawaii 96818

[2] Office of Science and Technology
National Marine Fisheries Service, NOAA
263 13th Avenue South
St. Petersburg, Florida 33701

[3] ECS Federal LLC
for Office of Science and Technology
National Marine Fisheries Service, NOAA
1315 East West Highway
Silver Spring, Maryland 20910

[4] Office of Science and Technology
National Marine Fisheries Service, NOAA
7600 Sand Point Way
Seattle, Washington 98115

[5] Institute for the Oceans and Fisheries
University of British Columbia
2202 Main Mall
Vancouver, British Columbia V6T 1Z4, Canada

[6] Dragonfly Data Science
P.O. Box 27535
Wellington 6141, New Zealand

Abstract—Environmental and anthropogenic processes have led to widespread changes in productivities and spatial distributions of marine fishery resources. As geographic distributions of fish stocks and subsequently fishing fleets shift, improved spatiotemporal data and spatial modeling will become necessary to estimate abundance and productivity. The goal of this paper is to propose a strategy for engineering a modeling platform for spatially explicit, next-generation stock assessment models. We recount our approach for developing a system prototype, the Metapopulation Assessment System (MAS), that is easy to use, modular, and extensible. The MAS prototype was designed to support complex metapopulation modeling, which includes handling multiple populations, areas, fleets, and surveys and sex differentiation. We describe the components of the software life cycle, engineering, and infrastructure design to support a spatially explicit, next-generation stock assessment system. Software infrastructure was designed and implemented with 3 components: GitHub for collaboration, version control, and code organization; the C++ language for coding fishery system dynamics and estimation modeling; and the R language for coding the input-output interface and systematic testing. Systematic testing was a key component of the MAS development life cycle and was applied to guarantee that system requirements, such as accurate estimation of quantities of interest, are successfully implemented. We conclude with a discussion of some lessons learned and future challenges for ongoing efforts to implement a next-generation stock assessment platform.

Manuscript submitted 19 June 2024.
Manuscript accepted 14 January 2025.
Fish. Bull. 123:88–104 (2025).
Online publication date: 3 February 2025.
doi: 10.7755/FB.123.2.2

The views and opinions expressed or implied in this article are those of the author (or authors) and do not necessarily reflect the position of the National Marine Fisheries Service, NOAA.

Environmental and anthropogenic factors increasingly affect the spatial distribution and productivities of marine fishery resources (Perry et al., 2005; Cheung et al., 2013; Free et al., 2019; Pinsky et al., 2020). As geographic distributions of fish stocks and fishing fleets shift (Gullestad et al., 2020; Palacios-Abrantes et al., 2023), improved spatiotemporal data (e.g., Maureaud et al., 2021) and spatial modeling (e.g., Koenigstein et al., 2016) will be needed to accurately estimate abundance and to predict changes in productivity. Some single-region stock assessments will need to be reconfigured as spatially explicit models or approximated as spatially implicit models to account for range shifts. Single-region assessment models can be extended to implicitly account for spatial patterning in selectivity among fishing fleets by using the "areas-as-fleets" modeling approach (e.g., Waterhouse et al., 2014). Although assessment approaches have continually evolved to improve population dynamics modeling, a next-generation platform is needed to handle the challenges of producing accurate stock assessments for populations exposed to regional changes in environmental conditions.

Improvements in modeling movements of fish and fishing fleets will be an important component of a next-generation stock assessment modeling platform that accounts for spatiotemporal effects of fisheries and environmental drivers under climate change (Berger et al., 2017; Punt, 2019). This platform will also need to support management strategy evaluations with spatially structured operating models (OMs), ensemble modeling, and ecosystem-based fishery management applications (Lynch et al., 2018). A next-generation modeling system will require a modular and extensible software infrastructure to handle changes in the data types used for assessment purposes, analytical approaches, and nonstationary environmental conditions.

Our goal with this paper is to propose a strategy for engineering a modeling system for spatially explicit, next-generation stock assessment models. To this end, we recount our development and testing of a prototype modeling platform for building spatially explicit assessment models that is modular, extensible, and easy to use. We describe the components of the software life cycle, engineering, and infrastructure design needed to support a spatially explicit, next-generation stock assessment modeling platform. Software infrastructure was designed and implemented with 3 components: GitHub for collaboration, version control, and code organization; the C++ language for coding fishery system dynamics and estimation modeling; and the R language for coding the input-output interface and systematic testing. We explain how a prototype, the Metapopulation Assessment System (MAS), was developed to meet these requirements. Systematic testing was a key component of the MAS development life cycle and was applied to guarantee that system requirements, such as accurate estimation of quantities of interest, are successfully implemented. We illustrate an application of simulation testing with the MAS estimation model (EM) for an age-structured OM. We discuss some lessons learned from the MAS project and future challenges for ongoing efforts to implement a next-generation stock assessment modeling platform.

Materials and methods

Engineering a next-generation modeling system is a key goal of this effort to support fishery assessments and management. In 2014, we initiated the development of the MAS. The MAS was conceptualized and developed as an informal collaboration between the NOAA Pacific Islands and Southeast Fisheries Science Centers (Brodziak et al., 2014, 2017). The vision for the MAS project was to build a spatial prototype to span future modeling needs while maintaining existing capabilities with an object-oriented programming (OOP) approach. This aim was consistent with NOAA's updated Stock Assessment Improvement Plan (Lynch et al., 2018), which outlined a future with improved continuity between regional stock assessment methods under a generalized stock assessment framework. It was also consistent with recommendations from the Center for the Advancement of Population Assessment Methodology workshop on next-generation stock assessment models and their requirements held in 2019 (Hoyle et al.[1]; Punt et al., 2020).

The MAS was conceived and designed to be a general software system to support an interoperable set of software modules for building stock assessment models. The main design features of the MAS are a modular and extensible software infrastructure engineered for flexibility and a development life cycle for maintainability and quality control. The MAS development strategy was to support alternative assessment model types with templates as well as to provide built-in ensemble modeling capabilities to handle parametric and structural uncertainty under the system life cycle.

System life cycle, engineering, and infrastructure

System life cycle The system life cycle supports a rigorous software engineering process by using "a systematic approach to the analysis, design, assessment, implementation, test, maintenance and reengineering of software" (Laplante, 2001). A system life cycle and quality control procedures are essential for engineering a next-generation stock assessment modeling platform.

Developing software to build an assessment modeling platform requires a total quality assurance and improvement cycle. The system life cycle is a sequence of 4 primary processes of software requirements, design, implementation, and testing. Each process is represented as a node in a directed graph that spans the set of one-step interactions among processes in the life cycle.

When fishery system dynamics change, either because of changes in our understanding of the system with increased data availability or in response to novel environmental conditions, the assessment modeling approach must also adapt. The design components of the software modeling system evolve in the development life cycle. The first step in the life cycle is to set requirements. Specifying the necessary software behaviors and attributes to implement system requirements conditioned on resource constraints is an iterative process. Technical requirements for a next-generation model were discussed and reviewed at the Center for the Advancement of Population Assessment Methodology workshop in 2019 (Hoyle et al.[1]) and summarized by Punt et al. (2020). These requirements include clear and thorough documentation, state-of-the-art diagnostic analyses, objective means to perform data weighting and model tuning, inherent capacity to account for spatial structure with stock components, capacity to include tagging observations including close-kin mark-recapture data, state-space modeling capacity with flexible implementation of random effects, and support for future stock projections and management strategy evaluations. The next-generation modeling system should support these technical requirements as well as be able to be used to implement ensemble modeling that directly accounts for structural uncertainty (e.g., Dormann et al., 2018; Jardim et al., 2021).

The design process is the second step and is used to identify how to meet requirements and satisfy constraints by evaluating alternative solutions and choosing the best available ones. Identifying the design tools and infrastructure needed to build the software follows the requirements. The implementation process sets the timing pattern of development tasks and their prioritization to manage potential risks to success. Developing efficient processes to precisely implement the software system requirements and build the design components is the third step of the life cycle.

[1] Hoyle, S. D., M. N. Maunder, and Z. T. A'mar. 2020. Frameworks for the next generation of general stock assessment models: 2019 CAPAM workshop report. N.Z. Fish. Assess. Rep. 2020/39, 33 p. Minist. Prim. Ind., Wellington, New Zealand. [Available from website.]

Quality assurance of stock assessments is inherently difficult because the exact estimated quantities and assessment results are nearly impossible to know. It is, however, critical to have a strong testing process that can at least address the performance of models. The testing process is the last step in the cycle and is used to set the methods for quality control and assurance for assessment software, in order to measure progress and to adjust other processes to achieve success. Unit and simulation testing procedures for reliably verifying software features for ongoing quality assurance and control are described in the "Systematic testing" section (see also Supplementary Materials [online only]). Taken together, the 4 steps of requirements, design, implementation, and testing are analogous to those of the Deming cycle used to achieve total quality improvement in manufacturing (Deming, 1982). Typically, the workflow for any production process, including software engineering, entails feedback. Such feedback can occur between pairs of life cycle processes. Accounting for feedback, the life cycle functions as a means to iteratively plan, implement, test, and rethink the interrelated processes needed to build the next-generation system. Overall, the conceptual design of the MAS is based on a system life cycle that focuses work on software engineering and infrastructure to achieve ongoing quality assurance and improvement.

Software engineering Given the system life cycle, it is important to emphasize the necessity of applying software engineering principles (e.g., Martin, 2009) in a systematic and measured approach to the development and maintenance of software. In the case of our development of a modeling system, the overall purpose was to structure the computer code needed to build a next-generation assessment platform. Under a systematic approach, one begins by analyzing the problem and breaking it down into smaller components, or modules. Modularity allows development of well-defined, independent components that have logically discrete functionality. The 3 basic modules in the MAS, for example, are *CalculateCatchAtAge()*, *CalculateSpawningBiomass()*, and *SetVarianceCovariance()*; these modules can be used to produce predictions of fishery catch at age and population spawning biomass and to set estimates of parameter covariances to their estimated values, respectively.

Each module is implemented and tested in isolation prior to integration. Unit testing can be used to write single test cases to confirm the accuracy of individual program modules. Modules also accommodate division of work and ultimately improve maintainability. This modular approach, in turn, leads to an improved capacity for extensibility, which is another key design feature of the MAS. Also, one of the challenges is to allow the flexibility of modular programming while also making the code run efficiently. With modular programming in the MAS, functional forms become object functors, all inherited from a base class with a virtual function that the child classes override. This eliminates the need for costly conditional statements that result in jumps in the machine code. In addition, multidimensional arrays are flattened to 1-dimensional arrays. This array flattening keeps memory contiguous and aids in the efficiency of the central processing unit cache, although the effects on runtime were not explicitly evaluated for this study.

Modularity can be applied in many places to help extend a generalized stock assessment framework to include new features for alternative model configurations. These model extensions include using alternative sub-models for life history characteristics, adding new observational data types, deploying alternative input and output options, applying different estimation methods, and changing the spatial assessment structure, to name a few. The MAS can handle such future changes because it is programmed by using the C++11 (ISO/IEC 14882:2011) and R (vers. 4.1.2; R Core Team, 2021) languages that provide for flexible and extensible software engineering.

Adhering to a structured software engineering approach also entails the consistent application of 2 important software paradigms, functional programming and OOP. In the MAS prototype, both functional programming and OOP are used to take advantage of their complementary natures. In functional programming, computer program structure is divided into individual modules that are small, encode one functional operation, and are simple to describe. This divide-and-conquer approach to coding facilitates understanding among developers and allows straightforward modification of existing code. Functional programming is a top-down design approach that leads to a software system that is logically divided into modular parts.

In comparison to functional programming, OOP is a software approach in which a model is constructed around objects. Under the OOP paradigm, data are compartmentalized into objects (i.e., data fields or attributes), and the contents and behavior of objects are defined through the declaration of classes (i.e., methods). The primary goal of OOP is to increase the flexibility and maintainability of code by organizing it around objects that represent real-world or conceptual entities. In theory, an object is a software representation of a real-world object. In practice, an object is a runtime state or instance of a class, where a class is a compile-time structure that comprises data and associated operations. Just as with real-world objects of modeling interest like fish or fishing fleets, software objects have state and behavior. For example, an oceanic fish has a state (species, morphological characteristics, and genetic signature) and behavior (feeding, spawning, and avoiding predation).

In the MAS, classes are defined for a variety of assessment system components, including structures for population dynamics, modeling information, spatial data, objective functions, thread management (the coordination and control of multiple independent sequences of execution to optimize performance within a program), output processes, and others. These classes are used to implement system-level concepts that relate object structures and their behaviors in an efficient manner. The MAS is one of a handful of fishery analysis platforms designed to embrace OOP and modular design for software infrastructure. Other platforms that use OOP design features include the FLR framework (Kell

et al., 2007; Fisheries Library in R, available from website), Data-limited Methods Toolkit (Carruthers and Hordyk, 2018; DLMtool, available from website), OSMOSE model (Shin and Cury, 2004; Object-oriented Simulator of Marine Ecosystems, available from website), and Casal2 (Doonan et al., 2016; available from website).

Software infrastructure The development of the MAS is based on a flexible and efficient software infrastructure. Initially, Git (available from website) was used for software version control, and the MAS project was deployed on GitHub. We used the GitHub application system (available from website) for version control, collaboration, hosting, and code distribution. Infrastructure features were important for organizing software development and facilitated the structured construction of the MAS prototype and the associated R package r4MAS (Supernaw et al., 2022).

Our general strategy for building the software infrastructure of the MAS was based on 4 principles of OOP: encapsulation, data abstraction, polymorphism, and inheritance. Encapsulation refers to an object's ability to hide its data attributes and behavior that are not necessary for its user or client process. Encapsulation allows an object's data members and methods to be represented as a single unit (e.g., a Kuan) with protection from client modification. The data (attributes) and the methods (functions or procedures) that operate on the data are bundled into a single unit or class. This concept helps in hiding the internal state of the object and in exposing only a controlled interface. The benefits of encapsulation are protection of data from accidental corruption as well as reduction of the coupling between code fragments. This access control, in turn, provides safeguards for data processing and improves code maintainability.

Data abstraction is the process of hiding the complex software implementation details and showing only the essential features of the object. It helps in reducing complexity and allows a programmer to focus on interactions at a high level. In a fishery stock assessment model, parameters such as growth rates or mortality can be refit by using a bootstrap procedure on the input data, a procedure that resamples the observed data and refits the model to generate new estimates of model parameters. This process can be encapsulated in a method like *refitModel()*, where the user triggers the model fitting procedure with bootstrapped data without needing to manage the underlying resampling logic. Data abstraction is achieved through encapsulation. By using encapsulation, the internal implementation details of a class can be hidden and only the necessary parts are exposed (through public methods). In general, data abstraction simplifies interactions with complex models by providing high-level operations that hide intricate computational processes.

Polymorphism refers to the ability to implement abstract programming entities in multiple ways to extend software features. In the context of OOP, polymorphism is the capacity to provide different kinds of functionality with the same interface. Polymorphism is implemented in the MAS by using template metaprogramming. An example of polymorphism is illustrated in Pseudocode Block 1, with 2 methods of *Evaluate* returning different outputs depending on the type of selectivity class selected by the

Pseudocode Block 1

```
Class SelectivityBase{
public:
        virtual double Evaluate(double age)=0;
};

class LogisticSelectivity : SelectivityBase{
        double a50; //age of 50% selectivity
        double s; //the rate of increase in selectivity at a50

virtual double Evaluate(double age) {
  return (1.0) / ((1.0) + exp(-1.0 + (age - a50) /s))/max_selectivity;
  }
};

class DoubleLogisticSelectivity : SelectivityBase {
        double a50; //age of 50% selectivity
        double alpha_asc; //ascending alpha
        double beta_asc; // ascending beta
        double alpha_desc; // descending alpha
        double beta_desc; // descending beta

virtual double Evaluate(double age) {
  variable a_= 1.0 / (1.0 + exp(-1.0 * (age -alpha_asc)/ beta_asc));
  variable b_ = 1.0 - (1.0 / (1.0 + exp(-1.0 * (age - alpha_desc) / beta_desc)));
  return (a_* b_)/max_selectivity;
```

user, either the logistic (2-parameter model) or the double-logistic (4-parameter model) form of fishery selectivity. This example also demonstrates how polymorphism can streamline the syntax of model specification. Note that, for brevity, the code for calculating *max_selectivity*, the maximum value of unscaled selectivity at age, is not provided in Pseudocode Block 1.

Inheritance in OOP allows new object definitions (children) to be based on existing ones (parents), such that "when a new kind of object class is defined, only those properties that differ from the properties of the specified existing classes need to be declared explicitly, while the other properties are automatically extracted from the existing classes and included in the new class" (Taivalsaari, 1996). An example can be taken from taxonomy. If a parent class *Fish* is defined, a property shared among all fish species (e.g., HasGills and IsAquatic) need not be redefined for the child class *CartilaginousFish* because it inherits these properties from its parent; however, definitions would be needed for properties of cartilaginous fishes (e.g., IsCartilaginous and SwimBladder=FALSE) that are not shared with bony fishes. Through inheritance, the definition and implementation of a new class can be derived from an existing base class, with the newly derived class inheriting attributes from the base class.

Inheritance provides an efficient way to extend the software infrastructure needed to create models with alternative sub-model components. For example, the parent class *SelectivityBase* in Pseudocode Block 1 has 2 child classes, *LogisticSelectivity* and *DoubleLogisticSelectivity*, that inherit the method *Evaluate* for calculation of selectivity values. The inheritance structure used for population dynamics in the MAS prototype (Figs. 1 and 2) includes base classes for fish recruitment, growth, mortality, maturity, selectivity, and a likelihood-based observation model. The child subclasses for modeling population dynamics for growth, recruitment, mortality, maturity, and selectivity have 6, 6, 2, 2, and 4 subclasses, respectively (Figs. 1 and 2). Similarly, the parent class for creating a joint negative log-likelihood function (*Negative-Loglikelihood*) has 5 subclasses corresponding to alternative probability distributions for likelihood components (Fig. 2). Overall, the structured nature of functional programming and the encapsulation, data abstraction, polymorphism, and inheritance aspects of OOP provide powerful tools for building a next-generation assessment platform.

The C++ language is the computational engine for the MAS, a next-generation stock assessment system. The MAS is coded in templated C++. The code is written in pure standard C++11 and is, therefore, portable across operating systems. The MAS is currently compiled with the Analytics Template Library (ATL, available from website) and can also be compiled with Template Model Builder (Kristensen et al., 2016; TMB, available from website). The ATL has several quasi-Newton minimizers available in its template library, and the TMB has R-based minimizers. The MAS is not limited to just these template libraries, and any C++-based optimization library could be used. When the R package r4MAS is used, an objective function can be minimized with any available R minimizer. As for output, the standard function value, parameter values, gradient, and Hessian matrix are captured along with all derived quantities and exported in JavaScript Object Notation or JSON format, which is easily parsed into a list object for output processing in R.

In the MAS, C++ is also used to accommodate flexible OOP structuring (Jana, 2005; Stroustrup, 2013) and to support template metaprogramming. Template metaprogramming is the capacity to construct functions or classes that have the capacity to operate on multiple different object types (e.g., Vandevoorde et al., 2018). Function templates, which are functions that are parameterized so that they represent a family of functions, or other template types, are used to achieve a plug-and-play modularity implemented in C++ code. These templates are based on the concept of functors, or a class object that can be called like a function, providing flexibility in the application of parameter optimization routines. For example, the minimum value functor *ad_min()* is as follows:

```
template <typename T> inline const atl::Variable<T>
ad_min(const atl::Variable<T>& a, const atl::Variable<T>& b, atl::Variable<T> C = 1e-5) { return (a + b - atl::ad_fabs(a - b,C))*0.5; }
```

This functor in the MAS has 3 arguments: the arguments a and b are the data pair being compared to find their minimum value, and the argument C is a small constant used for smoothing.

The functor *ad_min()* eliminates the need for a conditional *if* branch to calculate the minimum value. The lack of a branching statement in *ad_min()*, in turn, allows application of automatic differentiation algorithms (Griewank and Walther, 2008). Automatic differentiation cannot be used to optimize objective functions that include branching statements. This feature of branching avoidance is part of the MAS when used with the ATL or other automatic differentiation systems (e.g., CppAD, available from website). Another benefit of template metaprogramming is being able to plug in different estimation algorithms. For example, the Laplace approximation method can be applied to estimate the marginal likelihood for a state-space assessment model when it is a smooth unimodal function, but a more costly particle filtering method may be needed when the marginal likelihood is not sufficiently smooth (e.g., Auger-Méthé et al., 2021).

Plug-in flexibility is important because the next-generation platform needs to make it possible to formulate assessment models based on either frequentist (Fournier and Archibald, 1982; Methot, 1990; Legault and Restrepo, 1998) or Bayesian (Punt and Hilborn, 1997; Meyer and Millar, 1999) frameworks. This adaptability includes random-effects or mixed-model frameworks (Nielsen and Berg, 2014; Miller et al., 2016), which can be statistically formulated by using either frequentist or Bayesian estimators (e.g., Demidenko, 2004; Auger-Méthé et al., 2021). Overall, the statistical estimation framework needs to be flexible for general assessment applications.

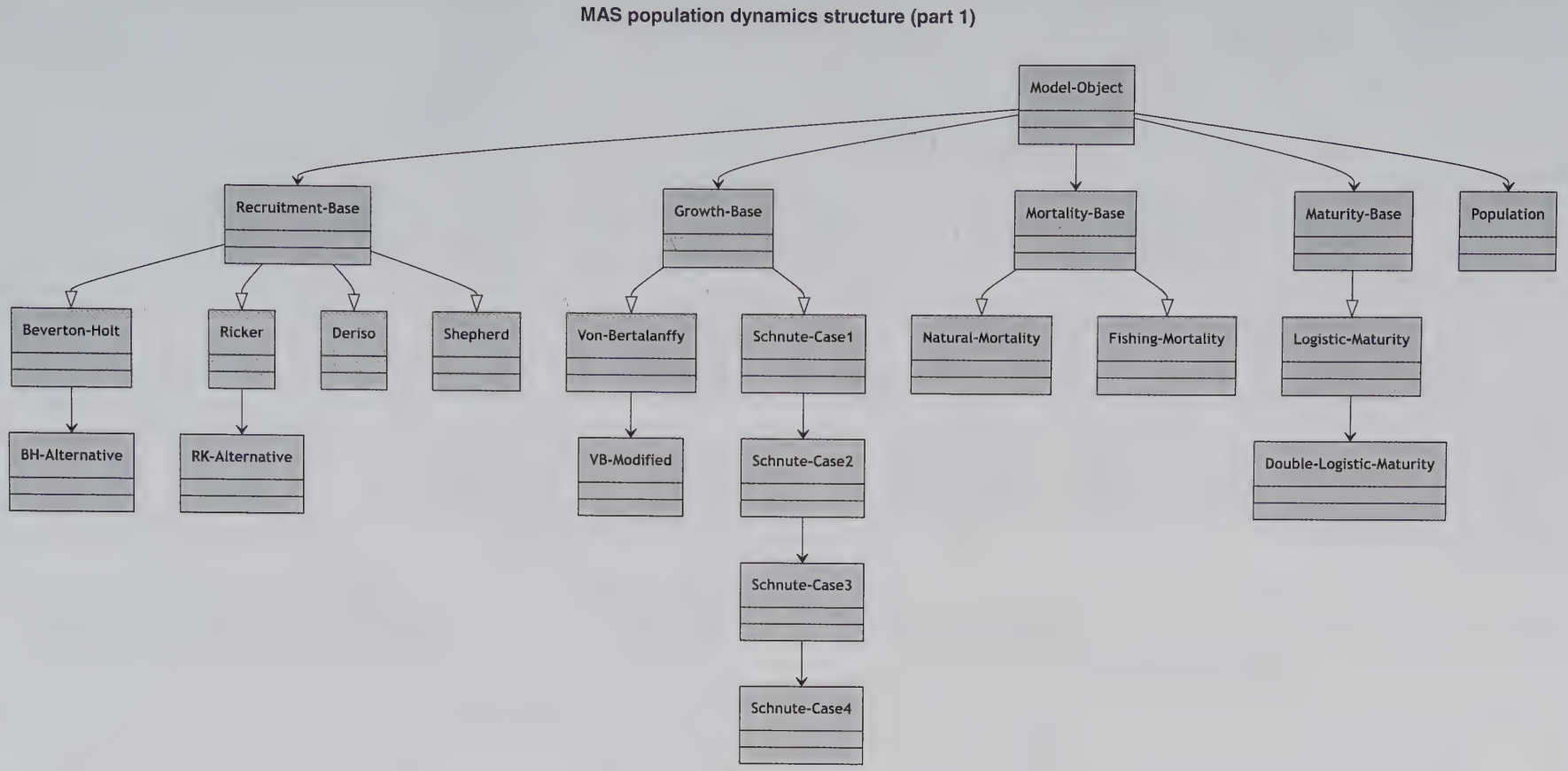

Figure 1

Schematic of some of the parent classes and inheritance structure for population dynamics in the Metapopulation Assessment System (MAS), a next-generation stock assessment modeling platform, including the base classes of Recruitment, Growth, Mortality, Maturity, and Population, along with their child subclasses. For a schematic with the other base classes, Selectivity, Negative-Loglikelihood, Fleet, Survey, Movement, and Information, see Figure 2.

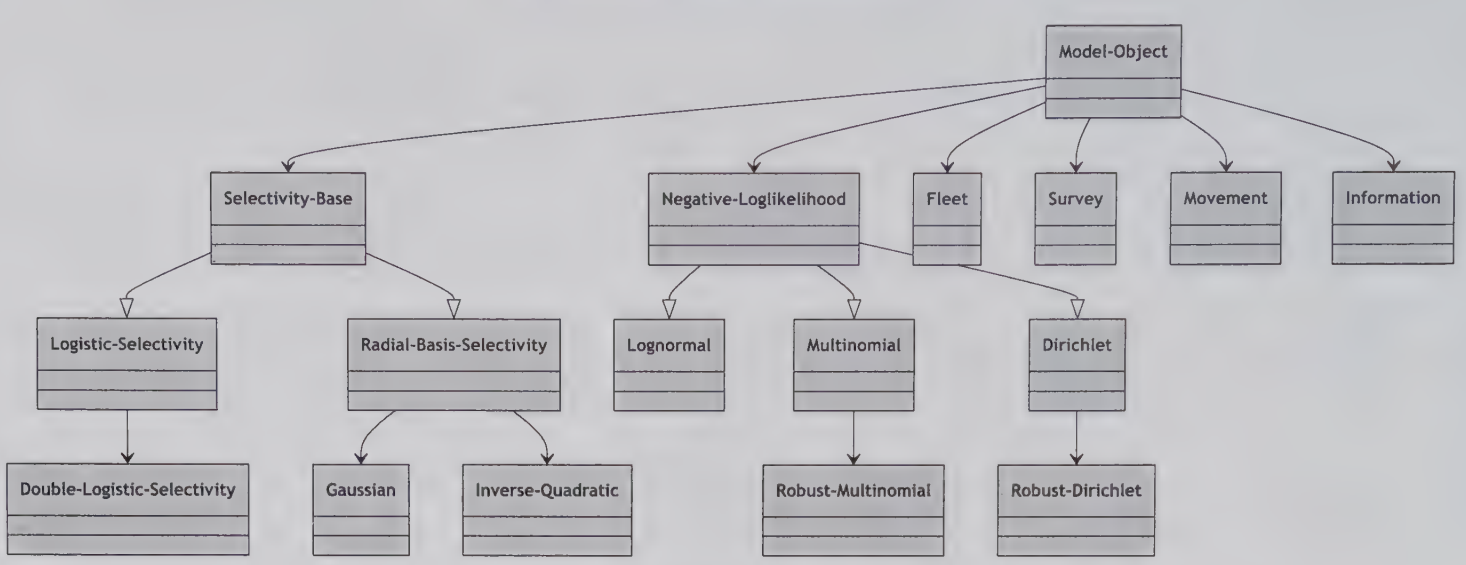

Figure 2

Schematic of some of the parent classes and inheritance structure for population dynamics in the Metapopulation Assessment System (MAS), a next-generation stock assessment modeling platform, including the base classes of Selectivity, Negative-Loglikelihood, Fleet, Survey, Movement, and Information, along with their child subclasses. For a schematic with the other base classes, Recruitment, Growth, Mortality, Maturity, and Population, see Figure 1.

In the MAS, the R language and environment is used to provide an application programming interface that supports interoperability, modifiability, and portability, with numerous extensions. Preprocessing and post-processing of MAS input and output data streams can be efficiently implemented by using the R language and its numerous extensions (Wickham, 2016; Wickham and Grolemund, 2017). The R language promotes the sharing of open-source scientific computing technology because of the dynamic documentation of reproducible numerical calculations and results (Xie, 2015; Xie et al., 2019) and the construction of R packages (Wickham, 2015). The combination of a scientific calculation engine based on the C++ language that can efficiently implement OOP (Stroustrup, 2013) with an interface and calculation engines based on the R language is a key design component for statistical computing (Eubank and Kupresanin, 2011) in a next-generation stock assessment system. This integration can be accomplished with the R package Rcpp (Eddelbuettel, 2013), which is a key tool for integrating the functionality of C++ and R.

Overall, the important components of software infrastructure needed for the design and implementation of the MAS prototype included the following: 1) Git for software version control; 2) GitHub for collaboration, version control, hosting, and organizing work; 3) the C++ language for coding the population dynamics and assessment estimation modeling; 4) the R language for coding the user interface and systematic testing; 5) an optimization template library, such as the ATL; and 6) the Rcpp package to smoothly integrate the functionality of C++ and R. These software infrastructure components are essential for implementing our strategy to build and maintain a next-generation stock assessment platform.

Model uncertainty and ensemble specification

Characterizing uncertainty in assessment model estimates is an important component of a next-generation stock assessment platform. In single-model assessments, characterizing uncertainty has been well addressed with standard methods (Smith et al., 1993; Patterson et al., 2001; Privitera-Johnson and Punt, 2020). However, accounting for structural uncertainties in predictive models is often needed (Peterman, 2004; Jardim et al., 2021; Ducharme-Barth and Vincent, 2022). For example, structural uncertainty about processes that influence spatial population dynamics under climate change is nontrivial because the environmental conditions have not been observed. An ensemble modeling approach may be needed to account for and bound structural uncertainties in spatial dynamics in order to reduce bias through model averaging (e.g., Dormann et al., 2018; Brooks and Brodziak, 2024). As a result, a requirement for any next-generation modeling system is the capacity to precisely specify each component of ensemble models, including different spatial structures as needed to account for structural uncertainties. This capacity includes the functionality to build spatially explicit models with one-to-many, many-to-one, or many-to-many relationships between regions and sub-model components. Overall, any next-generation system should be able to efficiently support spatial ensemble models.

The MAS was designed to support ensemble modeling for spatially explicit assessments, and ensemble modeling may be needed to represent the real-world knowledge base and process uncertainty in stock assessments. Ensemble construction requires identifying trade-offs among alternative model representations and setting the model weights needed to combine modeling results (e.g., Burnham and Anderson, 2002; Jardim et al., 2021). Estimates from an ensemble model should account for both estimation and model structural uncertainty (e.g., Brodziak and Piner, 2010; Ducharme-Barth and Vincent, 2022). Structural uncertainty includes the choice of the spatial structure used to model a fishery system.

For implementation of features, the MAS prototype includes an ensemble engine in C++ that can be used to construct ensemble models through template metaprogramming. Given a set of structural uncertainties, the engine can be used to create the ensemble as a factorial combination of all possible instances of sub-model factor levels or structural forms. For example, if the uncertainties consisted of a growth parameter, such as asymptotic length, and the functional form of an expected stock-recruitment function, the ensemble engine would iterate over all combinations of growth parameter values and recruitment sub-models to construct the members of the ensemble. The engine assigns each ensemble member, or individual assessment model, a unique identifier based on the signature of its sub-model components, automating the ensemble generation process. Each model is run in parallel by using Message Passing Interface (Message Passing Interface Forum, available from website) to decrease evaluation time. Structural uncertainties can also include whether a stock area is represented with a single-region or multiple-subregion model, but a feature that addresses this issue is not currently implemented in the ensemble engine of r4MAS.

Systematic testing

Systematic testing for quality assurance and control is a key to reliable product development. Regular scientific software testing procedures are highly recommended for maintaining functionality and creating new features (Wilson et al., 2014, 2017). For assessment modeling, the development and application of quality assurance entails making good decisions about the types and extent of empirical testing analyses along with ensuring that coverage of the space of plausible observation and process submodels is adequate.

One means to efficiently conduct quality control and assurance tests for the MAS has been to use a software collaboration platform like GitHub. This platform is used for quality control and assurance in the calculation engine written in C++ and for the input and output processing in the r4MAS package, the R language interface for the MAS. For example, we use unit tests to confirm the accuracy of

the Beverton–Holt recruitment module. These tests involve fixing all parameters within the module with known input values and assessing the module's output. Additionally, we have unit tests that verify whether the model estimates parameters when the *estimated* flags are turned on for the Beverton–Holt recruitment module. Furthermore, we conduct integration tests that load all modules of the MAS with predefined input values, comparing the MAS estimates with the expected true values. All the tests are written in R by using the *testthat* framework (Wickham, 2011). In general, it is a recommended practice to be explicit about uncertainty and to quantify it in complex models used for scientific policy analyses (e.g., Brodziak and Link, 2002; National Research Council, 2012). Systematic testing is an important component in the development of the MAS and the r4MAS package, and we illustrate this significance with an example in the next section.

In the rest of this section, we discuss how simulation testing can be used to evaluate how the r4MAS package performs as a stock assessment EM under one iteration of the software development life cycle. In a hypothetical systematic testing iteration, we addressed a hypothetical question about the performance of r4MAS in estimating stock status relative to reference points based on maximum sustainable yield (MSY). What is the relative accuracy of estimates of stock status from the r4MAS package? To illustrate the simulation testing approach, we applied the age-structured OM developed by Li et al. (2021) to evaluate the predictive accuracy of r4MAS as an EM. We used the exact same population simulation model and testing configuration used by Li et al. (2021) to examine estimation accuracy under their scenario for a hypothetical population based on life history traits for bottomfish species in the Atlantic Ocean off the southeastern United States. Model structures and equations of both the OM and the EM are detailed in the Supplementary Materials (online only). In what follows, we briefly describe the analysis approach of Li et al. (2021), the OM and EM, the test cases, and the performance measures for evaluating estimation performance.

Li et al. (2021) developed an age-structured OM to evaluate predictive accuracy and reliability of 4 primary age-structured stock assessment models used in the United States. The EMs for each platform were fitted to simulated data from the OM and the simulation-estimation process was iterated 100 times with time varying recruitment deviations and observation errors (Table 1) (Li et al., 2021). Their goal was to compare how well each EM could estimate key fishery management variables, such as spawning biomass and fishing mortality, relative to biological reference points under different configurations of the OM for the fishery system.

The OM was based on a standard stock assessment configuration for a simple fishery system. It consisted of an age-structured population dynamics model with a plus-group, pooled sexes, and discrete time steps corresponding to a 30-year period. Population dynamics were based on common formulations for an age-structured model of a population harvested by a single fishing fleet and monitored by a single research survey (Suppl. Materials [online only], Suppl. Tables 1–3 [online only]). Biological reference points for producing MSY and the spawning biomass and fishing mortality associated with MSY were evaluated for each iteration of the simulation-estimation process. The EM had the same model structure as the OM and was fitted to the simulated data in each iteration.

Two performance measures were used to quantify the expected estimation accuracy for quantities of interest produced by the EM conditioned on the OM assumptions and simulated data. The first performance measure was the mean over simulations (number of simulations [n]=100) of the median absolute relative error (MARE) for estimation across annual time steps (T=30). The MARE was used to measure the expected magnitude of unsigned errors for output quantities of interest Q as follows:

$$MARE = \frac{1}{T}\left[\sum_{t=1}^{T} \underset{s\in S}{median}\left\{\left|\frac{Q_{\mathrm{MAS},s,t} - Q_{\mathrm{true},s,t}}{Q_{\mathrm{true},s,t}}\right|\right\}\right], \quad (1)$$

where S = the set of simulations per simulation test (n=100);
$Q_{\mathrm{MAS},s,t}$ = the estimate of Q from the MAS in simulation s at time step t; and
$Q_{\mathrm{true},s,t}$ = the true value of Q in simulation s at time step t calculated from the OM.

The second performance measure was the mean of the median relative error (MRE), which provides an index of the expected directional estimation error for quantities of interest Q as follows:

$$MRE = \frac{1}{T}\left[\sum_{t=1}^{T} \underset{s\in S}{median}\left\{\frac{Q_{\mathrm{MAS},s,t} - Q_{\mathrm{true},s,t}}{Q_{\mathrm{true},s,t}}\right\}\right]. \quad (2)$$

These 2 measures of estimation performance are identical to measures used in Li et al. (2021), with MARE and MRE providing measures of the absolute estimation error and expected bias of the MAS estimator. We also calculated the median absolute deviation (MAD) of the MARE values to characterize their precision (Suppl. Table 4) (online only). The MAD for a data set provides a robust measure of the standard deviation of that data set. In our application of MAD, the data set $\underline{x}$ is the set of MARE values for a quantity of interest:

$$MAD(\underline{x}) = \underset{i}{median}\left(\left|x_i - \bar{x}\right|\right), \quad (3)$$

where x_i = the i^{th} MARE value; and
$\bar{x}$ = the average of the set of MARE values.

Two measures of stock status were chosen as quantities of interest for testing the estimation accuracy of the MAS. These were the relative spawning biomass, which is the ratio of spawning biomass to the spawning biomass required to produce MSY, and the relative fishing mortality, or the ratio of fishing mortality to the fishing mortality required to produce MSY. Estimation accuracies for 3 absolute quantities of interest, spawning biomass, recruitment, and fishing mortality, were also calculated for reference (Suppl. Materials) (online only). Overall, the performance

measures indicate that the estimates of relative spawning biomass and relative fishing mortality had the level of accuracy expected for estimates of spawning potential and fishing intensity relative to MSY-based reference points used in analysis of domestic fisheries of the United States.

We used 6 simulation tests to evaluate the estimation performance of the MAS (Table 1). For these evaluations, we used 5 simulation test cases that come directly from Li et al. (2021), with our test cases 1–5 corresponding to their cases 1, 4, 7, 8, and 9 (Li et al., 2021, table 3), and our sixth case was based on a scenario for underreported catch. The test cases for examining the accuracy of estimates of stock status were as follows:

Case 1. The base case
Case 2. The case in which fishing mortality has a pattern like a roller coaster
Case 3. The case with fishing mortality set at a constant high level
Case 4. The case with dome-shaped fishery selectivity
Case 5. The case with an additional research survey
Case 6. The case in which true catch is underreported by 20%

Li et al. (2021) established the base test (case 1), which had one fishing fleet and one survey, with fully selected fishing mortality linearly increasing with time and a time-invariant logistic selectivity function for both the fishing fleet and the survey. Case 1 represents a baseline assessment scenario and the other tests are variants of case 1. Cases 2 and 3 were used to examine the effects of different fishing mortality patterns. In case 2, the fishing mortality pattern linearly increases to a high level and then declines to a low level. In case 3, the fishing mortality pattern is constantly at a high level. Cases 4 and 5 were used to examine how having dome-shaped fishery selectivity or an additional research survey index would affect estimation, respectively. With case 6, we examined the effects of underreported catch biomass by reducing the observed catch biomass to 80% of the true catch biomass simulated in the OM. Therefore, input data for cases 1–5 are unbiased, but case 6 includes biased catch data.

Results

Simulation tests were completed under the scenario for a population simulated on the basis of life history traits, with a value of 0.2 set for the standard deviation of log-scale recruitment, in the same OM used by Li et al. (2021). Results from those tests indicate that the MAS produced adequate estimation accuracy for stock status (Fig. 3). The magnitudes of estimation error were consistently low with MARE values for relative spawning biomass and relative fishing mortality on the order of 5% or less. Cases 1–5 are directly comparable to those in Li et al. (2021), which had similar estimation accuracies under the 4 assessment EMs they examined. The MRE values for cases 1–5 indicate that the estimates of relative spawning biomass and relative fishing mortality were unbiased with interquartile ranges of relative errors from about −5% to about 5% (Fig. 4), similar to what the MARE values for these cases indicate. Results for case 6, with biased catch data, indicate that the magnitude of estimation bias depended on the magnitude of the misreported catch biomass, which for this case was centered at 20% less than the true amount in the OM. The underreporting of catch led to underestimation of the absolute quantities of spawning biomass and recruitment by about 25% or roughly equal to the sum of the 20% underreporting and a baseline MARE

Table 1

Description of the 6 test cases used to evaluate the estimation accuracy of the Metapopulation Assessment System under the scenario of the operating model for a simulated population based on life history traits, with settings for recruitment variability (σ_R), deviations in fishing mortality (F), temporal patterns in F, selectivity patterns, number of surveys, survey coefficient of variation (CV), initial condition, and amount of underreported catch by test case. A dash denotes that the value or information is the same as that given for the base case (case 1). Note that $\emptyset_F$ denotes spawning biomass per recruit at F, $\emptyset_0$ denotes unfished spawning biomass per recruit, and F_{High} denotes F set at a high level.

Description	Case	σ_R	F deviations	F patterns	Selectivity patterns	Number of surveys	Survey CV	Initial condition	Misreported catch
Base case	1	0.2	Same per iteration	Increase[1]	Logistic	1	0.2	$\emptyset_F \neq \emptyset_0$	0%
Pattern in F	2	–	–	Roller coaster[2]	–	–	–	–	–
Time series	3	–	–	F_{High}	–	–	–	–	–
Domed selectivity	4	–	–	–	Double-logistic	–	–	–	–
Additional survey	5	–	–	–	–	2	–	–	–
Underreported catch	6	–	–	–	–	–	–	–	−20%

[1] F linearly increases from 0.01 to 0.40 over the assessment period.
[2] F linearly increases from 0.01 to F_{High} in year 24 and then linearly decreases to a low level (F_{Low}) in year 30, where F_{High} and F_{Low} produce 80% of maximum sustainable yield (MSY) with $F_{High} > F_{MSY}$ (the F that would result eventually in the MSY of a population) and $F_{Low} < F_{MSY}$, as in the yield curve depicted in figure 1 of Li et al. (2021).

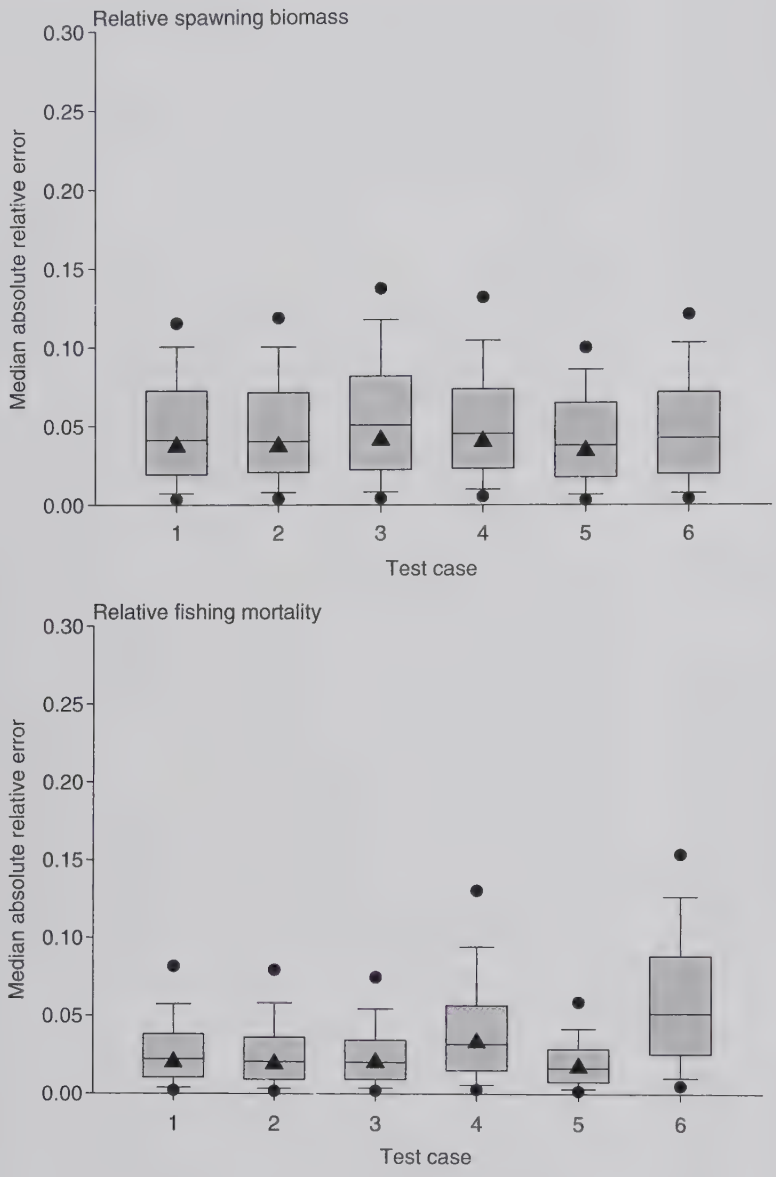

Figure 3

Box plots of the median absolute relative errors (MAREs) for estimation of relative spawning biomass, the ratio of spawning biomass to the spawning biomass required to produce maximum sustainable yield, and relative fishing mortality, the ratio of fishing mortality to the fishing mortality required to produce maximum sustainable yield, with 6 test cases in the Metapopulation Assessment System under the scenario for a simulated population based on life history traits. Case 1, the baseline assessment, involves one fishing fleet and one survey, with fully selected fishing mortality linearly increasing with time and a time-invariant logistic selectivity function for both the fishing fleet and the survey. In case 2, fishing mortality linearly increases to a high level and then declines to a low level. In case 3, fishing mortality is set at a constant high level. For case 4, fishery selectivity is dome shaped. Case 5 has an additional research survey. In case 6, true catch is underreported by 20%. In each box plot, the black line in the middle is the median. The upper and lower parts of each box represent the first and third quartiles (the 25th and 75th percentiles). The black circles indicate the 5th and 95th percentiles. The triangles indicate the minimum MARE values for tests 1–5 reported by Li et al. (2021). The whiskers extend above and below each box no more than 1.5 times the interquartile range.

of about 5% (Suppl. Materials [online only], Suppl. Figs. 1 and 2 [online only]). Overall estimation accuracy appeared adequate for stock status, and the results indicate that the performance of the MAS was similar to that of the 4 assessment platforms compared in Li et al. (2021), given the simulator assumptions and characteristics of the data collected.

Discussion

Lessons learned

We found that modular software infrastructure with good coding practices and model specification capacity increased the extensibility of a prototype for a next-generation stock assessment modeling system. Modularity entails having structured components for input-output processing, model specification and testing, and ensemble model capability. Extensibility means having components that can handle alternative spatiotemporal relations and interactions between populations, fleets, and environmental forcing, as well as having the capacity to reconfigure input data and include new observation types, such as close-kin mark-recapture data (Bravington et al., 2016). In this context, there is probably no single set of best practices to achieve modularity and extensibility, but we believe it is important to strive for the most advanced, yet acceptable software infrastructure to move forward. For the MAS, this goal led us to use GitHub, C++, the R language, and the Rcpp package to build the r4MAS package.

We have demonstrated that it is feasible to build a modeling platform that is based on R and C++ and is modular and fully extensible. For comparison, modularity is a structural feature of the design of AD Model Builder (ADMB) (Fournier et al., 2012), which is the modeling platform used in all the assessment models compared in Li et al. (2021). However, ADMB has limited extensibility because it does not support user-created C++ classes for extending the functionality of the modeling and estimation framework. The ADMB lacks this support because the platform is based on a template programming language that does not allow for additional OOP structuring in C++ (e.g., it does not allow inherited

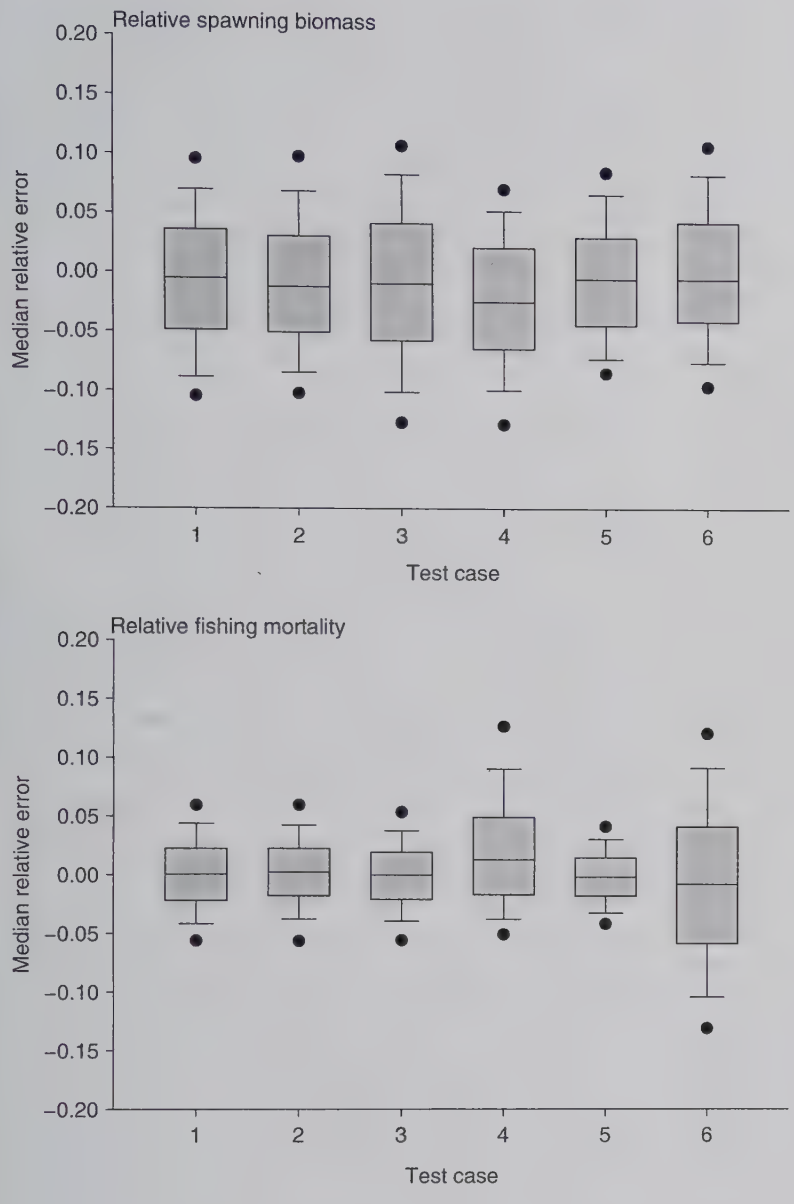

Figure 4

Box plots of the median relative errors (MREs) for estimation of relative spawning biomass, the ratio of spawning biomass to the spawning biomass required to produce maximum sustainable yield, and relative fishing mortality, the ratio of fishing mortality to the fishing mortality required to produce maximum sustainable yield, with 6 test cases in the Metapopulation Assessment System under the scenario for a simulated population based on life history traits. Case 1, the baseline assessment, involves one fishing fleet and one survey, with fully selected fishing mortality linearly increasing with time and a time-invariant logistic selectivity function for both the fishing fleet and the survey. In case 2, fishing mortality linearly increases to a high level and then declines to a low level. In case 3, fishing mortality is set at a constant high level. For case 4, fishery selectivity is dome-shaped. Case 5 has an additional research survey. In case 6, true catch is underreported by 20%. In each box plot, the black line in the middle is the median. The upper and lower parts of each box represent the first and third quartiles (the 25th and 75th percentiles). The black circles indicate the 5th and 95th percentiles. The whiskers extend above and below each box no more than 1.5 times the interquartile range.

or polymorphic objects). Further, ADMB development ended as of March 2024. In contrast, the MAS depends on the ATL, which fully supports C++ extensibility, is not limited by a template programming language requirement, and can be modified to use alternative class structures or optimizers, including neural network optimization.

Systematic testing should cover the range of possible assessment modeling situations, including models that include biased data (i.e., case 6). Testing expected performance of an EM when input data are imprecise or biased is important for characterizing the tradeoffs of alternative EM structures. Under case 6, use of the underreported catch data led to consistent underestimation of absolute quantities of spawning biomass and recruitment (Suppl. Materials [online only], Suppl. Figs. 1 and 2 [online only]) but resulted in reasonably accurate estimates of the scaled quantities of fishing mortality, relative spawning biomass, and relative fishing mortality (Figs. 3 and 4). Overall, simulation tests should strive to evaluate the predictive accuracy over a wide range of expected assessment conditions.

Many of the features and technical requirements for a next-generation system were elucidated in Punt et al. (2020). These insights provide solid technical guidance, but we believe software engineering will also play a key role in building a successful next-generation system. This is because extensibility to incorporate new data or information sources and to adapt to new analytical techniques, or knowledge acquisition models, will be essential for optimizing future assessment system performance. In this context, the r4MAS package makes model setup intuitive and is easy to use, an important user-oriented feature for any next-generation modeling platform.

The MAS project has illustrated the need to adapt the software infrastructure to the expected modeling needs and future requirements. The MAS prototype was designed to employ a mixture of both functional programming and OOP paradigms to produce a modular and extensible software system composed of code in the C++, Rcpp, and R languages. Although the MAS project lacked resources to develop an extensive input-output processing system, such

as the R package r4ss (Taylor et al., 2021; available from website), this functionality would be an ongoing requirement that would be expected to be addressed in the system life cycle. The focus on future extensibility of the MAS aligns with the general point that having a development team with diverse backgrounds and skill sets is important for enhancing creativity, flexibility, and productivity in new product management. In this context, software engineering is a key technical requirement to augment the features emphasized in the most recent workshop on next-generation assessment models (e.g., Hoyle et al.[1]; Punt et al., 2020). Other important software engineering components include object-oriented design, software unit testing requirements, parallel processing capacity, R language interfacing for input and output processing, and long-term extensibility with C++ template metaprogramming, as well as the capacity to efficiently handle ensemble model analyses, apply model averaging, and conduct management strategy evaluations. These engineering components will improve the practical implementation of any next-generation system.

Another lesson learned is that both constancy of purpose and adequate resources will be needed to efficiently produce a next-generation stock assessment modeling platform. This point is evident for the successful and ongoing Stock Synthesis project (Methot and Wetzel, 2013; available from website), which has had adequate resources and funding for student and postdoctoral contributors for many years. In comparison, the MAS project was allocated limited resources and was also affected by staff turnover, loss of institutional knowledge, and competing time commitments. When these limitations were recognized, the NOAA Stock Assessment Improvement Plan was updated to focus on a next-generation assessment system (Lynch et al., 2018). This emphasis on a next-generation platform led to the creation of the Fisheries Integrated Modeling System (FIMS) (FIMS Implementation Team, 2022), the development of which was initiated in 2020. Since then, the MAS prototype has been a research and development pipeline to the FIMS. Resources for the MAS have transitioned to focus solely on FIMS implementation. The FIMS project is developing the next-generation stock assessment platform supported by the National Marine Fisheries Service. To achieve this end, DevOps workflow approaches, such as GitHub, are actively used for the FIMS project—to efficiently build a next-generation assessment system that is agile and responsive to diverse needs of users at the National Marine Fisheries Service and other fisheries agencies. In this context, we emphasize that allocating sufficient resources and maintaining a constancy of purpose will be essential for the ongoing success of the FIMS project.

The technical influence of the MAS on the FIMS is significant in several aspects. Both systems share a foundation in object-oriented inheritance and similar design patterns, facilitating extensible module development and ensuring ease of unit testing. These systems have broad applicability and long-term viability because the principles of portability, maintainability, and extensibility are emphasized. Neither system is tied to a single estimation engine, enhancing their flexibility. Additionally, both systems can be compiled with the ATL and TMB, underlining their robust structural design as modeling frameworks rather than as static models. The interface of the Rcpp package enables seamless integration with R, with the FIMS project adopting a refactored naming convention to maintain an essentially identical interface to the MAS. This interface bridges R with underlying C++ code and reinforces the systems' interoperability and user accessibility.

Both the FIMS and MAS are designed to support complex metapopulation modeling, which includes handling multiple populations, fleets, surveys, and areas and sex differentiation. This capacity is essential for comprehensive fisheries management and assessment. Both systems can execute model runs in parallel, significantly enhancing computational efficiency. In terms of development cycles, the MAS is characterized by a highly agile development approach. The FIMS follows a similar agile method, allowing iterative improvements and rapid adaptation to new requirements. The shared technical characteristics and development philosophies between the MAS and FIMS highlight the substantial influence the MAS has exerted on the design and functionality of the FIMS, making the FIMS a versatile and extensible tool for fisheries modeling and assessment.

Future challenges

In the future, Breiman's (2001) 2 cultures of data modeling and machine learning modeling may need to be combined to produce the best predictive accuracy for integrated stock assessment models. This approach would contrast with the long-term fisheries modeling practice of deploying only statistical models to characterize the likelihood of observed data in stock assessment applications. The number of potential applications of machine learning models to directly support and inform fisheries stock assessments is increasing as automated data collection and the sizes of data sets on marine communities and environments increase (Malde et al., 2020). More frequent applications of machine learning for stock assessments can be expected. Such models have produced accurate predictions without explicit structure for species identification, discard estimation, and characterization of size composition (Beyan and Browman, 2020). Recent applications of machine learning for components of a next-generation assessment system include forecasting recruitment—an essential component of future stock projections (Smoliński, 2019); estimating natural mortality rates—a key life history parameter for age-structured stock assessments (Liu et al., 2020); and setting relative biomass prior distributions for the catch-only CMSY++ assessment model (Froese et al., 2023). Although there is no certainty about the future needs for stock assessment modeling, an important future challenge is to ensure that any next-generation assessment platform can be extended to incorporate data and assessment model

inputs produced by machine learning algorithms in an appropriate integrated estimation framework.

In recent years, it has become evident that the capacity to do ensemble modeling is likely important for structuring a next-generation assessment system (e.g., Lynch et al., 2018). Providing this capacity represents a major challenge given the multiplicity of assessment model structures that are consistent with typical observed data and knowledge for a fishery system. Ensemble model and multi-model inference are practical tools for implementing ecosystem-based fishery management in the face of uncertain system dynamics. An ongoing challenge will be to represent the fishery system with parsimonious but representative structures that address the trade-offs between the bias and variance of individual model results and the covariances between model results when combined to make ensemble model assessments and projections.

Some of the challenges we encountered in building a prototype of a next-generation modeling system naturally led to some unresolved issues. How to produce an analytical system whose components are maintainable and extensible and yet as low-cost and efficient as possible? To address this issue, the C++ language was used for coding the calculation engine and the R language was used for coding the system interface. How to incorporate diverse approaches for assessment model structure and stock status determination conditioned on available information on fishery systems ranging from data limited to data rich? We addressed this challenge by using template metaprogramming to produce a modular and extensible assessment system. How to ensure that diverse model structures and outputs are reproducible, well-documented, and transparent to support reliable scientific computing and open science practices for stock assessments (Lowndes et al., 2017; Wilson et al., 2017; Ramachandran et al., 2021). To address this issue, we used GitHub to provide version control and to archive source code and analytical approaches. These challenges underscore the point that any engineering strategy for building a next-generation system needs to be adaptive and will continually evolve.

Conclusions

In summary, our proposed engineering strategy includes specifications for the software life cycle, engineering, and infrastructure design needed to support a spatially explicit, next-generation stock assessment system, the MAS. Software infrastructure was designed by using OOP principles of encapsulation, data abstraction, polymorphism, and inheritance. Three primary components were used to implement the software infrastructure: GitHub for collaboration, version control, and code organization; the C++ language for coding fishery system dynamics and estimation modeling; and the R language for coding the input-output interface and systematic testing. Systematic testing was a key strategic element for iterative improvement under the life cycle of this next-generation stock assessment modeling platform.

Resumen

Los procesos ambientales y antropogénicos han provocado cambios generalizados en la productividad y la distribución espacial de los recursos pesqueros marinos. A medida que cambien las distribuciones geográficas de las poblaciones de peces y, por consiguiente, de las flotas pesqueras, será necesario mejorar los datos espaciotemporales y la modelación espacial para estimar la abundancia y la productividad. El objetivo de este artículo es proponer una estrategia para diseñar una plataforma de modelación espacialmente explícita para modelos de nueva generación para evaluación de poblaciones. Presentamos nuestro enfoque para desarrollar un prototipo de sistema, el Sistema de Evaluación de Metapoblaciones (MAS), que es fácil de usar, modular y extensible. El prototipo MAS se diseñó para dar soporte a modelos metapoblacionales complejos, que incluyen el manejo de múltiples poblaciones, áreas, flotas, prospecciones, así como la diferenciación de sexos. Describimos los componentes del ciclo de vida del software, la ingeniería y el diseño de la infraestructura para dar soporte a un sistema de nueva generación para la evaluación espacialmente explícita de poblaciones. La infraestructura de software se diseñó e implementó con 3 componentes: GitHub para la colaboración, el control de versiones y la organización del código; el lenguaje C ++ para codificar la dinámica del sistema pesquero y modelado de estimadores; y el lenguaje R para codificar la interfaz de entrada-salida y las pruebas sistemáticas. Las pruebas sistemáticas fueron un componente clave del ciclo de vida de desarrollo del MAS y se aplicaron para garantizar que los requisitos del sistema, como la estimación precisa de las cantidades de interés, se implementaran con éxito. Concluimos con la discusión de algunas lecciones aprendidas y futuros retos para los esfuerzos en curso para implementar una plataforma de evaluación de poblaciones de nueva generación.

Acknowledgments

We thank C. Porch, K. Shertzer, P. Lynch, and R. Methot for their insights and helpful discussions on the MAS project. For this research, no specific grants were received from funding agencies in the public, commercial, or not-for-profit sectors.

Literature cited

Auger-Méthé, M., K. Newman, D. Cole, F. Empacher, R. Gryba, A. A. King, V. Leos-Barajas, J. M. Flemming, A. Nielsen, G. Petris, et al.
2021. A guide to state–space modeling of ecological time series. Ecol. Monogr. 91(4):e01470.

Berger, A. M., D. R. Goethel, and P. D. Lynch.
2017 Introduction to "Space oddity: recent advances incorporating spatial processes in the fishery stock assessment and management interface." Can. J. Fish. Aquat. Sci. 74:1693–1697.

Beyan, C., and H. I. Browman.
2020. Setting the stage for the machine intelligence era in marine science. ICES J. Mar. Sci. 77:1267–1273.
Bravington, M. V., H. J. Skaug, and E. C. Anderson.
2016. Close-kin mark-recapture. Stat. Sci. 31:259–274.
Breiman, L.
2001. Statistical modeling: the two cultures. Stat. Sci. 16:199–231.
Brodziak, J., and J. Link.
2002. Ecosystem-based fishery management: what is it and how can we do it? Bull. Mar. Sci. 70:589–611.
Brodziak, J., and K. Piner.
2010. Model averaging and probable status of North Pacific striped marlin, *Tetrapturus audax*. Can. J. Fish. Aquat. Sci. 67:793–805.
Brodziak, J., M. Supernaw, and C. Porch.
2014. Object-oriented design of MAS, a metapopulation assessment system. 144th American Fisheries Society Annual Meeting; Quebec City, 17–21 August. Am. Fish. Soc., Bethesda, MD. [Abstract.] [Available from website.]
Brodziak, J., T. A'mar, and M. Supernaw.
2017. Designing a general MSE framework for a movement-based metapopulation assessment system. 147th American Fisheries Society Annual Meeting; Tampa, 18–24 August. Am. Fish. Soc., Bethesda, MD. [Abstract.] [Available from website.]
Brooks, E. N., and J. K. T. Brodziak.
2024. Simulation testing performance of ensemble models when catch data are underreported. ICES J. Mar. Sci. 81:1053–1072.
Burnham, K. P., and D. R. Anderson.
2002. Model selection and multimodel inference: a practical information-theoretic approach, 2nd ed., 488 p. Springer, New York.
Carruthers, T. R., and A. R. Hordyk.
2018. The data-limited methods toolkit (DLMtool): an R package for informing management of data-limited populations. Methods Ecol. Evol. 9:2388–2395.
Cheung, W. W. L., R. Watson, and D. Pauly.
2013. Signature of ocean warming in global fisheries catch. Nature 497:365–368.
Demidenko, E.
2004. Mixed models: theory and application, 704 p. John Wiley & Sons, Hoboken, NJ.
Deming, W. E.
1982. Out of the crisis, 507 p. MIT Press, Cambridge, MA.
Doonan, I., K. Large, A. Dunn, S. Rasmussen, C. Marsh, and S. Mormede.
2016. Casal2: New Zealand's integrated population modelling tool. Fish. Res. 183:498–505.
Dormann, C. F., J. M. Calabrese, G. Guillera-Arroita, E. Matechou, V. Bahn, K. Bartoń, C. M. Beale, S. Ciuti, J. Elith, K. Gerstner, et al.
2018. Model averaging in ecology: a review of Bayesian, information-theoretic, and tactical approaches for predictive inference. Ecol. Monogr. 88:485–504.
Ducharme-Barth, N. D., and M. T. Vincent.
2022. Focusing on the front end: a framework for incorporating uncertainty in biological parameters in model ensembles of integrated stock assessments. Fish. Res. 255:106452.
Eddelbuettel, D.
2013. Seamless R and C++ integration with Rcpp, 220 p. Springer, New York.
Eubank, R. L, and A. Kupresanin.
2011. Statistical computing in C++ and R, 540 p. CRC Press, Boca Raton, FL.
FIMS Implementation Team.
2022. NOAA-FIMS: the NOAA Fisheries Integrated Modeling System. R package, vers. 0.0.0.9000. [Available from website.]
Fournier, D., and C. P. Archibald.
1982. A general theory for analyzing catch at age data. Can. J. Fish. Aquat. Sci. 39:1195–1207.
Fournier, D. A., H. J. Skaug, J. Ancheta, J. Ianelli, A. Magnusson, M. N. Maunder, A. Nielsen, and J. Sibert.
2012. AD Model Builder: using automatic differentiation for statistical inference of highly parameterized complex nonlinear models. Optim. Methods Softw. 27:233–249.
Free, C. M., J. T. Thorson, M. L. Pinsky, K. L. Oken, J. Wiedenmann, and O. P. Jensen.
2019. Impacts of historical warming on marine fisheries production. Science 363:979–983.
Froese, R., H. Winker, G. Coro, M.-L. D. Palomares, A. C. Tsikliras, D. Dimarchopoulou, K. Touloumis, N. Demirel, G. M. S. Vianna, G. Scarcella, et al.
2023. New developments in the analysis of catch time series as the basis for fish stock assessments: the CMSY++ method. Acta Ichthyol. Piscat. 53:173–189.
Griewank, A., and A. Walther.
2008. Evaluating derivatives: principles and techniques of algorithmic differentiation, 2nd ed., 438 p. Soc. Ind. Appl. Math., Philadelphia, PA.
Gullestad, P., S. Sundby, and O. S. Kjesbu.
2020. Management of transboundary and straddling fish stocks in the Northeast Atlantic in view of climate-induced shifts in spatial distribution. Fish Fish. 21:1008–1026.
Jana, D.
2005. C++ and object-oriented programming paradigm, 2nd ed., 531 p. Raj Press, New Delhi, India.
Jardim, E., M. Azevedo, J. Brodziak, E. N. Brooks, K. F. Johnson, N. Klibansky, C. P. Millar, C. Minto, I. Mosqueira, R. D. M. Nash, et al.
2021. Operationalizing ensemble models for scientific advice to fisheries management. ICES J. Mar Sci. 78: 1209–1216.
Kell, L. T., I. Mosqueira, P. Grosjean, J.-M. Fromentin, D. Garcia, R. Hillary, E. Jardim, S. Mardle, M. A. Pastoors, J. J. Poos, et al.
2007. FLR: an open-source framework for the evaluation and development of management strategies. ICES J. Mar. Sci. 64:640–646.
Koenigstein, S., F. C. Mark, S. Gößling-Reisemann, H. Reuter, and H.-O. Poertner.
2016. Modelling climate change impacts on marine fish populations: process-based integration of ocean warming, acidification and other environmental drivers. Fish Fish. 17:972–1004.
Kristensen, K., A. Nielsen, C. W. Berg, H. Skaug, and B. M. Bell.
2016. TMB: automatic differentiation and Laplace approximation. J. Stat. Softw. 70(5):1–21.
Laplante, P. A. (ed.).
2001. Comprehensive dictionary of computer science, engineering and technology, 560 p. CRC Press, Boca Raton, FL.
Legault, C. M., and V. R. Restrepo.
1998. A flexible forward age-structured assessment program. Collect. Vol. Sci. Pap. ICCAT 49:246–253.
Li, B., K. W. Shertzer, P. D. Lynch, J. N. Ianelli, C. M. Legault, E. H. Williams, R. D. Methot Jr., E. N. Brooks, J. J. Deroba, A. M. Berger, et al.
2021. A comparison of 4 primary age-structured stock assessment models used in the United States. Fish. Bull. 119:149–167.

Liu, C., S. Zhou, Y.-G. Wang, and Z. Hu.
2020. Natural mortality estimation using tree-based ensemble learning models. ICES J. Mar. Sci. 77:1414–1426.
Lowndes, J. S. S., B. D. Best, C. Scarborough, J. C. Afflerbach, M. R. Frazier, C. C. O'Hara, N. Jiang, and B. S. Halpern.
2017. Our path to better science in less time using open data science tools. Nat. Ecol. Evol. 1:0160.
Lynch, P. D., R. D. Methot, and J. S. Link (eds.).
2018. Implementing a next generation stock assessment enterprise. An update to the NOAA Fisheries Stock Assessment Improvement Plan. NOAA Tech. Memo. NMFS-F/SPO-183, 127 p.
Malde, K., N. O. Handegard, L. Eikvil, and A.-B. Salberg.
2020. Machine intelligence and the data-driven future of marine science. ICES J. Mar. Sci. 77:1274–1285.
Martin, R. C.
2009. Clean code: a handbook of agile software craftsmanship, 431 p. Pearson Educ., Boston, MA.
Maureaud, A. A., R. Frelat, L. Pécuchet, N. Shackell, B. Mérigot, M. L. Pinksy, K. Amador, S. C. Anderson, A. Arkhipkin, A. Auber, et al.
2021. Are we ready to track climate-driven shifts in marine species across international boundaries? - A global survey of scientific bottom trawl data. Global Change Biol. 27:220–236.
Methot, R. D.
1990. Synthesis model: an adaptable framework for analysis of diverse stock assessment data. Int. North Pac. Fish. Comm. Bull. 50:259–277.
Methot, R. D., Jr., and C. R. Wetzel.
2013. Stock synthesis: a biological and statistical framework for fish stock assessment and fishery management. Fish. Res. 142:86–99.
Meyer, R., and R. B. Millar.
1999. BUGS in Bayesian stock assessments. Can. J. Fish. Aquat. Sci. 56:1078–1087.
Miller, T. J., J. A. Hare, and L. A. Alade.
2016. A state-space approach to incorporating environmental effects on recruitment in an age-structured assessment model with an application to southern New England yellowtail flounder. Can. J. Fish. Aquat. Sci. 73:1261–1270.
National Research Council.
2012. Assessing the reliability of complex models: mathematical and statistical foundations of verification, validation, and uncertainty quantification, 106 p. Natl. Acad. Press, Washington, DC. [Available from website.]
Nielsen, A., and C. W. Berg.
2014. Estimation of time-varying selectivity in stock assessments using state-space models. Fish. Res. 158:96–101.
Palacios-Abrantes, J., S. Crosson, C. Dumas, R. Fujita, A. Levine, C. Longo, and O. P. Jensen.
2023. Quantifying fish range shifts across poorly defined management boundaries. PLoS ONE 18(1):e0279025.
Patterson, K., R. Cook, C. Darby, S. Gavaris, L. Kell, P. Lewy, B. Mesnil, A. Punt, V. Restrepo, D. W. Skagen, and G. Stefánsson.
2001. Estimating uncertainty in fish stock assessment and forecasting. Fish Fish. 2:125–157.
Perry, A. L., P. J. Low, J. R. Ellis, and J. D. Reynolds.
2005. Climate change and distribution shifts in marine fishes. Science 308:1912–1915.
Peterman, R. M.
2004. Possible solutions to some challenges facing fisheries scientists and managers. ICES J. Mar. Sci. 61:1331–1343.
Pinsky, M. L., R. L. Selden, and Z. J. Kitchel.
2020. Climate-driven shifts in marine species ranges: scaling from organisms to communities. Annu. Rev. Mar. Sci. 12:153–179.
Privitera-Johnson, K. M., and A. E. Punt.
2020. A review of approaches to quantifying uncertainty in fisheries stock assessments. Fish. Res. 226:105503.
Punt, A. E.
2019. Spatial stock assessment methods: a viewpoint on current issues and assumptions. Fish. Res. 213:132–143.
Punt, A. E., and R. Hilborn.
1997. Fisheries stock assessment and decision analysis: the Bayesian approach. Rev. Fish Biol. Fish. 7:35–63.
Punt, A. E., A. Dunn, B. Elvarsson, J. Hampton, S. D. Hoyle, M. N. Maunder, R. D. Methot, and A. Nielsen.
2020. Essential features of the next-generation integrated fisheries stock assessment package: a perspective. Fish. Res. 229:105617.
R Core Team.
2021. R: a language and environment for statistical computing. R Foundation for Statistical Computing, Vienna, Austria. [Available from website, accessed November 2021].
Ramachandran, R., K. Bugbee, and K. Murphy.
2021. From open data to open science. Earth Space Sci. 8:e2020EA001562.
Shin, Y.-J., and P. Cury.
2004. Using an individual-based model of fish assemblages to study the response of size spectra to changes in fishing. Can. J. Fish. Aquat. Sci. 61:414–431.
Smith, S. J., J. J. Hunt, and D. Rivard (eds.).
1993. Risk evaluation and biological reference points for fisheries management. Can. Spec. Publ. Fish. Aquat. Sci. 120, 436 p.
Smoliński, S.
2019. Incorporation of optimal environmental signals in the prediction of fish recruitment using random forest algorithms. Can. J. Fish. Aquat. Sci. 76:15–27.
Stroustrup, B.
2013. The C++ programming language, 4th ed., 1346 p. Addison-Wesley, Boston, MA.
Supernaw, M., C. Stawitz, and B. Li.
2022. r4MAS: read and write input and output for MAS model. R package. [Available from website.]
Taivalsaari, A.
1996. On the notion of inheritance. ACM Comput. Surveys 28:438–479.
Taylor, I. G., K. L. Doering, K. F. Johnson, C. R. Wetzel, and I. J. Stewart.
2021. Beyond visualizing catch-at-age models: lessons learned from the r4ss package about software to support stock assessments. Fish. Res. 239:105924.
Waterhouse, L., D. B. Sampson, M. Maunder, and B. X. Semmens.
2014. Using areas-as-fleets selectivity to model spatial fishing: asymptotic curves are unlikely under equilibrium conditions. Fish. Res. 158:15–25.
Wickham, H.
2011. testthat: get started with testing. R J. 3(2):5–10.
2015. R packages: organize, test, document, and share your code, 182 p. O'Reilly Media, Sebastopol, CA.
2016. ggplot2: elegant graphics for data analysis, 2nd ed., 260 p. Springer, New York.
Wickham, H., and G. Grolemund.
2017. R for data science: import, tidy, transform, visualize, and model data, 492 p. O'Reilly Media, Sebastopol, CA.

Wilson, G., D. A. Aruliah, C. T. Brown, N. P. Chue Hong, M. Davis, R. T. Guy, S. H. D. Haddock, K. D. Huff, I. M. Mitchell, M. D. Plumbley, et al.
2014. Best practices for scientific computing. PLoS Biol. 12(1):e1001745.

Wilson, G., J. Bryan, K. Cranston, J. Kitzes, L. Nederbragt, and T. K. Teal.
2017. Good enough practices in scientific computing. PLoS Comput. Biol. 13(6):e1005510.

Xie, Y.
2015. Dynamic documents with R and knitr, 2nd ed., 294 p. CRC Press, Boca Rotan, FL.

Xie, Y., J. J. Allaire, and G. Grolemund.
2019. R markdown: the definitive guide, 303 p. CRC Press, Boca Rotan, FL.

Vandevoorde, D., N. M. Josuttis, and D. Gregor.
2018. C++ templates: the complete guide, 2nd ed., 788 p. Addison-Wesley, New York.

National Marine Fisheries Service
NOAA

Fishery Bulletin
established in 1881

Spencer F. Baird
First U.S. Commissioner of Fisheries and founder of *Fishery Bulletin*

The structure of the larval fish assemblage of Massachusetts Bay in 2008–2012 and 2015–2022

Paul Geoghegan (contact author)[1]
Michael D. Murphy[1]
Maureen Madray[1]
M. Conor McManus[2]
Eric Nestler[1]
Ann E. Pembroke[1]

Email address for contact author: pgeoghegan@normandeau.com

[1] Normandeau Associates
25 Nashua Road
Bedford, New Hampshire 03110

[2] Northeast Fisheries Science Center
National Marine Fisheries Service, NOAA
28 Tarzwell Drive
Narragansett, Rhode Island 02882

Abstract—Ichthyoplankton samples were collected monthly at 2 stations in Massachusetts Bay from 2008 to 2012 and from 2015 to 2022 to characterize the larval fish assemblage for this area. The fauna was composed of 2 major assemblages that were 87% dissimilar from each other and associated with season and water temperature. A cold-water assemblage of low density (43.26 larvae/1000 m^3) occurred from November through May at mean water column temperatures between 4.1°C and 10.3°C, with sand lances (*Ammodytes* spp.) the dominant taxon as a group. A warmwater assemblage of higher density (432.58 larvae/1000 m^3) occurred from June through October at mean water column temperatures between 12.3°C and 16.1°C, with the silver hake (*Merluccius bilinearis*) the dominant taxon. Within the cold-water assemblage, statistically distinct groups occurred in November, December–March, and April–May. The Atlantic herring (*Clupea harengus*), sand lances, and the American plaice (*Hippoglossoides platessoides*) were the dominant taxa in those periods, respectively. Within the warmwater assemblage, statistically distinct groups occurred in June–August and September–October, with the cunner (*Tautogolabrus adspersus*) and true hakes as a group (*Urophycis* spp.) the dominant taxa in those periods, respectively. Water temperature explained 28% of the annual variation in the cold-water assemblage, and there was no significant relationship between temperature and annual variation in the warmwater assemblage. This larval fish characterization provides a baseline against which potential changes in the assemblages in this area can be measured.

Manuscript submitted 10 September 2024.
Manuscript accepted 24 February 2025.
Fish. Bull. 123:105–118 (2025).
Online publication date: 10 March 2025.
doi: 10.7755/FB.123.2.3

The views and opinions expressed or implied in this article are those of the author (or authors) and do not necessarily reflect the position of the National Marine Fisheries Service, NOAA.

Sampling the early life stages of fish can further our understanding of changes in variability in fish stock sizes and catch (Llopiz et al., 2014), as well as provide a characterization of baseline conditions for environmental assessments. Such data are often used to characterize areas that may be important in supporting fish stocks by providing habitats for fish eggs and larvae. Long-term datasets are preferable because data can be integrated over time and the influence of a few potentially anomalous years or seasons (i.e., interannual variability) can be minimized. Long-term monitoring programs also provide the data necessary for resource management and for descriptions of population abundance and community composition on both temporal and spatial scales (McClatchie et al., 2014). Data from a monitoring program with intensive temporal sampling can be used to accurately describe changes over time in the region sampled and provide an important benchmark against which potential changes can be measured.

Regional ichthyoplankton sampling in the continental shelf system of the northeastern United States has been conducted since the 1970s to understand broad-scale changes in the system's oceanography and plankton community. The Marine Resources Monitoring, Assessment, and Prediction Program and the Ecosystem Monitoring (EcoMon) program, both of the National Marine Fisheries Service, have provided valuable data on the seasonality and species composition of the larval fish assemblage on the northeastern U.S. shelf and in the Gulf of Maine. Using these data, Walsh et al. (2015) found that some fish larval distributions in the Gulf of Maine and Georges Bank shifted to offshore and shallower regions. Although these data are valuable in understanding the broad, long-term changes in the larval fish assemblage in this area, the spatiotemporal sampling frequencies of the surveys of these programs do not provide the fine-scale sampling frequency needed to understand local seasonal (or temporal) changes in the larval fish assemblage of Massachusetts Bay.

Sampling at a spatial scale finer than those of these programs has occurred in the larger Gulf of Maine system. Runge and Jones (2012) sampled 2 stations in Massachusetts Bay, 1 station

in Ipswich Bay, and 4 nearby stations off the coasts of New Hampshire and southern Maine, usually 3 times per month in 2007 and 2008. The ichthyoplankton of Cape Cod Bay was monitored monthly from 1974 to 1976 as part of the Pilgrim Power Station monitoring program (Scherer, 1984). Chenoweth (1973), Townsend (1983, 1984), and Lazzari (2001) reported on the ichthyoplankton assemblages in inshore areas along the coast of Maine north and east of Massachusetts Bay. However, despite their finer scale, these examinations did not produce time series necessary to understand local seasonal changes in the larval fish assemblage of Massachusetts Bay.

We conducted ichthyoplankton monitoring monthly from 2008 to 2012 and from 2015 to 2022 to assess the potential effects of the operation of an offshore liquified natural gas regasification facility in Massachusetts Bay. Data from this program, collected over 13 years at a level of temporal detail not previously available, provide a description of the seasonality and structure of the larval fish assemblage in Massachusetts Bay at the start of the 21st century.

Materials and methods

Field procedures

Ichthyoplankton sampling was conducted in the central part of Massachusetts Bay about 22 km south of Gloucester, Massachusetts, and about 30 km east of Boston, Massachusetts, at 2 stations for 13 years from 2008 to 2012 and from 2015 to 2022 (Fig. 1, Suppl. Table 1 [online only]). Massachusetts Bay is an embayment of the western Gulf of Maine, generally south of Gloucester and west of Stellwagen Bank. To the south, Massachusetts Bay merges into Cape Cod Bay. There is a weak counterclockwise flow in Massachusetts Bay with a residence time for surface water of 20–45 d (Geyer et al., 1992). The water column is usually stratified from April through October and well-mixed in the winter (Leo et al.[1]). The maximum depth in Massachusetts Bay is about 90 m in Stellwagen Basin.

From 2008 to 2012, sampling was typically conducted twice per month. From 2015 to 2022, sampling typically occurred twice per month in January, February, and December and once per month from March through November. On each sampling date, 3 samples were collected during both night and day; night was defined as more than 2 h after sunset to more than 2 h before sunrise and day was defined as more than 2 h after sunrise to more than 2 h before sunset. Generally, 6 samples were collected on each sampling date (3 samples in each of 2 periods). Each sample consisted of an oblique tow through the water column from near bottom to the surface with a target volume of 1000 m^3. The collection gear was a conical ring net equipped with a calibrated flowmeter. The net had a mesh size of 0.33 mm and a diameter of 1.0 m at the mouth, with a 4:1 ratio of length to mouth opening. Equipped with a swivel and a depressor hanging from the swivel, the net was towed off the stern quarter of the boat with a bridle in front of the net. Flowmeter readings before and after deployment were recorded to estimate the volume of water filtered by the net. Samples were preserved in 5%–10% buffered formalin for later identification of organisms. Coincident with ichthyoplankton sampling, water depth was recorded and temperature data were collected at depths of <0.5 m (surface), 0.5–2.5 m (near surface), 9.0–16.0 m (mid-depth), and 18.0–24.0 m (near bottom).

Laboratory procedures

All larvae were identified to the lowest practical taxon, usually to species, and enumerated. Primary references used for identifications were Jones et al. (1978), Elliott and Jimenez (1981), Richards (2005), and Fahay (2007). Because of morphometric similarities, some taxa were grouped to genus. Red hake (*Urophycis chuss*), white hake (*U. tenuis*), and spotted hake (*U. regia*) were grouped together as true hakes (*Urophycis* spp.). Similarly, American sand lance (*Ammodytes americanus*) and northern sand lance (*A. dubius*) were grouped as sand lances (*Ammodytes* spp.). Nomenclature followed Page et al. (2023), and a list of the taxa used, with common and scientific names and months of occurrence, is presented in Supplementary Table 2 (online only).

For taxa with clearly defined developmental stages, individuals were assigned to the appropriate life stage, such as egg, yolk-sac larvae, post-yolk-sac larvae, young of the year, and yearling or older. Yolk-sac and post-yolk-sac larvae were the focus of our analysis for this study and hereafter are referred to as *larvae*. Yolk-sac larvae ranged from hatchlings to individuals with a complete and functional digestive system. Post-yolk-sac larvae included individuals after the yolk sac stage up to transformation to the young-of-the-year form, which included a full complement of fin rays.

For quality control, 10% of samples (randomly selected out of batches of 10 samples) were reexamined to ensure that a minimum of 95% of the ichthyoplankton individuals were removed. For taxonomic quality control, a randomly selected 10% of samples were reanalyzed by a senior taxonomist to ensure a minimum taxonomic efficiency of 95%. Data quality control followed procedures in Geoghegan (1996). Data were subject to univariate and multivariate error checking routines and then audited against original field and laboratory data sheets.

Data analysis

Temporal patterns in the overall composition of larval fish assemblages in the sampling area were examined through multivariate analyses performed by using functions

[1] Leo, W., R. Geyer, and M. Mickelson. 2003. Physical and biological oceanography of Massachusetts Bay. *In* Briefing for OMSAP workshop on ambient monitoring revisions, June 18–19, 2003. Environ. Qual. Dep. Rep. 2003-ms-085, p. 4-1–4-21. Mass. Water Resources Auth., Boston, MA. [Available from website.]

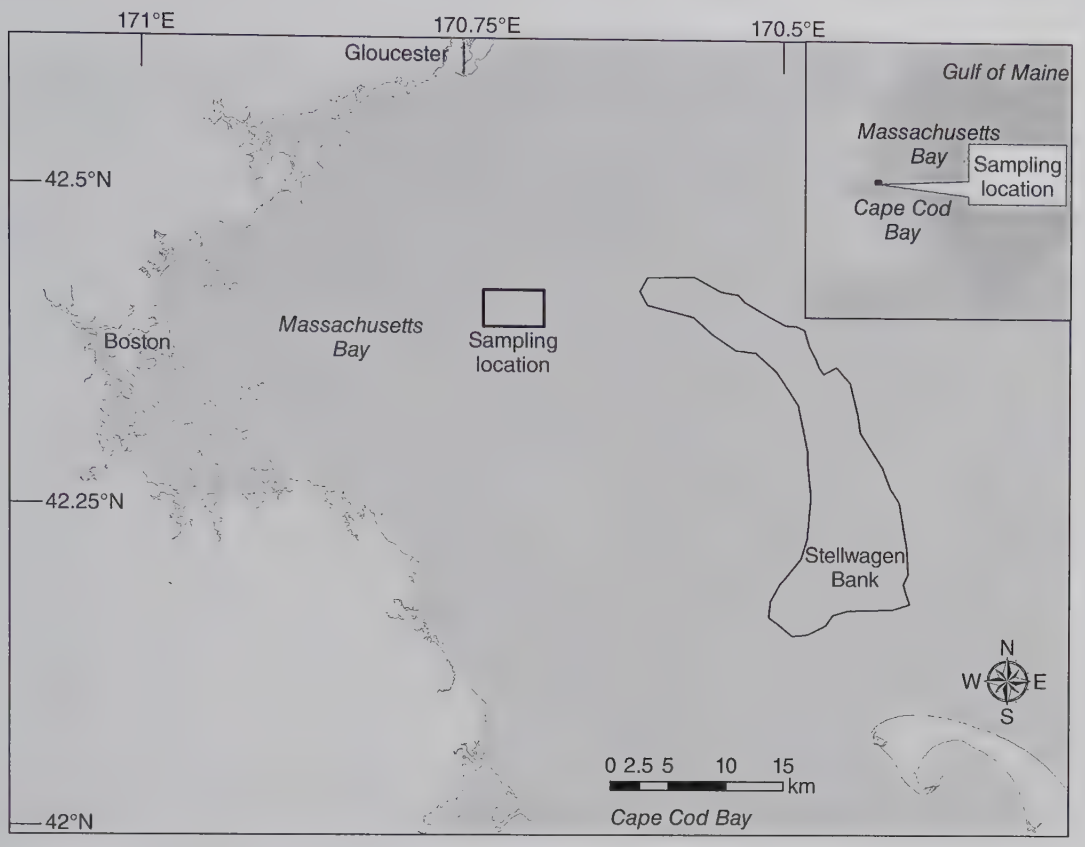

Figure 1

Map of Massachusetts Bay showing the location of ichthyoplankton sampling in 2008–2012 and 2015–2022. Fish larvae were sampled at 2 stations in an area about 22 km south of Gloucester, Massachusetts, and 30 km east of Boston, Massachusetts. Background mapping data are from Esri and MassGIS.

within the R package vegan (vers. 2.6-2; Oksanen et al., 2022) in R (vers. 4.2.1; R Core Team, 2022). The species-specific densities for larvae captured in each collection, measured as the number of larvae per 1000 m^3, were $\log_{10}(x+1)$ transformed to ensure that all taxa regardless of catch magnitude could contribute to similarity measures. Results are considered statistically significant if the P-value is less than 0.05. The average transformed density (geometric mean) for each month of each year of this study was determined, and these values were used to calculate a dissimilarity matrix by using the Bray–Curtis dissimilarity index (Bray and Curtis, 1957). Values of the Bray–Curtis index range from 0% for absolute similarity to 100% for absolute dissimilarity. We used Bray–Curtis index values to perform hierarchical clustering using the unweighted pair group method (Sokal and Michener, 1958) to visualize potential seasonal (across-months) groupings for each year in the study.

These multivariate analyses were originally performed for all years combined to visualize the integrated monthly patterns in the larval community. Then they were performed separately for each year to visualize if the monthly patterns found in the multiyear analyses also occurred in individual years. Using observed $\log_{10}$(density+1) values, each for a given species in a particular month and year of this study, we calculated means for each species in each month and year. These species-specific means for each month were averaged across all years to get species-specific grand means for each month, and these grand means were used to calculate Bray–Curtis indices between months. The hierarchical clustering described in the previous paragraph was used to reveal the levels of dissimilarity for larval fish assemblages characterized by the monthly grand means.

A similarity profile permutation test was used to determine the significant groups within the cluster dendrogram of the larval fish assemblages for each month (Clarke et al., 2008). At each dendrogram node (starting with the least similar), 1000 permutations of the samples were used to calculate similarities used to represent the distribution of the similarity profile under the hypothesis of no multivariate structure within the samples. If the null hypothesis was rejected ($P<0.01$, to account for multiple tests) for the actual observed similarity profile, the process was repeated at the next lower (more similar) node until the null hypothesis could not be rejected.

Logical contiguous groupings determined from the results of the annual cluster analyses were visualized by using nonmetric multidimensional scaling ordination to produce plots in which the distance between samples represented rank ordered similarities with closer proximity in the plot representing higher similarity. Stress metrics were used as a measure of adequacy of the representation of similarities in the ordination plot. Stress levels ≥0.1 and <0.2 provide an adequate representation but should be evaluated in conjunction with the dendrogram based on Bray–Curtis index values (Clarke and Warwick, 2001). Together, results from the cluster analysis and nonmetric multidimensional scaling ordination provide insight into the similarity among samples at the community level. Similarity percentage analysis (Clarke, 1993; Clarke and Warwick, 2001) was used to determine the contribution of each species to the average Bray–Curtis index between the major ichthyoplankton assemblages identified as groups in the dendrogram from cluster analysis. Larval densities were back-transformed to the arithmetic scale for presentation in tables as geometric mean densities of larvae for months and years, and group means were identified by numerical classification.

Mean temperatures in the upper 2.5 m of the water column (surface and near surface temperatures) were averaged with mid-depth and near-bottom temperatures to estimate water column temperature (hereafter referred to as *water temperature*). Monthly average water temperatures were calculated from values for each depth strata sampled each month. The overall mean water temperature (for all years combined) for a given month was calculated as the mean of the averages for that month. Mean monthly water temperatures were compared between the 2 sampling periods, 2008–2012 and 2015–2022, by using paired *t*-tests. Results of these 2-sample *t*-tests and correlations between water temperature and occurrence of larval taxa are considered statistically significant if the *P*-value is less than 0.05.

Distance-based redundancy analysis was employed to explore the relationship between water temperature and larval fish community composition (Legendre and Anderson, 1999). This examination acts as a version of principle component analysis in which Bray–Curtis dissimilarities are constrained by the linear relation to water temperature and provides a measure of the variation in larval fish community attributed to water temperature. A permutation test similar to an analysis of variance was used to determine the significance of the level of explained variation.

Results

Water temperature

Mean water temperature followed a monthly pattern in which it was highest in August and September and lowest in February and March (Table 1). The difference of 0.3°C in water temperatures between periods (2008–2012 and 2015–2022) is significant (P=0.036). There was no significant difference in mean water temperature for any month between 2008–2012 and 2015–2022, according to the results of the 2-sample *t*-tests. The maximum differences in mean monthly water temperatures occurred in January and July, when mean temperatures were 1.0°C and 0.8°C warmer in 2015–2022.

Table 1

Mean monthly water column temperatures in Massachusetts Bay during 2008–2012 and 2015–2022. Also provided are the *P*-values from the paired *t*-test used to compare mean temperatures between the 2 sampling periods. The significance level for this test is 0.05.

Month	Mean temperature (°C)		Difference (°C)	*P*-value
	2008–2012	2015–2022		
January	4.9	6.0	1.0	0.17
February	3.8	4.3	0.4	0.36
March	4.2	4.2	0.0	0.94
April	6.4	6.5	0.1	0.84
May	8.9	9.2	0.2	0.78
June	12.5	12.2	−0.3	0.61
July	14.0	14.8	0.8	0.20
August	15.5	16.1	0.6	0.35
September	16.0	16.2	0.1	0.80
October	13.4	13.6	0.1	0.85
November	10.4	10.1	−0.3	0.63
December	8.0	8.3	0.3	0.60
All months	9.8	10.1	0.3	0.04

Larval fish assemblages

The 2 major larval assemblages apparent in the Bray–Curtis dendrogram are 87% dissimilar with all years combined (Table 2, Fig. 2). The density of the cold-water assemblage that occurred in November–May at mean monthly water temperatures from 4.1°C (in February) to 10.3°C (in November) (43.26 larvae/1000 m^3; Table 2) was lower than the density of the warmwater assemblage that occurred in June–October at mean monthly water temperatures from 12.3°C (in June) to 16.1°C (in September) (432.58 larvae/1000 m^3; Table 2). The cold-water assemblage was dominated by sand lances, Atlantic cod (*Gadus morhua*), and American plaice (*Hippoglossoides platessoides*). The warmwater assemblage was dominated by silver hake (*Merluccius bilinearis*), true hakes, and cunner (*Tautogolabrus adspersus*). None of the 5 most abundant taxa in either assemblage were among the 5 most abundant taxa in the other assemblage, confirming the degree of dissimilarity between assemblages.

Among the abundant taxa in the cold-water and warmwater assemblages, the silver hake (12%), true hakes (11%), and the cunner (8%) contributed most to the total dissimilarity (87%) between major assemblages (Table 2). These taxa were found almost exclusively in the

Table 2

Geometric mean density of fish larvae captured in the 2 major assemblages associated with season and water column temperature in Massachusetts Bay during 2008–2012 and 2015–2022. The cold-water assemblage occurred in November–May at mean temperatures of 4.1°C–10.3°C, and the warmwater assemblage occurred in June–October at mean temperatures of 12.3°C–16.1°C. Also provided for each taxon are the mean contribution to the Bray–Curtis dissimilarity index, the ratio of that mean contribution to the standard deviation of that mean, the contribution to total dissimilarity, and the *P*-value from the similarity percentage analysis. Values are provided for the abundant taxa that made statistically significant ($P<0.05$) contributions to the total dissimilarity between the 2 assemblages. Asterisks denote the 5 highest densities in each assemblage.

	Mean density (larvae/1000 m^3)					
Taxon	Cold-water assemblage	Warmwater assemblage	Mean contribution to dissimilarity	Ratio	Contribution to total dissimilarity (%)	*P*-value
American plaice	2.23*	3.64	0.03	1.06	3.90	1.00
Atlantic cod	7.75*	0.75	0.04	1.25	4.28	0.18
Atlantic herring	2.00*	1.29	0.03	0.94	3.89	1.00
Cunner	0.09	58.07*	0.07	1.28	7.98	0.01
Fourbeard rockling	0.72	42.20*	0.07	2.99	7.65	0.01
Pollock	3.33*	0.06	0.03	1.10	3.48	0.94
Sand lances	21.77*	0.00	0.06	1.26	7.20	0.69
Silver hake	0.08	184.78*	0.11	4.54	12.01	<0.01
True hakes	0.04	103.90*	0.10	2.39	11.08	<0.01
Yellowtail flounder	0.60	12.25*	0.05	1.58	5.17	0.05
All other taxa	4.65	25.64	–	–	–	–
Total (all taxa)	43.26	432.58	–	–	87.40	–

warmwater assemblage. The relatively high ratio of mean contribution to dissimilarity to the standard deviation of that mean indicates that these taxa were consistently influential in identifying assemblages.

The cold-water and warmwater assemblages were present in every year of the study (Fig. 3). The cold-water assemblage started to occur as early as October in 2008, 2012, and 2016 (at water temperatures of 12.6°C–15.2°C) and as late as December in 2009, 2011, 2015, and 2020–2022 (at water temperatures of 7.3°C–9.8°C). In 2020 and 2021, the cold-water assemblage may have begun to occur in November, but no sampling was done that month in either year. The warmwater assemblage started to occur as early as April in 2016 and 2018 (at water temperatures of 6.2°C–6.4°C) and as late as June in 2011, 2015, 2017, and 2020–2022 (at water temperatures of 9.3°C–13.6°C). In 2022, the warmwater assemblage may have begun to occur in May, but no sampling was done that month.

There were 5 statistically significant seasonal groups of fish larvae within the 2 major assemblages when all larval data were combined (Figs. 2 and 3). Three groups occurred within the cold-water assemblage: group 1 in November (at a water temperature of 10.3°C), group 2 in December–March (at water temperatures of 4.1°C–8.2°C), and group 3 in April and May (at water temperatures of 6.5°C–9.1°C). Group 1 was dominated by Atlantic herring (*Clupea harengus*) and occurred in the years 2015, 2017, and 2022, when larval Atlantic herring were present at high mean densities (45.32 larvae/1000 m^3; Table 3). Group 2 was dominated by sand lances and Atlantic cod and occurred in every year. A transitional group between the cold-water and warmwater assemblages, group 3 occurred in April and May in each of the years 2009–2011 and in 2018, when the American plaice was the dominant taxon.

Two high-density groups occurred within the warmwater assemblage: group 4 in June–August (at water temperatures of 12.3°C–15.9°C), with a density of 1448.29 larvae/1000 m^3, and group 5 in September and October (at water temperatures of 13.5–16.1°C), with a density of 177.63 larvae/1000 m^3 (Figs. 2 and 3, Table 3). Group 4 was dominated by cunner, silver hake, and true hakes and occurred every year. A transitional group between the warmwater and cold-water assemblages, group 5 occurred in 2009 and 2018. True hakes and silver hake were also dominant in group 5 but at lower densities than they were found in group 4.

Groups 2 and 4 (which occur in December–March and June–August, respectively) form the core of the major cold-water and warmwater assemblages because they were present in every year (Fig. 3). Cunner, silver hake, and true hakes contributed significantly and most to the 95% dissimilarity between these groups (Table 4). These taxa were the 3 most abundant in group 4 and occurred at lower densities in group 2 (Table 3).

The nonmetric multidimensional scaling plot confirms the strong seasonal pattern evident in the Bray–Curtis dendrogram (Fig. 4). Group 1 (which occurs in November) appears at the bottom center of the nonmetric multidimensional scaling plot, and the months cycle counterclockwise around the plot, emphasizing the seasonal component of the larval assemblages. Some overlap in the nonmetric multidimensional scaling plot occurs among groups

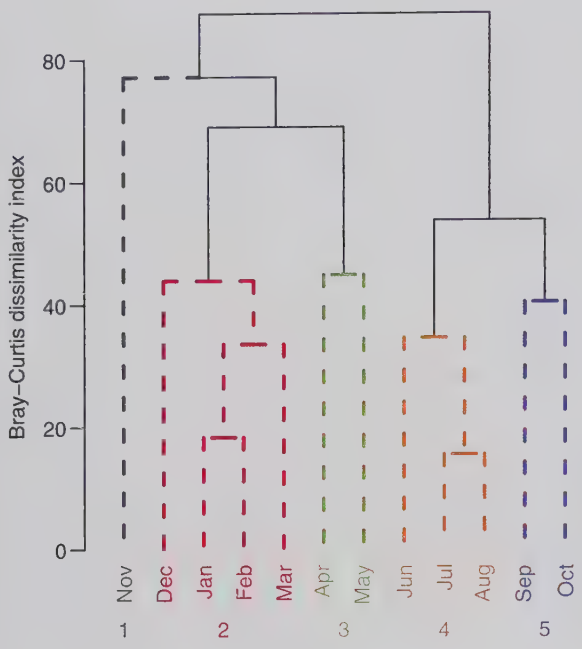

Figure 2

Dendrogram of the 5 statistically distinct seasonal groups of larval fish within the 2 major assemblages in Massachusetts Bay during 2008–2012 and 2015–2022, identified through cluster analysis with Bray–Curtis dissimilarity index values. Solid lines designate statistically distinct groups, and dashed lines indicate groups that are not statistically distinct. Numerals at the bottom of the figure indicate the groups, which are based on temporal changes in the cold-water assemblage (groups 1–3) and warmwater assemblage (groups 4 and 5). The cold-water assemblage occurred in November–May at mean temperatures of 4.1°C–10.3°C, and the warmwater assemblage occurred in June–October at mean temperatures of 12.3°C–16.1°C. Mean monthly densities for taxa were used to calculate Bray–Curtis dissimilarity index values.

identified in the Bray–Curtis dendrogram (Fig. 2). The least amount of overlap between adjacent groups occurs between groups 1 and 2, confirming the 73% Bray–Curtis dissimilarity between these groups (Fig. 2). Similarly, the overlap between adjacent groups 3 and 4, which form a boundary between the major cold-water and warmwater assemblages, is minimal (72% dissimilarity). Groups 1 and 5 also had minimal overlap (65% dissimilarity), and these groups are boundaries between the warmwater and cold-water assemblages.

The results of distance-based redundancy analysis indicate that the variation in composition of the cold-water assemblage (which occurs in November–May) was significantly, but weakly, correlated with mean water temperature (coefficient of correlation=0.28, P=0.011). No significant correlation was found between water temperature and the variation in composition of the warmwater assemblage (which occurs in June–October). The silver hake, Atlantic herring, and witch flounder (*Glyptocephalus cynoglossus*) were the taxa with the highest significant positive correlation between mean density and mean water temperature (Table 5, Figs. 5 and 6). However, the 10 years with no catch of witch flounder and the 3 years of relatively large catches of witch flounder strongly influenced the positive relationship for this taxon. Densities of Atlantic wolffish (*Anarhichas lupus*), wrymouth (*Cryptacanthodes maculatus*), and snakeblenny (*Lumpenus lampretaeformis*) were negatively correlated with water temperature (Table 5, Fig. 6). However, as with witch flounder, the relationship between density of Atlantic wolffish and water temperature was strongly influenced by 10 years with no catch and 3 years with relatively higher densities.

Discussion

We detected seasonal patterns in the local larval fish assemblage in central Massachusetts Bay by sampling ichthyoplankton at a high frequency over 13 years. Frequent sampling within a small area is useful in efforts to describe phenological changes (Staudinger et al., 2019) because potential spatial variability is minimized. The focus on the central location within Massachusetts Bay resulted in data that can be used for characterization not just of the larval fish assemblage in the sampling area but of the assemblage in the entire Massachusetts Bay.

Our data are in general agreement with the EcoMon program data collected in Massachusetts Bay during our study period (NEFSC[2]). A total of 36 ichthyoplankton samples were collected during 7 months in Massachusetts Bay as part of the EcoMon program in 2008–2012 and 2015–2022. No samples were collected in Massachusetts Bay as part of the EcoMon program in January, March, July, September, and December. The 3 most abundant taxa in the EcoMon data were among the 5 most abundant taxa in our study in 4 of the 5 seasonal groups defined in this study (those that occur in November, December–March, April–May, and June–August) (Table 6). The rank order of the 3 most abundant taxa were identical between the programs in 2 of the 5 groups (those that occur in December–March and April–May). Only in September and October was one of the most abundant taxa, the Atlantic menhaden (*Brevoortia tyrannus*), in the EcoMon program data not among the top 5 taxa in our study; however, only 2 samples were collected during September and October as part of the EcoMon program.

The agreement between our data and data from earlier work elsewhere in the southern Gulf of Maine and Massachusetts Bay is also a strong indication that our data are representative of the larger Massachusetts Bay.

[2] NEFSC (Northeast Fisheries Science Center). 2019. Zooplankton and ichthyoplankton abundance and distribution in the North Atlantic collected by the Ecosystem Monitoring (EcoMon) Project from 1977-02-13 to 2021-11-15 (NCEI Accession 0187513). NOAA Natl. Centers Environ. Inf. [Dataset.] [Available from website, accessed October 2024.]

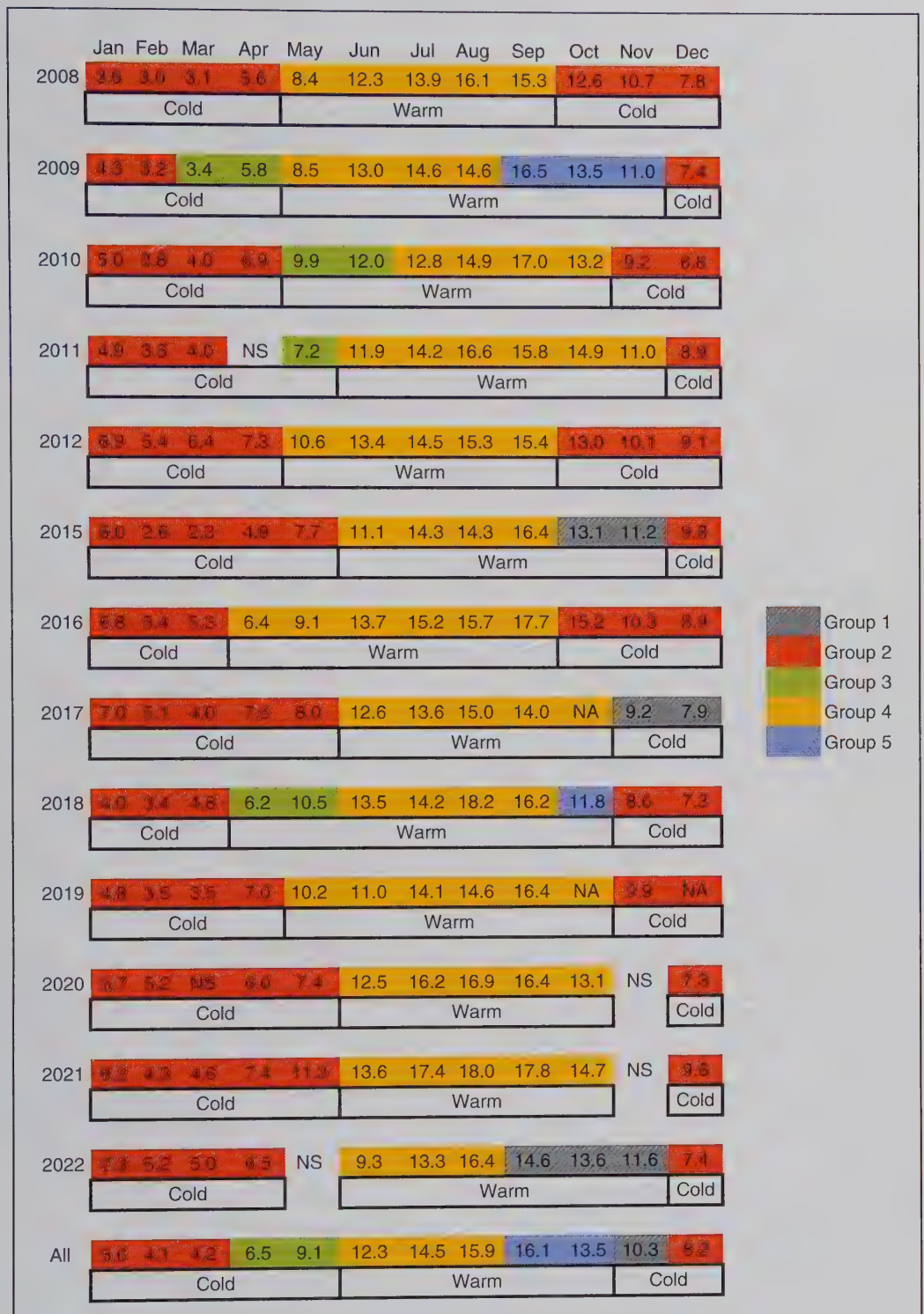

Figure 3

The 5 statistically distinct groups identified through cluster analysis with Bray–Curtis dissimilarity index values for the larval fish assemblage in Massachusetts Bay in 2008–2012 and 2015–2022, with mean monthly water column temperatures in degrees Celsius. Groups 1–3 were discerned within the cold-water assemblage, which occurred in November–May, and groups 4 and 5 were found within the warmwater assemblage, which occurred in June–October. NS=not sampled; NA=not available because water column temperatures were not collected.

Table 3

Geometric mean density for 5 statistically distinct groups of fish larvae captured in Massachusetts Bay during 2008–2012 and 2015–2022. The groups occurred in different seasons: group 1 in November, group 2 in December–March, group 3 in April and May, group 4 in June–August, and group 5 in September and October. Asterisks denote the 5 highest densities in each group.

	Seasonal group density (larvae/1000 m^3)				
Taxon	1	2	3	4	5
American plaice	0.00	0.22	36.88*	11.18	0.09
Atlantic cod	1.93*	12.23*	4.28*	1.53	0.00
Atlantic menhaden	0.75*	0.07	0.03	10.06	3.93
Atlantic herring	45.32*	2.02*	0.06	<0.01	6.89*
Cunner	0.00	0.00	0.37	767.90*	0.26
Fourbeard rockling	0.77*	0.03	3.92	93.10*	12.44*
Haddock	0.00	0.37	4.44*	0.05	0.00
Longhorn sculpin	0.00	1.09*	0.46	0.00	0.00
Pollock	0.37	8.57*	0.39	0.05	0.07
Sand lances	0.00	73.34*	4.49*	0.00	0.00
Silver hake	1.31*	<0.01	0.04	356.79*	68.51*
True hakes	0.34	0.02	0.00	129.55*	74.55*
Windowpane	0.00	0.01	0.03	0.89	4.23*
Winter flounder	0.00	0.15	10.80*	0.90	0.00
Yellowtail flounder	0.00	0.00	4.17	45.90*	0.99
All other taxa	0.62	1.19	3.36	30.38	5.67
Total (all taxa)	51.41	99.32	73.72	1448.29	177.63

In addition, our data agree with those of Jury et al.[3], who compiled temporal and spatial distribution data on 58 invertebrate and fish species found in embayments and estuaries of Massachusetts, New Hampshire, and Maine, including in Massachusetts Bay. Each of the dominant taxa in our study (Table 3) were considered either "highly abundant" or "abundant" in Massachusetts Bay by Jury et al.[3] during the months they were dominant in our study.

Our data are also in agreement with those of Runge and Jones (2012), who sampled 2 stations in Massachusetts Bay and found that Atlantic herring, pollock (*Pollachius virens*), and sand lances were abundant in the winter months, similar to the composition of the cold-water assemblage defined in our study (Table 2). They also identified cunner, silver hake, red hake, American plaice, and daubed shanny (*Leptoclinus maculatus*) as dominant in the summer months, similar to the composition of the warmwater assemblage defined in our study, with some exceptions: the fourbeard rockling (*Enchelyopus cimbrius*) and yellowtail flounder (*Myzopsetta ferruginea*) were among the 5 most abundant warmwater taxa in our data, and we collected no daubed shanny.

In Cape Cod Bay, to the south of our sampling area, Scherer (1984) found that larval densities were highest from June through September, when fourbeard rockling, Atlantic mackerel (*Scomber scombrus*), true hakes, and cunner larvae were most abundant. The seasonality and composition of high larval densities in Cape Cod Bay from June through September is similar to the high-density warmwater assemblage that occurs from June through October and was identified in our study (Table 2), except that Atlantic mackerel were not abundant in our data. The spawning stock biomass of Atlantic mackerel is currently greatly reduced from the levels of the 1970s when Scherer (1984) sampled Cape Cod Bay, and this difference in spawning stock biomass likely explains the low levels of larval Atlantic mackerel in our data (NEFSC[4]). Each of the 5 most abundant taxa in our cold-water assemblage (November–May) was at its highest abundance in Cape Cod Bay from November through May (Scherer, 1984).

Mean water temperature increased by 0.3°C between the periods 2008–2012 and 2015–2022. Significant increases in surface water temperature in the Gulf of Maine and Northwest Atlantic Ocean have been widely reported (Mills et al., 2013; Pershing et al., 2015, 2021; Gonçalez Neto et al., 2021; Mills et al., 2024). In each of these studies, a longer time series of sea-surface temperatures was used, and linear models were sometimes used to illustrate increases in water temperature. The lack of sampling in 2013 and 2014 in our study prevented the use of methods for time-series analysis. The warmest mean water temperatures in our study were recorded in 2012, 2016, 2017, 2010, 2020, and 2021, and those years were among those with the greatest deviation from mean sea-surface temperatures reported by Mills et al. (2024) for the period 1982–2021. Our inclusion of colder mid-depth and near-bottom temperatures below the thermocline in the summer may have tempered an increase that would have been larger if we had used only sea-surface temperatures, although increases in bottom water temperatures have been reported from additional studies (Record et al., 2019; Friedland et al., 2020).

In our study, mean water temperature explained 28% of the variability in the composition of the cold-water larval assemblage but did not significantly explain the variability in the warmwater assemblage. Our data indicate that, in the cold-water assemblage, abundance of some of the taxa that range far to the north of Massachusetts Bay, such as the Atlantic wolffish, snakeblenny, and wrymouth, were negatively correlated with temperature. These 3 taxa can

[3] Jury, S. H., J. D. Field, S. L. Stone, D. M. Nelson, and M. E. Monaco. 1994. Distribution and abundance of fishes and invertebrates in North Atlantic estuaries. Estuar. Living Mar. Resources Progam, ELMR Rep. 13, 221 p. Strateg. Environ. Assess. Div., Natl. Ocean Serv., NOAA, Silver Spring, MD. [Available from website.]

[4] NEFSC (Northeast Fisheries Science Center). 2022. Management track assessment June 2021. Northeast Fish. Sci. Cent. Ref. Doc. 22-10, 79 p. [Available from website.]

Table 4

Geometric mean density, mean contribution to the Bray–Curtis dissimilarity index, ratio of that mean contribution to the standard deviation of that mean, and contribution to total dissimilarity for abundant taxa that made statistically significant ($P<0.05$) contributions to total dissimilarity (95%) between 2 statistically distinct groups of fish larvae collected in Massachusetts Bay during 2008–2012 and 2015–2022. One group occurred in December–March, and the other occurred in June–August. The P-values are from the similarity percentage analysis.

Taxon	Density (larvae/1000 m^3)		Mean contribution to dissimilarity	Ratio	Contribution to total dissimilarity (%)	P-value
	December–March	June–August				
Cunner	0.00	767.90	0.11	6.83	12.08	<0.01
Fourbeard rockling	12.23	93.10	0.08	7.41	8.27	0.01
Silver hake	<0.01	356.79	0.10	4.47	10.68	0.01
True hakes	0.02	129.55	0.08	1.99	8.77	0.05
Yellowtail flounder	0.00	45.90	0.07	4.17	7.05	0.01

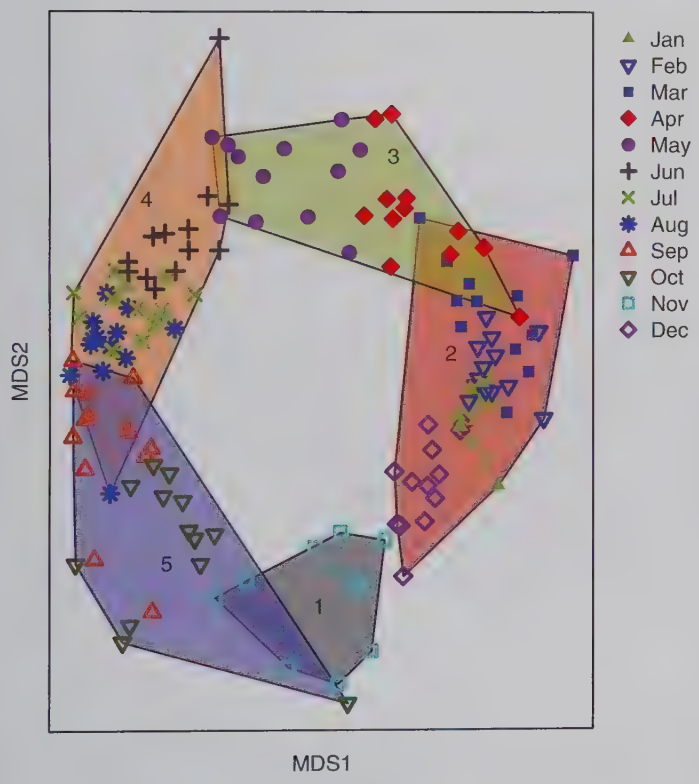

Figure 4

Nonmetric multidimensional scaling (MDS) plot of 5 statistically distinct seasonal groups within the larval fish assemblage of Massachusetts Bay in 2008–2012 and 2015–2022, identified through cluster analysis with Bray–Curtis dissimilarity index values. Each symbol represents a month-year combination. Polygons delineate and numerals indicate the groups, which are also illustrated in the dendrogram in Figure 2. The groups occurred in different seasons: group 1 in November, group 2 in December–March, group 3 in April and May, group 4 in June–August, and group 5 in September and October. The calculated stress level is 0.11.

Table 5

Taxa with a significant ($P<0.05$) correlation between geometric mean density and mean water column temperature for the cold-water assemblage in Massachusetts Bay during 2008–2012 and 2015–2022. The cold-water assemblage occurred in November–May at mean temperatures of 4.1°C–10.3°C. r=coefficient of correlation.

Taxon	r	P-value
Atlantic herring	0.66	0.02
Atlantic wolffish	−0.85	<0.01
Fourbeard rockling	0.58	0.04
Silver hake	0.65	0.02
Snakeblenny	−0.76	<0.01
True hakes	0.56	0.05
Witch flounder	0.61	0.03
Wrymouth	−0.72	0.01
Yellowtail flounder	0.60	0.03

be considered northern fish because they occur as far north as Davis Strait, between western Greenland and Baffin Island (Atlantic wolffish: Rountree, 2002; snakeblenny: Collette, 2002a), and Labrador (wrymouth: Collette, 2002b). Abundance of these cold-water taxa may decrease if water temperatures in the cold-water season continue to rise. The thermal habitat of each of these 3 taxa is projected with medium-to-low uncertainty to decrease in waters of the northeastern United States or eastern Canada under predicted greenhouse gas scenarios (Morley et al., 2018). Abundances of snakeblenny and wrymouth were low in the 2 warmest years of 2012 and 2016, although these species were found in samples in

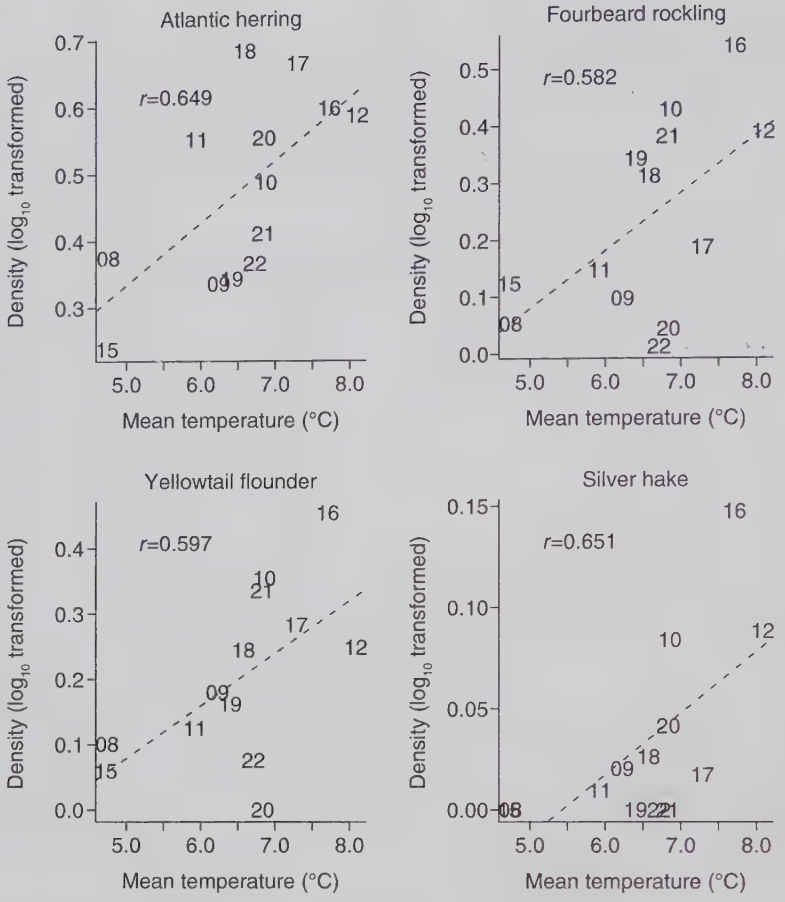

Figure 5

Significant (P<0.05) relationships between $\log_{10}(x+1)$-transformed density of fish larvae and mean water column temperature for Atlantic herring (*Clupea harengus*), fourbeard rockling (*Enchelyopus cimbrius*), yellowtail flounder (*Myzopsetta ferruginea*), and silver hake (*Merluccius bilinearis*) captured in the cold-water assemblage in Massachusetts Bay during 2008–2012 and 2015–2022. The cold-water assemblage occurred in November–May at mean temperatures of 4.1°C–10.3°C. The coefficient of correlation (r) for each trend line (dashed line) is given in each graph. Numerals in the graphs indicate years of occurrence. Densities of larvae in raw data from ichthyoplankton sampling are recorded as number of larvae per 1000 m^3.

most years. Atlantic wolffish occurred only in the coldest years of 2008, 2015, and 2011; however, the occurrence of this taxon is too limited to draw a strong conclusion.

Larval abundances of 5 taxa (the Atlantic herring, fourbeard rockling, silver hake, witch flounder, and yellowtail flounder) in the cold-water assemblage were positively correlated with increasing mean water temperature. The center of distribution of larvae of these taxa, except for Atlantic herring and witch flounder, moved significantly northward between the period 1977–1987 and the period 1999–2008 along the northeast U.S. continental shelf (Walsh et al., 2015). Furthermore, the distribution of adults of the fourbeard rockling, silver hake, and yellowtail flounder also moved north along the northeast U.S. continental shelf between the period 1970–2009 and the period 2010–2019 (Mills et al., 2024), potentially contributing to the increase in abundance of larvae with the rise in temperature observed in our study area. The positive relationship with increasing water temperatures during the cold-water period may indicate that these taxa will become more abundant in our study area during cold-water seasons as water temperatures continue to rise. Witch flounder were not abundant in any year in our study area, and the low density of this taxon observed in our study (Fig. 6) does not support major inferences.

A single variable, whether environmental or biological, is not likely to entirely explain the spatial and temporal occurrence of larvae. The incorporation of environmental

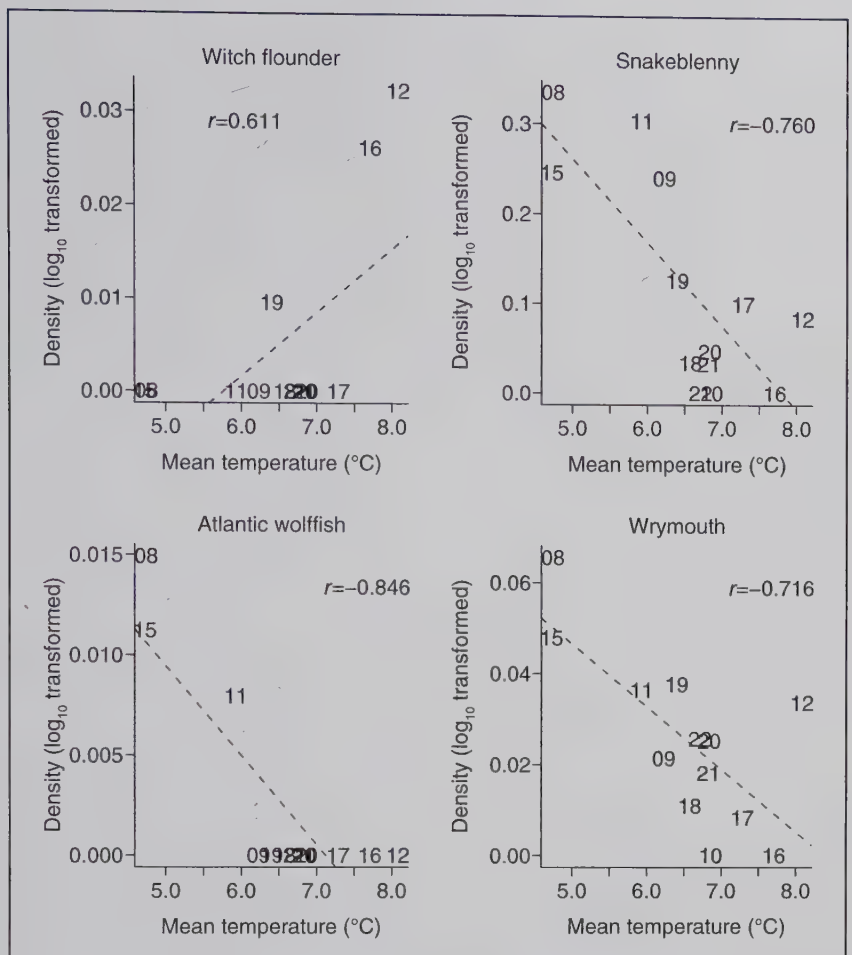

Figure 6

Significant (P<0.05) relationships between $\log_{10}(x+1)$-transformed density of fish larvae and mean water column temperature for witch flounder (*Glyptocephalus cynoglossus*), snakeblenny (*Lumpenus lampretaeformis*), Atlantic wolffish (*Anarhichas lupus*), and wrymouth (*Cryptacanthodes maculatus*) captured in the cold-water assemblage in Massachusetts Bay during 2008–2012 and 2015–2022. The cold-water assemblage occurred in November–May at mean temperatures of 4.1°C–10.3°C. The coefficient of correlation (r) for each trend line (dashed line) is given in each graph. Numerals in the graphs indicate years of occurrence. Densities of larvae in raw data from ichthyoplankton sampling are recorded as number of larvae per 1000 m^3.

variables, such as water temperature, can improve the performance of fishery models, but several factors can limit their usefulness (Keyl and Wolff, 2008). The spawning stock of adults and environmental factors, such as circulation patterns that retain or advect propagules, can be important to the occurrence and abundance of fish larvae in a particular location. Churchill et al. (2011) found that spring-spawned larval Atlantic cod were retained in the western Gulf of Maine and transported to areas favorable to juvenile development during periods of winds favorable for downwelling. However, Hare et al. (2015) incorporated updated estimates of spawning stock biomass and recruitment into the model of Churchill et al. (2011) and found a decreased correlation between recruitment and wind direction, indicating that the influence of environmental variables on ecosystem processes can vary.

The phenology of fish larvae in the Gulf of Maine is changing in "complex and inconsistent ways" (Staudinger et al., 2019). Patterns in the occurrence of fish larvae outlined by Walsh et al. (2015) partially support the expectation that changes in fish larval phenology along the northeastern coast of the United States between the periods 1977–1987 and 1999–2008 could be attributed to changes in water temperature. The season of occurrence changed for about half of the 45 larval taxa examined by Walsh et al. (2015). Among larvae that had a change in occurrence, those common in the summer and fall shifted their occurrence most often to later in the season, and

Table 6

Comparison of the rank order of density of taxa collected in 5 statistically distinct seasonal groups within the larval fish assemblage in Massachusetts Bay during 2008–2012 and 2015–2022, between the sampling of the Ecosystem Monitoring (EcoMon) program and the sampling of this study. Density was measured as number of larvae per 10 m^2 in the EcoMon program and as number of larvae per 1000 m^3 in this study.

	Seasonal group									
	November		December–March		April and May		June–August		September and October	
Taxon	EcoMon	This Study	EcoMon	This Study	EcoMon	This Study	EcoMon	This Study	EcoMon	This Study
Atlantic herring	1	1							1	4
Atlantic cod	2	2	3	2						
Atlantic menhaden									2	
American plaice					3	1				
Cunner							1	1		
Fourbeard rockling	3	4					2	4		
Pollock			2	3						
Sand lances			1	1	1	3				
True hakes									3	1
Winter flounder					2	2				
Yellowtail Flounder							3	5		

those common in the winter and spring shifted most often to earlier in the season. In addition, sometimes organisms made "wrong-way migrations" to less-than-favorable habitat in response to larval transport (Fuchs et al., 2020) and possibly to increasing population size (Mills et al., 2024).

This study resulted in the first quantitative description of the larval fish assemblage of Massachusetts Bay and the influence of water temperature on this assemblage. Our data have the potential to aid identification of larval taxa that might be susceptible to climate change by using the projections and criteria of Hare et al. (2016). It is expected that the density of larvae of at least 4 commercially important fish taxa among the 5 most abundant taxa that we identified in the cold-water assemblage (the Atlantic herring, Atlantic cod, pollock, and American plaice) will be negatively affected by continued warming in Massachusetts Bay. Among the 5 most abundant taxa of larvae in the warmwater assemblage, at least 3 commercially important taxa (the white hake, silver hake, and yellowtail flounder) are expected to be negatively affected by increasing temperatures in Massachusetts Bay.

Conclusions

The time-integrated description of the structure of the ichthyoplankton assemblage in Massachusetts Bay in the early 21st century, based on our 13-year dataset, serves as an important baseline against which future changes in the assemblage may be compared. We identified 2 major larval fish assemblages that were 87% different from each other, a low-density cold-water assemblage present from November through May and a warmwater assemblage present at a higher density from June through October. Within the cold-water assemblage, 3 groups were found to occur at different times of year or seasons: November, December–March, and April–May. Within the warmwater assemblage, 2 groups were present at different seasons: June–August and September–October.

Water temperature explained 28% of the interannual variability in the cold-water assemblage but did not significantly explain any variability in the warmwater assemblage. However, it is apparent from our study and others that temperature alone does not control the composition and phenology of larval communities and that other factors, such as hydrography and local environmental conditions, can be important (Starko et al., 2024; Weisberg et al., 2024). The interaction between larvae and additional factors, such as hydrography, spawning stock, and changes in population size (Hare et al., 2015; Staudinger et al., 2019, Mills et al., 2024), warrant further investigation into their influences on ichthyoplankton assemblages.

Resumen

Se colectaron muestras de ictioplancton mensualmente en 2 estaciones de la bahía de Massachusetts de 2008 a 2012 y de 2015 a 2022 para caracterizar el ensamble

de peces larvarios de esta zona. La fauna se componía de 2 conjuntos principales que eran un 87% diferentes entre sí y estaban asociados con la estación y la temperatura del agua. Un grupo de agua fría de baja densidad (43.26 larvas/1000 m^3) apareció de noviembre a mayo a temperaturas medias de la columna de agua entre 4.1°C y 10.3°C, con lanzón (*Ammodytes* spp.) como taxón dominante. Entre junio y octubre se observo un ensamblaje de aguas cálidas de mayor densidad (432.58 larvas/1000 m^3) con temperaturas medias de la columna de agua entre 12.3°C y 16.1°C, siendo la merluza plateada (*Merluccius bilinearis*) el taxón dominante. Dentro del conjunto de especies de aguas frías, se observaron grupos estadísticamente diferentes en noviembre, diciembre–marzo y abril–mayo. El arenque Atlántico (*Clupea harengus*), los lanzones y el lenguado americano (*Hippoglossoides platessoides*) fueron los taxones dominantes en esos periodos, respectivamente. Dentro del ensamble de aguas cálidas, se produjeron grupos de especies estadísticamente diferenciados en junio-agosto y septiembre-octubre, siendo el salmonete (*Tautogolabrus adspersus*) y el grupo de merluzas (*Urophycis* spp.) los taxones dominantes en esos periodos, respectivamente. La temperatura del agua explica el 28% de la variación anual del esnamble de aguas frías, y no existe una relación significativa entre la temperatura y la variación anual del ensamble de aguas cálidas. Esta caracterización de larvas de peces proporciona una línea base con la que se pueden medir los cambios potenciales en los ensambles de esta área.

Acknowledgments

All work in the field and laboratory was completed by Normandeau Associates Inc. for Exelerate Energy LP, as a subcontractor to Tetra Tech Inc. E. Fel'Dotto supervised field collections. K. Adair, J. Buckingham, A. Bullock, A. Coutu, H. Proctor, and J. Strube supervised laboratory identifications of ichthyoplankton. D. Anderson, D. Pelletier, and N. Stockley assisted in the preparation of tables and figures.

Literature cited

Bray, J. R., and T. J. Curtis.
1957. An ordination of upland forest communities of southern Wisconsin. Ecol. Monogr. 27:325–349.

Chenoweth, S. B.
1973. Fish larvae of the estuaries and coast of central Maine. Fish. Bull. 71:105–113.

Churchill, J. H., J. Runge, and C. Chen.
2011. Processes controlling retention of spring-spawned Atlantic cod (*Gadus morhua*) in the western Gulf of Maine and their relationship to an index of recruitment success. Fish. Oceanogr. 20:32–46.

Clarke, K. R.
1993. Non-parametric multivariate analyses of changes in community structure. Aust. J. Ecol. 18:117–142.

Clarke, K. R., and R. M. Warwick.
2001. Change in marine communities: an approach to statistical analysis and interpretation, 2nd ed., 144 p. PRIMER-E, Plymouth, U.K.

Clarke, K. R., P. J. Somerfield, and R. N. Gorley.
2008. Testing of null hypotheses in exploratory community analyses: similarity profiles and biota-environment linkage. J. Exp. Mar. Biol. Ecol. 366:56–69.

Collette, B. B.
2002a. Wrymouths. Family Cryptacanthodidae. *In* Bigelow and Schroeder's fishes of the Gulf of Maine, 3rd ed. (B. B. Collette and G. Klein-MacPhee, eds.), p. 483–485. Smithson. Inst. Press, Washington, DC.
2002b. Pricklebacks. Family Stichaeidae. *In* Bigelow and Schroeder's fishes of the Gulf of Maine, 3rd ed. (B. B. Collette and G. Klein-MacPhee, eds.), p. 474–481. Smithson. Inst. Press, Washington, DC.

Elliott, E. M., and D. Jimenez.
1981. Laboratory manual for the identification of ichthyoplankton from the Beverly-Salem Harbor area, 230 p. Div. Mar. Fish., Commonw. Mass. Dep. Fish Wildl. Rec. Vehicles, Boston, MA.

Fahay, M. P.
2007. Early stages of fishes in the western North Atlantic Ocean (Davis Strait, Southern Greenland and Flemish Cap to Cape Hatteras), vols. 1 and 2, 1696 p. NAFO, Dartmouth, Canada.

Friedland, K. D., R. E. Morse, J. P. Manning, D. C. Melrose, T. Miles, A. G. Goode, D. C. Brady, J. T. Kohut, and E. N. Powell.
2020. Trends and change points in surface and bottom thermal environments of the US Northeast Continental Shelf Ecosystem. Fish. Oceanogr. 29:396–414.

Fuchs, H. L., R. J. Chant, E. J. Hunter, E. N. Curchitser, G. P. Gerbi, and E. Y. Chen.
2020. Wrong-way migrations of benthic species driven by ocean warming and larval transport. Nat. Clim. Change 10:1052–1056.

Geoghegan, P.
1996. The management of quality control and quality assurance systems in fisheries science. Fisheries 21(8):14–18.

Geyer, W. R., G. B. Gardner, W. S. Brown, J. Irish, B. Butman, T. Loder, and R. P. Signell.
1992. Physical oceanographic investigation of Massachusetts and Cape Cod Bays: executive summary. Report to the Massachusetts Bay Program. Mass. Bay Program, MBP-92-03S, 23 p. [Available from website.]

Gonçalez Neto, A., J. A. Langan, and J. B. Palter.
2021. Changes in the Gulf Stream preceded rapid warming of the Northwest Atlantic Shelf. Commun. Earth Environ. 2:74.

Hare, J. A., E. N. Brooks, M. C. Palmer, and J. H. Churchill.
2015. Re-evaluating the effect of wind on recruitment in Gulf of Maine Atlantic cod (*Gadus morhua*) using an environmentally-explicit stock recruitment model. Fish. Oceanogr. 24:90–105.

Hare, J. A., W. E. Morrison, M. W. Nelson, M. M. Stachura, E. J. Teeters, R. B. Griffis, M. A. Alexander, J. D. Scott, L. Alade, R. J. Bell, et al.
2016. A vulnerability assessment of fish and invertebrates to climate change on the Northeast U.S. Continental Shelf. PLoS ONE 11(2):e0146756.

Jones, P. W., F. D. Martin, and J. D. Hardy.
1978. Development of fishes of the Mid-Atlantic Bight: an atlas of egg, larvae and juvenile stages. Vols. 1–6. U.S. Fish Wildl. Serv. Biol. Serv. Program FWS/OBS-78/12.

Keyl, F., and M. Wolff.
2008. Environmental variability and fisheries: what can models do? Rev. Fish Biol. Fish. 18:273–299.

Lazzari, M. A.
2001. Dynamics of larval fish abundance in Penobscot Bay, Maine. Fish. Bull. 99:81–93.

Legendre, P., and M. J. Anderson.
1999. Distance-based redundancy analysis: testing multispecies responses in multifactorial ecological experiments. Ecol. Monogr. 69:1–24.

Llopiz, J. K., R. K. Cowen, M. J. Hauff, R. Ji, P. L. Munday, B. A. Muhling, M. A. Peck, D. E. Richardson, S. Sogard, and S. Sponaugle.
2014. Early life history and fisheries oceanography: new questions in a changing world. Oceanography 27(4):26–41.

McClatchie, S., J. Duffy-Anderson, J. C. Field, R. Goericke, D. Griffith, D. S. Hanisko, J. A. Hare, J. Lyczkowski-Schultz, W. T. Peterson, W. Watson, et al.
2014. Long time series in US fisheries oceanography. Oceanography 27(4):48–67.

Mills, K. E., A. J. Pershing, C. J. Brown, Y. Chen, F.-S. Chiang, D. S. Holland, S. Lehuta, J. A. Nye, J. C. Sun, A. C. Thomas, et al.
2013. Fisheries management in a changing climate: lessons from the 2012 ocean heat wave in the Northwest Atlantic. Oceanography 26(2):191–195.

Mills, K. E., A. Kemberling, L. A. Kerr, S. M. Lucey, R. S. McBride, J. A. Nye, A. J. Pershing, M. Barajas, and C. S. Lovas.
2024. Multispecies population-scale emergence of climate change signals in an ocean warming hotspot. ICES J. Mar. Sci. 81:375–389.

Morley, J. W., R. L. Selden, R. J. Latour, T. L. Frölicher, R. J. Seagraves, and M. L. Pinsky.
2018. Projecting shifts in thermal habitat for 686 species on the North American continental shelf. PLoS ONE 13(5):e0196127.

Oksanen, J., G. L. Simpson, F. G. Blanchet, R. Kindt, P. Legendre, P. R. Minchin, R. B. O'Hara, P. Solymos, M. H. H. Stevens, E. Szoecs, et al.
2022. vegan: community ecology package. R package, vers. 2.6-2. [Available from website, accessed October 2022.]

Page, L. M., K. E. Bemis, T. E. Dowling, H. Espinosa-Pérez, L. T. Findley, C. R. Gilbert, K. E. Hartel, R. N. Lea, N. E. Mandrak, M. A. Neighbors, et al.
2023. Common and scientific names of fishes from the United States, Canada, and Mexico, 8th ed. Am. Fish. Soc., Spec. Publ. 37, 439 p. Am. Fish. Soc., Bethesda, MD.

Pershing, A. J., M. A. Alexander, C. M. Hernandez, L. A. Kerr, A. Le Bris, K. E. Mills, J. A. Nye, N. R. Record, H. A. Scannell, J. D. Scott, et al.
2015. Slow adaptation in the face of rapid warming leads to the collapse of the Gulf of Maine cod fishery. Science 350:809–812.

Pershing, A. J., M. A. Alexander, D. C. Brady, D. Brickman, E. N. Curchitser, A. W. Diamond, L. McClenachan, K. E. Mills, O. C. Nichols, D. E. Pendleton, et al.
2021. Climate impacts on the Gulf of Maine ecosystem: a review of observed and expected changes in 2050 from rising temperatures. Elementa Sci. Anthr. 9(1):00076.

R Core Team.
2022. R: a language and environment for statistical computing. R Foundation for Statistical Computing, Vienna, Austria. [Available from website, accessed June 2022.]

Record, N. R., J. A. Runge, D. E. Pendleton, W. M. Balch, K. T. A. Davies, A. J. Pershing, C. L. Johnson, K. Stamieszkin, R. Ji, Z. Feng, S. D. Kraus, et al.
2019. Rapid climate-driven circulation changes threaten conservation of endangered North Atlantic right whales. Oceanography 32(2):162–169.

Richards, W. J. (ed.).
2005. Early stages of Atlantic fishes: an identification guide for the western central North Atlantic, vols. 1 and 2, 2636 p. CRC Press, Boca Raton, FL.

Rountree, R. A.
2002. Wolffishes. Family Anarhichadidae. *In* Bigelow and Schroeder's fishes of the Gulf of Maine (B. B. Collette and G. Klein-MacPhee, eds.), p. 485–496. Smithson. Inst. Press, Washington, DC.

Runge, J. A., and R. J. Jones.
2012. Results of a collaborative project to observe coastal zooplankton and ichthyoplankton abundance and diversity in the western Gulf of Maine: 2003–2008. Am. Fish. Soc. Symp. 79:345–360.

Scherer, M. D.
1984. The ichthyoplankton of Cape Cod Bay. *In* Observations on the ecology and biology of western Cape Cod Bay, Massachusetts. Lecture notes on coastal and estuarine studies, vol. 11 (J. D. Davis and D. Merriman, eds.), p. 151–190. Springer, New York.

Sokal, R. R., and C. D. Michener.
1958. A statistical method for evaluating systematic relationships. Univ. Kansas Sci. Bull. 38(part 2):1409–1438.

Starko, S., M. van der Mheen, A. Pessarrodona, G. V. Wood, K. Filbee-Dexter, C. J. Neufeld, S. Montie, M. A. Coleman, and T. Wernberg.
2024. Impacts of marine heatwaves in coastal ecosystems depend on local environmental conditions. Global Change Biol. 30:e17469.

Staudinger, M. D., K. E. Mills, K. Stamieszkin, N. R. Record, C. A. Hudak, A. Allyn, A. Diamond, K. D. Friedland, W. Golet, M. E. Henderson, et al.
2019. It's about time: a synthesis of changing phenology in the Gulf of Maine ecosystem. Fish. Oceanogr. 28:532–566.

Townsend, D. W.
1983. The relations between larval fishes and zooplankton in two inshore areas of the Gulf of Maine. J. Plankton Res. 5:145–173.
1984. Comparison of inshore zooplankton and ichthyoplankton populations of the Gulf of Maine. Mar. Ecol. Prog. Ser. 15:79–90.

Walsh, H. J., D. E. Richardson, K. E. Marancik, and J. A. Hare.
2015. Long-term changes in the distributions of larval and adult fish in the Northeast U.S. Shelf Ecosystem. PLoS ONE 10(9):e0137382.

Weisberg, S. J., S. M. Roberts, L. K. Gruenberg, T. G. Schwemmer, T. Menz, I. F. Fenwick, J. A. Nye, and R. G. Asch.
2024. Gulf Stream intrusions associated with extreme seasonal fluctuations among larval fishes. Mar. Ecol. Prog. Ser. 739:157–172.

National Marine Fisheries Service
NOAA

Fishery Bulletin
established in 1881

Spencer F. Baird
First U.S. Commissioner of Fisheries and founder of *Fishery Bulletin*

Assessing postrelease mortality in hook-and-line fishing of a large coastal sciaenid, the white seabass (*Atractoscion nobilis*)

Ruairi MacNamara (contact author)
Michael Shane
Victor Bach Muñoz
Mark Drawbridge

Email address for contact author: rmacnamara@hswri.org

Hubbs-SeaWorld Research Institute
2595 Ingraham Street
San Diego, California 92109

Abstract—White seabass (*Atractoscion nobilis*) are highly prized on the Pacific coast of North America. Size-based, seasonal, and spatial harvest regulations are in place for this species, leading to the release of live fish in hook-and-line fisheries. To better understand how releases may be affecting the population of this species in the Southern California Bight, 161 white seabass (420–1425 mm in total length [TL]) were captured by hook and line over a 4-year period (2021–2024). Biological, environmental, and fishing data were recorded for each capture event, and fish were subsequently released into a large (630-m^3) net pen. The short-term postrelease mortality of white seabass (i.e., within 24 h) was 14.9% overall. When assessed by using logistic regression, the best-supported model of mortality included *hooking location* and its interaction with *fish TL*. Model-predicted mortality was generally lower for fish hooked in the lip (0%–67%) than for fish hooked in the oral cavity or deeper (21%–63%), although mortality increased substantially in lip-hooked individuals >1000 mm TL (10%–67%). A small number of white seabass (11 individuals) had signs of barotrauma, with the results of a separate analysis indicating that these fish were significantly larger and captured at deeper sites than those without barotrauma. These findings can help improve fisheries management decision-making for a species that is heavily targeted by hook-and-line fishing.

Manuscript submitted 6 September 2024.
Manuscript accepted 25 February 2025.
Fish. Bull. 123:119–126 (2025).
Online publication date: 12 March 2025.
doi: 10.7755/FB.123.2.4

The views and opinions expressed or implied in this article are those of the author (or authors) and do not necessarily reflect the position of the National Marine Fisheries Service, NOAA.

In fishery systems, captured fish may be voluntarily returned to the water alive (as in catch-and-release fishing) or may be returned as a result of regulations that limit harvest. The release (or discard) of fish is an important part of managing fisheries, but quantifying postrelease mortality can be challenging. Relative to net-based gears, capture by hook and line can have distinctive effects on fish that are released (e.g., Veldhuizen et al., 2018). Species-specific studies of hook-and-line fishing are therefore necessary to understand the effects on intentionally or incidentally captured fish that are released.

Along the west coasts of the United States (California) and Mexico (Baja California), the white seabass (*Atractoscion nobilis*) is targeted commercially with gears that include hook and line, and this sciaenid is also popular among recreational anglers (Valero and Waterhouse, 2016; MacNamara et al., 2022). According to logbook records, a sizeable proportion of the white seabass captured by anglers on commercial passenger fishing vessels is released (Valero and Waterhouse, 2016). Although some work has been undertaken to examine postrelease mortality of juvenile white seabass (Aalbers et al., 2004), little is known about this issue in larger individuals (>600 mm in total length [TL]).

In the Southern California Bight, white seabass are collected from the wild to be used as broodstock for a long-standing stock-enhancement program (Drawbridge et al., 2021; MacNamara et al., 2022). Fish are captured by hook and line under a scientific collecting permit (S-201600001-21118-001) from the California Department of Fish and Wildlife that waives many recreational harvest regulations for this species (CDFW[1]). White seabass are held and monitored in a large net pen at Santa Catalina Island, an offshore island in the Southern California Bight, before being brought to the hatchery of the Hubbs-SeaWorld Research Institute on the mainland. Using this net pen, we were able to assess the effects of fishing and the biological and environmental factors that influence postrelease mortality of white seabass. The results of this multiyear study will help improve

[1] CDFW (California Department of Fish and Wildlife). 2025. Scientific collecting permits. [Web page available from website, accessed February 2025.]

the harvest regulations and stock assessments required for management of this important species.

Material and methods

Harvest regulations

Although voluntary catch and release is likely low, various size-based, seasonal, and spatial harvest regulations lead to the release of white seabass captured by hook and line. Both recreational and commercial fisheries for white seabass in California are subject to the minimum legal length of 711 mm TL (California. . .2025). A daily bag limit of 3 white seabass per angler is in effect statewide for recreational fishing, decreasing to 1 fish between 15 March and 15 June from Point Conception to the border of the United States and Mexico (i.e., in the Southern California Bight). Lastly, California's extensive network of marine protected areas includes several state marine conservation areas (CDFW[2]) in the Southern California Bight in which white seabass cannot be harvested by hook and line but similar species can be. As a result, incidental capture of white seabass may occur in those areas.

Fishing

Fishing of white seabass for this study took place annually at Santa Catalina Island in late spring and early summer from 2021 to 2024. Boat-fishing tackle commonly used to catch white seabass (30- to 50-lb test) was fished by 5–10 experienced anglers each year. Large (4/0–8/0) non-offset circle hooks and J-hooks were used; the latter were a type called *jig head* that has a small lead weight affixed to the upper shank near the eye. Live California market squid (*Doryteuthis opalescens*) were used as bait close to the seabed while at anchor. The depth at each fishing site was recorded by using the boat's echo sounder (NavNet vx2[3], Furuno Electric Co. Ltd., Nishinomiya, Japan), as an indicator of capture depth, although it is possible that some fish were hooked higher up in the water column. Sea-surface temperatures at the times of capture were obtained from the NOAA National Data Buoy Center for station 46222, located between Santa Catalina Island and the mainland (33°37′5″N, 118°19′1″W; data available from website). This data buoy, which records temperature at a depth of 0.5 m, was selected as it is the closest to the fishing grounds (approximately 28–35 km away) and data from it were available across all 4 years of the study. During scientific gill-net surveys at Santa Catalina Island (Allen et al., 2007), sea-surface temperatures in summer were only 1°C warmer on average than bottom temperatures within the depth range at which angling for white seabass took place.

Once hooked, white seabass were brought to the boat as quickly as possible (fight time was not recorded) and were landed with a large, knotless mesh landing net. Fish were placed in a 0.36-m^3 transport tank (inside dimensions: 0.98 m long by 0.65 m wide by 0.57 m high) with a seawater flow rate of approximately 75 L/min. For each fish, hooking location was recorded as occurring in the lip, roof of the mouth, or deeper (i.e., in the gills, esophagus, or stomach) (Fig. 1). Bleeding was noted but was difficult to estimate quantitatively; therefore, hooking location was used as an index of injury. The hook was removed with long-nose pliers (except in 3 deep-hooked individuals for which the line had to be cut), TL was measured to the nearest millimeter, and each fish's cheek was scanned for the presence of a coded wire tag that indicates hatchery origin. Only fish of wild origin (i.e., without a coded wire tag) were used in this study. A passive integrated transponder was injected in the left dorsoposterior musculature of each fish for identification of individuals. Each fish was kept submerged during handling, which typically lasted <1.5 min and was performed by onboard scientists. A lid was then placed over the transport tank, and the boat was driven to the net pen. All fishing occurred within 10 km of the net pen to minimize transport time (i.e., the time from being placed in the transport tank to being transferred to the net pen). Fish that died immediately upon capture were assigned a transport time of 0 min.

Fish were transferred from the transport tank to the net pen in a landing net or in a vinyl fish sling. Most fish were able to descend unaided in the net pen within a few seconds. When a live fish floated at the surface, efforts were made to right the body position and gently submerge the fish to a depth of about 1 m. If the fish did not swim away after this effort was made several times, the swim bladder was deflated (hereafter referred to as *vented*) to allow the fish to descend. Venting involved carefully penetrating the body wall at a shallow angle (<45°) from the posterior direction by using a spinal needle (1.2 by 90.0 mm) with stylet (BD Medical, Franklin Lakes, NJ). Although generally discouraged among recreational anglers in California (CDFW[4]), venting was approved for this study because of the difficulty of using a descending device within the net pen, which was shallower than most of the fishing sites and posed a snagging risk at the bottom for descended fish. Loss of equilibrium and the need to deflate the swim bladder served as an indicator of barotrauma in this study, as other gross external signs, such as exophthalmia or protrusion of the organs from the body, were generally not present (note that 2 vented individuals did have mild stomach eversion in their oral cavity).

[2] CDFW (California Department of Fish and Wildlife). 2024. California marine protected areas (MPAs). [Web page available from website, accessed November 2024.]

[3] Mention of trade names or commercial companies is for identification purposes only and does not imply endorsement by the National Marine Fisheries Service, NOAA.

[4] CDFW (California Department of Fish and Wildlife). 2024. Rockfish barotrauma and descending devices. [Web page available from website, accessed November 2024.]

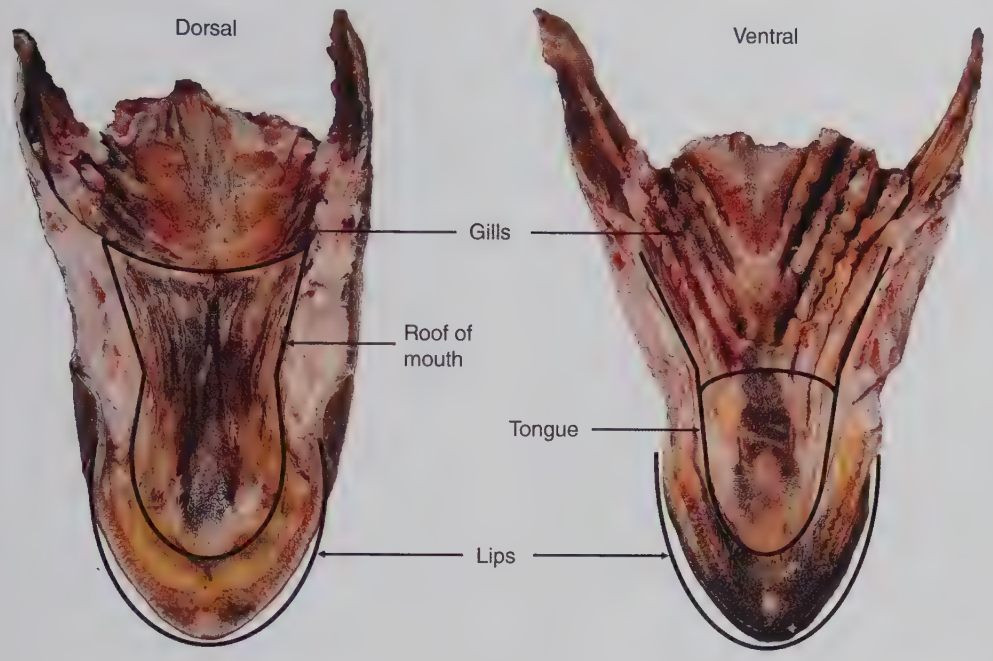

Figure 1

Horizontal plane view of the dorsal and ventral mouth parts of an adult white seabass (*Atractoscion nobilis*) caught in the Southern California Bight in 2024, showing the hooking locations for fish categorized as lip hooked and as internally hooked (roof of mouth and gills shown, esophagus and stomach not shown). Note that the tongue is shown on the ventral side for reference, although no fish were hooked in the tongue in this study.

Holding

The net pen is located in a protected cove in water with mean lower low water of 21.7 m. The pen consists of a floating frame measuring 9.7 m long by 9.7 m wide, with a containment net (3.2-cm square mesh) suspended to a depth of 6.7 m from the frame. The total volume of the containment net is 630 m^3. The containment net is surrounded by a predator net (10.0-cm square mesh). White seabass were monitored for 24 h after being placed in the net pen, and any dead fish were removed and identified by using their passive integrated transponder. White seabass that were not removed during this period were assumed to have survived short-term after release. Fish were held for several months before being transported to the hatchery of the Hubbs-SeaWorld Research Institute, but after the first 24 h, monitoring became less regular (i.e., occurring every 2–3 d, when fish were being fed). Therefore, only short-term postrelease mortality (i.e., within 24 h) could be quantitatively assessed.

Data analysis

Data for all 4 years were combined, and results from initial data exploration indicate collinearity between the variables *fish TL* and *fishing site depth*: smaller white seabass tended to be captured at shallower fishing sites and larger white seabass at deeper fishing sites (Suppl. Figure) (online only). *Fishing site depth*, therefore, was removed from the primary analysis, given that *fish TL* is more easily measured and commonly reported in fishing logs or by fishery samplers. Because depth is important in the context of fisheries management, analysis was also done with an alternative generalized linear model (GLM) in which *fish TL* is substituted for *fishing site depth* (the results of this alternative GLM are presented in Supplementary Tables 1 and 2 [online only]). Generalized linear models with the binomial response *white seabass mortality within 24 h* (0 or 1) were fitted by using a logit link in R, vers. 4.3.1 (R Core Team, 2023). The R package brglm2 (vers. 0.9.2; Kosmidis, 2023) was used because it is better suited to dealing with quasi-complete separation and rare occurrence of events in small datasets than standard GLMs, giving more conservative model estimates.

The main variable of interest was *hooking location*, which was coded as a binary categorical variable of either lip hooked or internally hooked (i.e., any fish hooked in the roof of the mouth, gills, esophagus, or stomach). The continuous predictor variables *fish TL* and *water temperature at capture* were included as main effects or as interactive effects with *hooking location*. *Transport time* was also modeled to better estimate if it may have contributed to mortality, given that fish not harvested in typical hook-and-line fishing are immediately released following capture. Multicollinearity was checked (it was detected if the variance inflation factor was >2), and

selection of candidate models was performed with Akaike information criterion corrected for small sample sizes (AICc). The model with the fewest parameters and a difference in AICc <2 between it and the best-fit model was selected. The R package ggeffects (vers. 1.7.0; Lüdecke, 2018) was used to plot values with 95% confidence intervals (CIs).

The study design limited the identification of barotrauma to individuals that survived long enough to be transported to, and placed in, the net pen. Furthermore, fish exhibiting barotrauma underwent venting to allow them to descend in the net pen; therefore, this handling step differed from the handling of fish without barotrauma. Although fish with barotrauma were included in the GLM analysis, barotrauma was not explicitly modeled as a predictor variable. Instead, a separate analysis compared *fish TL*, *fishing site depth*, *transport time*, and *water temperature at capture* among fish that had signs of barotrauma and those that did not. Mann–Whitney *U*-tests were used because of the non-normality of the data and the highly unequal group sizes.

Results

A total of 161 white seabass were captured, with sizes ranging between 420 and 1425 mm TL (mean: 837 mm TL [standard deviation (SD) 253]). Of those fish, 69 individuals had lengths less than and 92 individuals had lengths greater than the minimum legal length of 711 mm TL (Fig. 2A). White seabass were captured at fishing sites with depths of 4.6–21.3 m (mean: 10.6 m [SD 5.0]) (Fig. 2B), and more were lip hooked (number of fish [*n*]=135) than internally hooked (*n*=26) (Fig. 2C). Transport time ranged between 0 and 264 min (mean: 62 min [SD 39]) (Fig. 2D), and water temperature at the time of capture was 16.9°C–21.7°C (mean: 18.3°C [SD 1.0]) (Fig. 2E). Of the captured white seabass, 11 individuals had signs of barotrauma, 144 fish did not, and 6 individuals that died immediately upon capture could not be assessed for barotrauma (Fig. 2F). For an overall mortality of 24 white seabass (14.9%) in this study, 6 fish died immediately upon capture (all internally hooked), and an additional 18 individuals died within 24 h (Table 1).

For the GLMs, AICc values indicate clear support for the model in which the interaction of the variables *hooking location* and *fish TL* is used to examine mortality over the other candidate models (Table 2). The 95% CIs do not overlap with zero, indicating that short-term postrelease mortality of white seabass was statistically significant for hooking location and for the interaction between lip hooking and fish TL in the selected model (Table 3). Internally hooked white seabass were more likely to suffer postrelease mortality than lip-hooked white seabass (95% CI: 5.590–15.505). Mortality increased for lip-hooked white seabass as fish TL increased (95% CI: 0.003–0.011), but no statistically significant mortality trend occurred with fish TL for internally hooked white seabass (95% CI: –0.005–0.001) (Table 3).

Model-predicted mortality for a lip-hooked white seabass increased from 0% (95% CI: 0%–3%) for a 420-mm-TL fish to 67% (95% CI: 33%–89%) for a 1425-mm-TL fish; this trend was gradual up to about 1000 mm TL (mortality <10%) and much steeper between 1000 and 1425 mm TL (mortality increased from 10% to 67%) (Fig. 3A). Although not statistically significant, the estimated mortality for internally hooked white seabass decreased between 63% (95% CI: 32%–86%) for a 420-mm-TL fish and 21% (95%

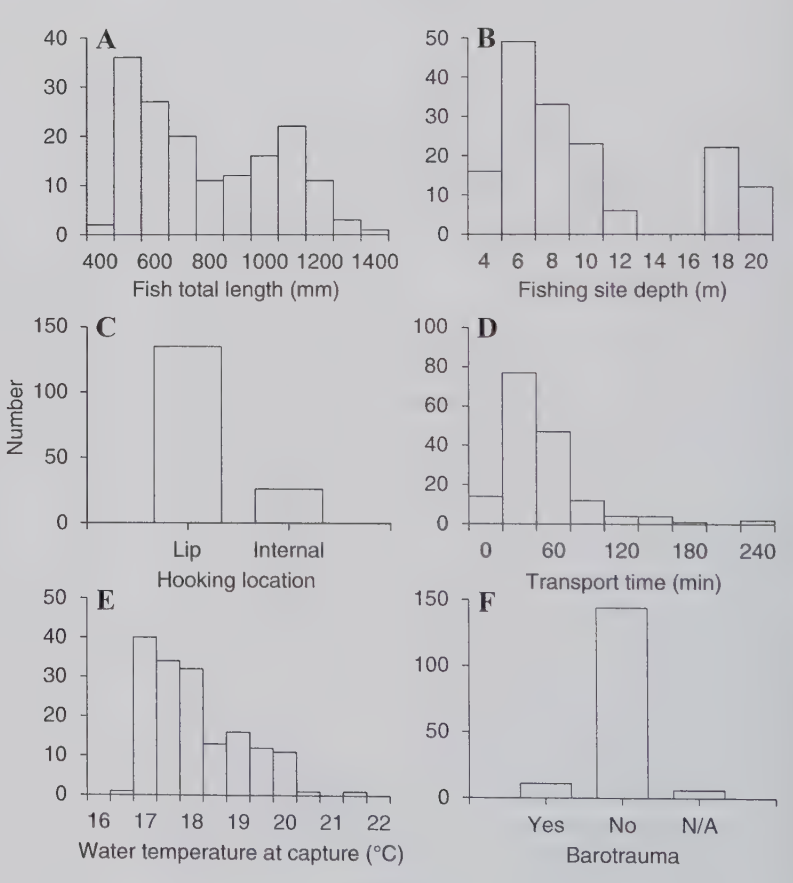

Figure 2

Frequencies of (**A**) fish total length, (**B**) fishing site depth, (**C**) hooking location, (**D**) transport time, (**E**) water temperature at capture, and (**F**) barotrauma for 161 white seabass (*Atractoscion nobilis*) captured by hook and line between 2021 and 2024 in the Southern California Bight. In panel F, *N/A* is the label for fish that died immediately upon capture and could not be assessed for barotrauma.

Table 1

Number of white seabass (*Atractoscion nobilis*) captured by hook and line in the Southern California Bight during each year of the study and all years combined. Also provided are the numbers of captured fish that died within 24 h of release and the associated rates of short-term postrelease mortality.

Year	Number captured	Postrelease mortalities	
		Number	Rate (%)
2021	33	8	24.2
2022	55	5	9.1
2023	41	4	9.8
2024	32	7	21.9
All years	161	24	14.9

CI: 3%–69%) for a 1425-mm-TL fish (Fig. 3B). Results from the use of the alternative GLM, with *fishing site depth* substituted for *fish TL*, indicate that postrelease mortality of white seabass was statistically significant for the main effects of *hooking location* and *fishing site depth* (Suppl. Tables 1 and 2) (online only).

For the subset of 155 white seabass that did not die immediately upon capture, 9 of the 11 individuals with barotrauma suffered postrelease mortality (81.8%). Fish TLs were significantly different between fish that had barotrauma and those that did not ($P<0.001$; Fig. 4A), as were the fishing site depths at which they were captured ($P<0.001$; Fig. 4B). White seabass with barotrauma were all large (850–1425 mm TL) and were captured at the deepest sites (9.1–21.3 m). In contrast, between fish that had barotrauma and those that did not, there were no differences in transport time ($P=0.931$; Fig. 4C) or water temperature at capture ($P=0.895$; Fig. 4D).

Table 2

Candidate generalized linear models used to describe short-term postrelease mortality (within 24 h) for white seabass (*Atractoscion nobilis*) captured by hook and line. The number of predictor variables in the model (K), Akaike information criterion corrected for small sample sizes (AICc), difference in AICc between the given model and the best-performing model (ΔAICc), individual model weight (AICc weight), and log-likelihood value (LL) are provided for each model. Predictor variables are *fish total length*, *hooking location*, *transport time*, and *water temperature at capture*. The selected model is the one in which the interaction of *hooking location* and *fish total length* is used. Models were fitted to data for fish caught from 2021 through 2024 in the Southern California Bight.

Model	K	AICc	ΔAICc	AICc weight	LL
Hook × length	4	100.36	0.00	1.00	−46.05
Hook + length	3	116.98	16.63	0.00	−55.41
Hook + length + temperature	4	119.10	18.74	0.00	−55.42
Hook	2	120.97	20.61	0.00	−58.45
Hook + temperature	3	122.81	22.45	0.00	−58.33
Hook × temperature	4	124.24	23.88	0.00	−57.99
Transport	2	131.31	30.96	0.00	−63.62
Null	1	137.62	37.27	0.00	−67.80

Discussion

In this study, we quantified the short-term postrelease mortality of white seabass captured by hook and line and found that hooking location is a key determinant, as has been documented for other marine fish species, including the related red drum (*Sciaenops ocellatus*) (e.g., Flaherty et al., 2013). Expanding the earlier findings of Aalbers et al. (2004) on juvenile white seabass, the results of our work indicate that mortality in larger individuals was generally low for fish hooked in the lip in comparison to mortality for those hooked in the oral cavity or deeper. The rate of internal hooking was relatively low (16.1%), but a larger sample size of fish captured using practices representative of the entire recreational fishery would allow for a better assessment of fine-scale hooking locations, as the severity of injury likely increases with proximity to sensitive areas (e.g., gills). Despite our having to create a single *internally hooked* category because of constraints on sample size, our findings highlight the need for managers to consider outreach on tactics like the use of circle hooks that have the potential to increase hooking in external mouth parts (Aalbers et al., 2004; Cooke and Suski, 2004). Any effort to change anglers' choice of hook type should be coupled with studies on how hook type might influence catch composition and size selectivity (Garner et al., 2017) and on how hook type, regardless of hooking location, might affect postrelease mortality (Vecchio and Wenner, 2007).

Fish size was another significant predictor of postrelease mortality and was examined across the size range typically captured by hook and line in California (Valero and Waterhouse, 2016). Mortality increased with size for lip-hooked white seabass, a result that has been found in some other hook-and-line capture studies (e.g., Grixti et al., 2008; Wegner et al., 2021). The increase in mortality was gradual up to a fish size of about 1000 mm TL, after which a more rapid increase occurred (albeit with fewer data points and wider CIs). This size effect could be driven by the inclusion of several large, lip-hooked individuals that were captured at the deepest fishing sites and that had barotrauma and died. Large fish (e.g., >1000 mm TL) may also have incurred disproportionately more stress due to handling, higher transport density, or longer fight times (the latter was not recorded but tends to be related to fish size in hook-and-line fishing; e.g., Zemeckis et al., 2020). The inverse size–mortality pattern for internally hooked white

Table 3

Model coefficients (estimates, standard errors, and 95% confidence intervals on a logit scale) for the selected generalized linear model fitted to data for short-term postrelease mortality (within 24 h) of white seabass (*Atractoscion nobilis*) captured by hook and line during 2021–2024 in the Southern California Bight. The selected model includes the interaction of *hooking location* and *fish total length*. *Hooking location* is coded either as lip hooked or as internally hooked (in the roof of the mouth, gills, esophagus, or stomach). The reference level for *hooking location* is lip hooked.

			95% confidence interval	
Parameter	Estimate	Standard error	Lower value	Upper value
Intercept	−9.235	2.217	−13.579	−4.890
Hooking location	10.548	2.530	5.590	15.505
Hooking location (internal) × fish total length	−0.002	0.002	−0.005	0.001
Hooking location (lip) × fish total length	0.007	0.002	0.003	0.011

seabass may be a result of this category including fewer individuals than the category for lip-hooked fish or of larger fish being more resilient than smaller fish to internal hooking damage or hook removal.

Neither short-term postrelease mortality nor the occurrence of barotrauma appear to be influenced by water temperature, but it remains to be seen if cumulative temperature effects over periods longer than 24 h lead to delayed mortality or behavioral impairment (e.g., Gale et al., 2013). The depths of fishing sites in this study (4.6–21.3 m) were similar to observed swimming depths of tagged adult white seabass during summer months (Aalbers and Sepulveda, 2015). Few white seabass had signs of barotrauma (7.1%), and the results of our analysis indicate that this condition was limited to large individuals captured at the deepest fishing sites. Venting, which may work in other species (e.g., Zemeckis et al., 2020), ultimately does not appear to be effective in white seabass (as evidenced by the deaths of 9 of the 11 vented individuals). The maximum depth of the net pen (6.7 m) may also have constrained the ability of vented individuals to remain submerged. Recompression with a descending device should be explored for reducing mortality in large white seabass that float on the surface after release.

Postrelease mortality has been assessed for recreationally targeted marine fish species in California by using electronic tags (e.g., Sepulveda et al., 2020; Wegner et al., 2021) and was documented in our study during captive monitoring of white seabass in a large enclosure. Regardless of their experimental approach, studies of postrelease mortality have limitations and potential biases. The net pen used in our study was large enough to hold white seabass at very low densities (<0.1 fish/m^3), but our use of it precluded replication because of the challenges of operating multiple pens. In addition, the net pen offered protection to compromised individuals that otherwise may have been susceptible to predation (Raby et al., 2014). Because white seabass are patchily distributed in space and time, the collection of a large number of fish from the wild for use as hatchery broodstock provided a valuable opportunity to quantify postrelease mortality. However, broodstock collection techniques differ from typical hook-and-line fishery

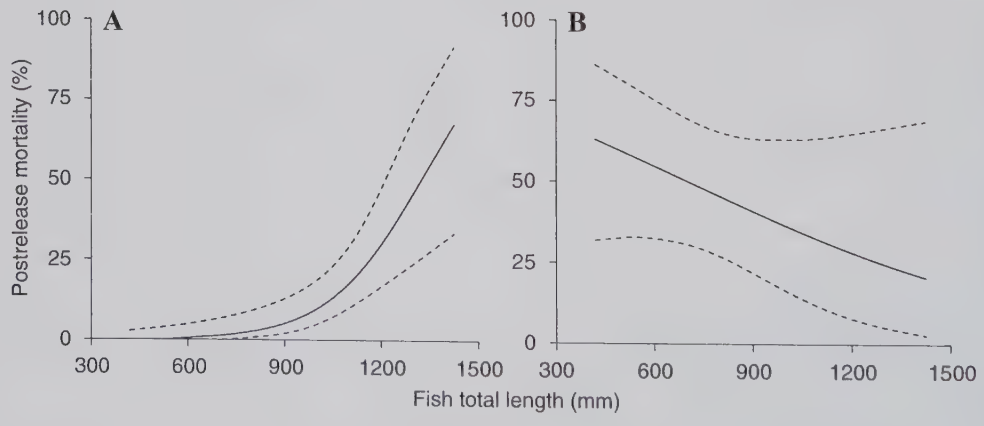

Figure 3

Model response curves showing the relationship between short-term postrelease mortality (within 24 h) and fish total length (**A**) when lip hooked or (**B**) when internally hooked for white seabass (*Atractoscion nobilis*) captured by hook and line during 2021–2024 in the Southern California Bight. Dashed lines indicate 95% confidence intervals.

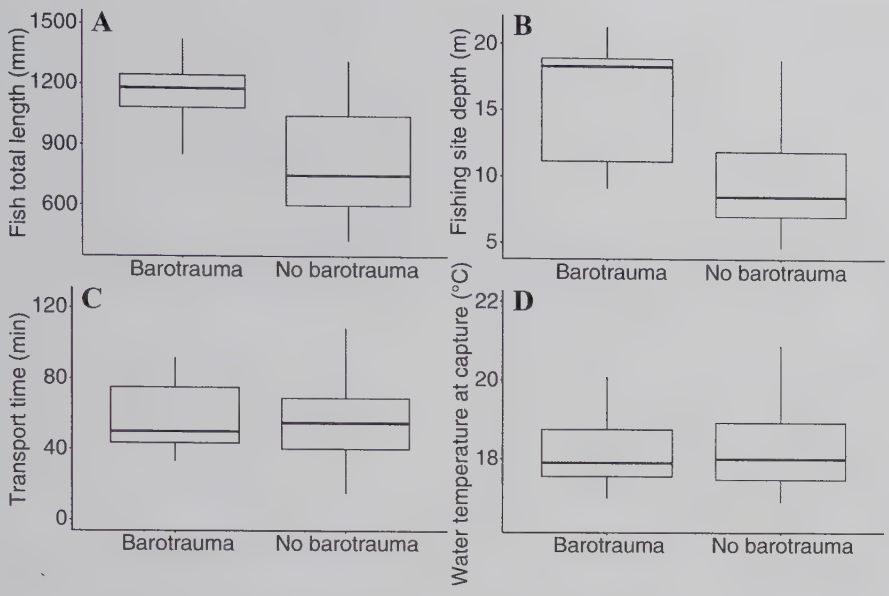

Figure 4

Box plots of (**A**) fish total length, (**B**) fishing site depth, (**C**) transport time, and (**D**) water temperature at capture for 2 groups of white seabass (*Atractoscion nobilis*) captured by hook and line from 2021 through 2024 in the Southern California Bight: fish with barotrauma (number of fish [*n*]=11) and without barotrauma (*n*=144). In each box plot, the horizontal line is the median. The upper and lower parts of each box represent the first and third quartiles (the 25th and 75th percentiles). The whiskers extend 1.5 times the interquartile range. Outliers have been removed for visual clarity.

practices; in particular, stress or trauma may be caused by transport to the net pen or by the handling process used for collections. This study also focused only on short-term mortality (within 24 h), but delayed effects are known to be important in some species (e.g., Wegner et al., 2021). Indeed, 15 white seabass died during long-term holding (1–8 months) in the 4 years of this study (Hubbs-SeaWorld Research Institute, unpubl. data), indicating that delayed or captivity effects can manifest in the net pen. Complementary techniques like blood chemistry analysis (e.g., Gallagher et al., 2014; Sepulveda et al., 2020) could allow the physiological effects of capture, handling, transport, and holding on white seabass to be better distinguished in the future.

Conclusions

Model-predicted mortality was low for lip-hooked white seabass of sublegal and legal sizes up to around 1000 mm TL, relative to those for internally hooked fish. Mortality was higher in larger fish, possibly because of barotrauma, a finding that warrants investigation of an appropriate technique for alleviation. Postrelease mortality estimates can help inform stock assessment models that were developed previously without such data being available (Valero and Waterhouse, 2016), allowing improvement of harvest regulations to better account for hook-and-line releases.

Resumen

La corvina blanca (*Atractoscion nobilis*) es muy apreciada en la costa del Pacífico de América del Norte. Existen regulaciones de captura basadas en el tamaño, la temporada y espacio para esta especie, lo que lleva a la liberación de peces vivos en las pesquerías con anzuelo y línea. Para comprender mejor cómo las liberaciones pueden estar afectando a la población de esta especie en la bahía del sur de California, se capturaron 161 corvinas blancas (420–1425 mm de longitud total [LT]) con anzuelo y línea durante un período de 4 años (2021–2024). Se registraron datos biológicos, ambientales y de pesca para cada evento de captura, y luego los peces fueron liberados en un corral de red grande (630 m^3). La mortalidad a corto plazo posterior a la liberación de la corvina blanca (es decir, dentro de las 24 h) fue del 14.9 % en total. Cuando se evaluó mediante regresión logística, el modelo de mortalidad mejor respaldado incluyó *el lugar del anzuelo* y su interacción con la *TL* del pez. La mortalidad predicha por el modelo fue, en general, menor para los peces enganchados en el labio (0%–67%) que para los peces enganchados en la cavidad oral o a mayor profundidad (21%–63%), aunque la mortalidad aumentó sustancialmente en los individuos enganchados en el labio >1000 mm TL (10%–67%). Un pequeño número de corvinas blancas (11 individuos) presentaban signos de barotrauma, y los resultados de un análisis separado indicaron que estos peces eran significativamente

más grandes y se capturaban en lugares más profundos que los que no presentaban barotrauma. Estos resultados pueden contribuir a mejorar la toma de decisiones de manejo pesquero para una especie que es objeto de una pesca intensiva con anzuelo y línea.

Acknowledgments

We thank J. Albright, C. Albright, D. Elm, and their crews for supporting the study. E. Hernandez, C. Brewer, C. Macherzak, J. Johnson, and members of the Coastal Conservation Association of California assisted in the field. Comments from 3 anonymous reviewers helped improve the manuscript. The work was funded by the Ocean Resources Enhancement and Hatchery Program of the California Department of Fish and Wildlife and supported in part by the Catalina Seabass Fund and SeaWorld Busch Gardens Conservation Fund.

Literature cited

Aalbers, S. A., and C. A. Sepulveda.
2015. Seasonal movement patterns and temperature profiles of adult white seabass (*Atractoscion nobilis*) off California. Fish. Bull. 113:1–14.

Aalbers, S. A., G. M. Stutzer, and M. A. Drawbridge.
2004. The effects of catch-and-release angling on the growth and survival of juvenile white seabass captured on offset circle and J-type hooks. N. Am. J. Fish. Manag. 24:793–800.

Allen, L. G., D. J. Pondella II, and M. A. Shane.
2007. Fisheries independent assessment of a returning fishery: abundance of juvenile white seabass (*Atractoscion nobilis*) in the shallow nearshore waters of the Southern California Bight, 1995–2005. Fish. Res. 88:24–32.

California Fish and Game Code §8383.5 (2025). [Available from website, accessed February 2025.]

Cooke, S. J., and C. D. Suski.
2004. Are circle hooks an effective tool for conserving marine and freshwater recreational catch-and-release fisheries? Aquat. Conserv. 14:299–326.

Drawbridge, M., M. Shane, and C. Silbernagel.
2021. The status of white seabass, *Atractoscion nobilis* as a commercially ready species for marine US aquaculture. J. World Aquac. Soc. 52:647–661.

Flaherty, K. E., B. L. Winner, J. L. Vecchio, and T. S. Switzer.
2013. Spatial and size distribution of red drum caught and released in Tampa Bay, Florida, and factors associated with post-release hooking mortality. Gulf Caribb. Res. 25:29–41.

Gale, M. K., S. G. Hinch, and M. R. Donaldson.
2013. The role of temperature in the capture and release of fish. Fish Fish. 14:1–33.

Gallagher, A. J., J. E. Serafy, S. J. Cooke, and N. Hammerschlag.
2014. Physiological stress response, reflex impairment, and survival of five sympatric shark species following experimental capture and release. Mar. Ecol. Prog. Ser. 496:207–218.

Garner, S. B., W. F. Patterson III, and C. E. Porch.
2017. Experimental assessment of circle vs. J hook performance and selectivity in the northern Gulf of Mexico recreational reef fish fishery. ICES J. Mar. Sci. 74:1437–1447.

Grixti, D., S. D. Conron, A. Morison, and P. L. Jones.
2008. Estimating post-release survival and the influential factors for recreationally caught black bream (*Acanthopagrus butcheri*) in the Glenelg River, south eastern Australia. Fish. Res. 92:303–313.

Kosmidis, I.
2023. brglm2: bias reduction in generalized linear models. R package, vers. 0.9.2. [Available from website, accessed July 2024.]

Lüdecke, D.
2018. ggeffects: tidy data frames of marginal effects from regression models. J. Open Source Softw. 3(26):772.

MacNamara, R., M. Shane, and M. Drawbridge.
2022. Understanding the long-term movement patterns of hatchery-reared white seabass. Environ. Biol. Fishes 105:1797–1808.

R Core Team.
2023. R: a language and environment for statistical computing. R Foundation for Statistical Computing, Vienna, Austria. [Available from website, accessed July 2024.]

Raby, G. D., J. R. Packer, A. J. Danylchuk, and S. J. Cooke.
2014. The understudied and underappreciated role of predation in the mortality of fish released from fishing gears. Fish Fish. 15:489–505.

Sepulveda, C. A., S. A. Aalbers, M. Wang, J. Kneebone, and D. Bernal.
2020. Post-release survivorship of Pacific bluefin tuna (*Thunnus orientalis*) captured in the California recreational fishery. Fish. Res. 223:105413.

Valero, J., and L. Waterhouse.
2016. California white seabass stock assessment in 2016, 191 p. Cent. Adv. Popul. Assess. Methodol., La Jolla, CA. [Available from website.]

Vecchio, J. L., and C. A. Wenner.
2007. Catch-and-release mortality in subadult and adult red drum captured with popular fishing hook types. N. Am. J. Fish. Manag. 27:891–899.

Veldhuizen, L. J. L., P. B. M. Berentsen, I. J. M. De Boer, J. W. van de Vis, and E. A. M. Bokkers.
2018. Fish welfare in capture fisheries: a review of injuries and mortality. Fish. Res. 204:41–48.

Wegner, N. C., E. J. Portner, D. T. Nguyen, L. Bellquist, A. P. Nosal, A. L. Pribyl, K. L. Stierhoff, P. Fischer, K. Franke, R. D. Vetter, et al.
2021. Post-release survival and prolonged sublethal effects of capture and barotrauma on deep-dwelling rockfishes (genus *Sebastes*): implications for fish management and conservation. ICES J. Mar. Sci. 78:3230–3244.

Zemeckis, D. R., J. Kneebone, C. W. Capizzano, E. A. Bochenek, W. S. Hoffman, T. M. Grothues, J. W. Mandelman, and O. P. Jensen.
2020. Discard mortality of black sea bass (*Centropristis striata*) in a deepwater recreational fishery off New Jersey: role of swim bladder venting in reducing mortality. Fish. Bull. 118:105–119.

National Marine
Fisheries Service
NOAA

Fishery Bulletin
established in 1881

Spencer F. Baird
First U.S. Commissioner
of Fisheries and founder
of *Fishery Bulletin*

Age structure and seasonal movement of Atlantic sturgeon (*Acipenser oxyrinchus*) aggregating in eastern Long Island Sound and the Connecticut River

Kelli C. Mosca[1]
Thomas F. Savoy[1]
Jacqueline B. Roberts[1]
Evan C. Ingram[2]
Eric T. Schultz[3]
Hannes Baumann (contact author)[4]

Email address for contact author: hannes.baumann@uconn.edu

[1] Fisheries Division
Connecticut Department of Energy and
Environmental Protection
333 Ferry Road
Old Lyme, Connecticut 06371

[2] School of Marine and Atmospheric Sciences
Stony Brook University
Stony Brook, New York 11794

[3] Department of Ecology and
Evolutionary Biology
University of Connecticut
75 North Eagleville Road
Unit 3043
Storrs, Connecticut 06269

[4] Department of Marine Science
University of Connecticut
1080 Shennecossett Road
Groton, Connecticut 06340

Abstract—Atlantic sturgeon (*Acipenser oxyrinchus*) seasonally aggregate in Long Island Sound and the Connecticut River, but their size and age structure and use of the river remain insufficiently understood. We analyzed all available length data from monitoring efforts (1988–2021: number of samples [*n*]=3544), estimated age from sections of pectoral-fin spines (*n*=296), and measured annuli widths for retrospective size-at-age analysis (*n*=166). Fish ranged from 21 to 218 cm in total length ([TL], mean: 105.2 cm TL), but 87% of them measured 50–130 cm TL. Ages ranged from 0 to 18 years (mean: 8.1 years), with 92% of all individuals estimated to be younger than 12 years. Annuli widths indicate that faster growing fish selectively disappeared from the study area over time. To reveal movement patterns, particularly for the upper Connecticut River (freshwater), we analyzed 3 years (2019–2021) of acoustic detections of 85 individuals. These fish occurred in the study area from March through November but stayed on average only 54–91 d. The majority of fish entering the receiver arrays in Long Island Sound also moved into the river but largely utilized its lower, brackish estuary. Still, a large proportion of individuals (35%–66%) made upriver excursions into freshwater, and the timing coincided with low flow and warm river temperatures in late summer. Therefore, both the brackish and freshwater portions of the Connecticut River serve as important seasonal feeding habitats for Atlantic sturgeon ≤130 cm TL.

Manuscript submitted 24 August 2024.
Manuscript accepted 28 February 2025.
Fish. Bull. 123:127–142 (2025).
Online publication date: 19 March 2025.
doi: 10.7755/FB.123.2.5

The views and opinions expressed or implied in this article are those of the author (or authors) and do not necessarily reflect the position of the National Marine Fisheries Service, NOAA.

Sturgeon (Acipenseridae) are among the most endangered fish groups in the world, as historic overexploitation and habitat destruction have long decimated the populations of most of its extant 25 species (Pikitch et al., 2005). The Atlantic sturgeon (*Acipenser oxyrinchus*) is an anadromous species that occurs in waters along the Atlantic coast of North America from the Florida peninsula to the Gulf of St. Lawrence in Canada (a range approximately from 30°N to 52°N; Hilton et al., 2016). Juveniles remain in their natal rivers for 1–6 years before entering marine waters (Dovel and Berggren, 1983). Subadults, a group that includes fish 50–130 cm in total length [TL], then form aggregations and migrate along the coast, where they utilize natal and non-natal river estuaries to feed (Waldman et al., 2013). Overexploitation of this large, slow-growing, and late-maturing species during the 19th and 20th centuries caused severe population declines and triggered a coast-wide fishing moratorium in 1998 (Secor, 2002). River pollution, obstruction of freshwater spawning habitats by dams, vessel strikes, and dredging all acted to exacerbate negative abundance trends (Waldman et al., 2019). Today, all 5 genetically distinct population segments (DPSs) in the United States (i.e., the South Atlantic, Carolina, Chesapeake Bay, New York Bight, and Gulf of Maine DPSs) are listed as either endangered or threatened under the Endangered Species Act (Federal Register, 2012a, 2012b). Spawning populations are thought to have been lost from 13–19 of the 38 rivers across the Atlantic seaboard where they have historically been found (ASSRT, 2007; ASMFC, 2017; Waldman et al., 2019).

The Connecticut River is the largest river in New England (653 km long) and the main freshwater source to Long Island Sound (Koppelman et al., 1976). Historical records indicate

that Atlantic sturgeon utilized and presumably spawned in several upstream locations in the Connecticut River (Galligan, 1960), but all spawning runs probably ceased in the early 20th century. Yet, both the Connecticut River and Long Island Sound still provide essential habitat for Atlantic sturgeon (Federal Register, 2017) because Atlantic sturgeon of all 5 DPSs are known to aggregate there from late spring to early fall presumably to feed or seek physiological refuge (Savoy and Pacileo, 2003; Waldman et al., 2013). The upper, freshwater portion of the Connecticut River (which begins at river kilometer [rkm] 22) could be of particular importance because Atlantic sturgeon appear to use it as either foraging ground or again as potential spawning habitat, the latter indicated by the recent discovery of pre-migratory juveniles in the river (Savoy et al., 2017).

The Connecticut Department of Energy and Environmental Protection (DEEP) has monitored Atlantic sturgeon in the area of Long Island Sound and the Connecticut River since 1988, by collecting samples of pectoral-fin spines for age determination and, more recently, by deploying receivers to detect acoustically tagged individuals (Savoy[1]). Fin spines of Atlantic sturgeon have been sampled nonlethally and can be used to determine age from annuli counts with acceptable precision (Stevenson and Secor, 1999). Furthermore, the proportionality of somatic and fin spine growth in sturgeons (Sunde, 1961; Kehler et al., 2018) is similar to the known coupling of somatic and otolith or scale growth in other fish species (Campana, 1990; Baumann et al., 2013), allowing back-calculation of lengths and growth characterization for individuals.

In this study, we analyzed the DEEP fin spine collection and recent DEEP telemetry data[2] because they both hold relevant, complementary information for conservation of Atlantic sturgeon in Long Island Sound and the Connecticut River. For example, size-at-age analyses allowed inferring whether the area is utilized only by juveniles and subadults or also to some extent by adults and how their respective length-at-age patterns compare to those of Atlantic sturgeon from other studied aggregations. In addition, the acoustic detections of tagged Atlantic sturgeon allowed us to develop detailed insights into what areas of Long Island Sound and the Connecticut River are of particular importance to Atlantic sturgeon and in what season, information that is critical for refining conservation measures.

The first objective of this study therefore was to quantify the length and age structure of Atlantic sturgeon by analyzing already existing samples of pectoral-fin spines. We hypothesized that the aggregation of Atlantic sturgeon in Long Island Sound and the Connecticut River consists predominantly of subadults and that their length-at-age patterns are similar to those recently compiled for Atlantic sturgeon in the New York Bight (Dunton et al., 2016). Back-calculation of the lengths of individuals specifically allowed us to test for changes in the variability of growth phenotypes with increasing age at capture. Our second objective was to analyze 3 years (2019–2021) of existing telemetry records for Atlantic sturgeon to determine their habitat utilization and areas of seasonal occupancy in the sound and the estuarine and freshwater portions of the river. We were particularly interested in the sizes of Atlantic sturgeon that make freshwater excursions into the upper Connecticut River to infer whether such behavior could be related to spawning. Lastly, we correlated the seasonal occupancy patterns to 2 environmental parameters, temperature and discharge volume in the Connecticut River, to identify signals for upriver movements.

Materials and methods

Fin spine samples: age and growth

Atlantic sturgeon were caught with gill nets or skiff trawls in the Connecticut River (rkm 0–52) and in adjacent eastern Long Island Sound (Fig. 1) from April through November in 1988–2021 by using procedures detailed in Damon-Randall et al. (2010). Gill nets had 100.0-by-2.3-m panels of different mesh sizes (7.6–25.4-cm stretched mesh) to maximize catchability across the expected size spectrum for Atlantic sturgeon (20–200 cm TL) (Moser et al., 2000; Damon-Randall et al., 2010). Gill nets were deployed for ≤2 h, and trawl nets (9.7 by 7.0 m, 2-cm codend mesh) were towed for ≤12 min at 1.5 kt. All captured Atlantic sturgeon were measured for TL and operationally classified as juveniles (<50 cm TL), subadults (50–130 cm TL), and adults (>130 cm TL) on the basis of permitting definitions of the National Marine Fisheries Service (NMFS[3]; Ingram et al., 2019). Because their sex and spatial origin were not known, we purposefully defined adults as broadly as possible, potentially including fish from southern DPSs (the South Atlantic and Carolina DPSs) that can be mature at 130 cm TL (Collins et al., 2000; Balazik et al., 2012). Samples for aging were taken from a subset of 50 individuals per year (25 fish that were <100 cm TL and 25 fish that were >100 cm TL) by clipping off a roughly 2-cm section of the right pectoral-fin spine (Suppl. Fig. 1) (online only). Immediately following these procedures, individuals were released. All methods used for capture and sampling of Atlantic sturgeon were approved and permitted by NOAA permits 16323 (prior to 2017) and 19641 (beginning in 2017).

A total of 301 pectoral-fin spines from Atlantic sturgeon were available in the DEEP collection for age analysis. Samples were air dried for at least 2 months prior to

[1] Savoy, T. 2017. Assessing reproduction of Atlantic and shortnose sturgeon in the Connecticut River, 15 p. Annual federal aid report for the State Wildlife Grant Program. [Available from Conn. Dep. Energy Environ. Prot., 333 Ferry Rd., Old Lyme, CT 06371.]

[2] Source data from this study are available upon request from the senior and contact authors.

[3] NMFS (National Marine Fisheries Service). 2024. Authorizations and permits for protected species (APPS): location/take information. [Web page available from website, last modified March 2024.]

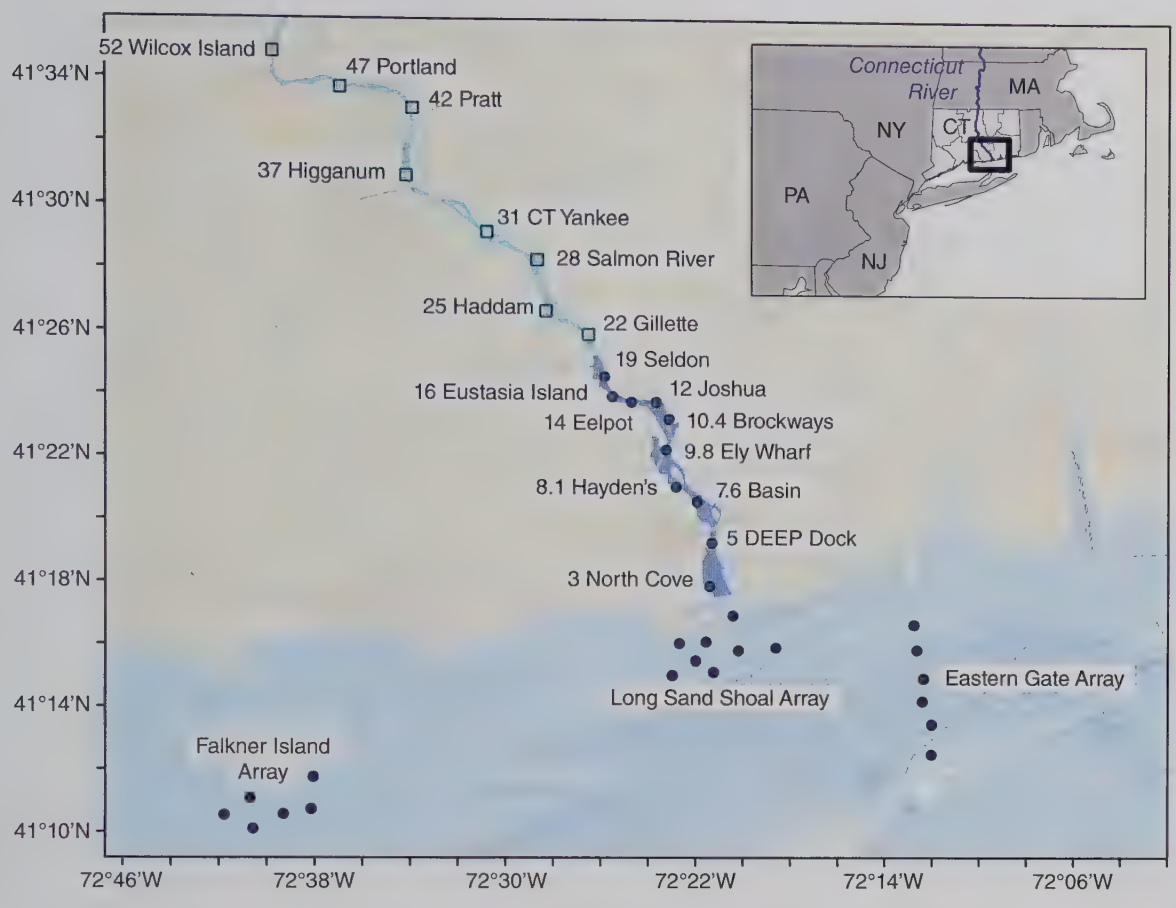

Figure 1

Map of the study area of eastern Long Island Sound and the Connecticut River in the northeastern United States, showing the locations where Atlantic sturgeon (*Acipenser oxyrinchus*) were captured and tagged from April through November during 2019–2021. Fish were tagged at the mouth of and all along the river, up to river kilometer (rkm) 52. Each receiver in the river is labeled with a numeral for the river kilometer of its location and the station name assigned to it by the Connecticut Department of Energy and Environmental Protection. For analysis and presentation of data from this study, receivers in the river are grouped into 2 areas: the brackish estuary (rkm 3–19; blue circles and river shading) and the freshwater upper section (rkm 22–52; cyan squares and river shading). Dark blue circles indicate the acoustic receivers that make up the 3 arrays in the sound, Long Sand Shoal, Eastern Gate, and Falkner Island. Data from receivers placed in the river beyond rkm 52 (at Wilcox Island) were omitted because those receivers recorded no detections of Atlantic sturgeon during the study period. Basemap data sources: NOAA OCS, Esri, DeLorme, and NaturalVue.

sectioning by using an IsoMet Low Speed Saw (Buehler Lake Bluff, IL) equipped with double diamond-dusted blades to produce sections approximately 0.4 mm thick. Calibrated images of each fin spine section on a dark background were taken with an Axiocam 105 digital camera (Zeiss, Oberkochen, Germany) connected to a Zeiss Discovery V8 stereomicroscope with transmitted light at 15× magnification. Analysis of these images was done with Image-Pro Premier software (vers. 9.0 and 10.0; Media Cybernetics, Rockville, MD). Each annulus was defined as an opaque zone paired with an adjacent translucent zone, except for the first annulus, which always takes the form of a star- or tree-shaped translucent ring (Kehler et al., 2018). We counted only annuli with translucent zones traceable around most of the spine (Baremore and Rosati, 2014) and measured interannular distances along a consistent straight axis (Suppl. Fig. 1) (online only). A considerable proportion of spine sections (n=130, 43%) contained inclusions, which are secondary fin rays that get absorbed into the lobes of the primary spine (Suppl. Fig. 1) (online only). Such samples could still be aged with confidence but precluded measurements of interannular distances for length back-calculation. Five samples were removed because of poor image quality, yielding 296 aged specimens, 90% of them caught after 2006.

Samples were examined blind 3 times by the primary age reader and 1 time by a second age reader, who did not know the age estimates of the primary reader. Aging

precision was estimated within and between readers. We first computed the coefficient of variation (CV) for each fish j:

$$CV_j = 100\frac{\sqrt{\sum_{i=1}^{N}\frac{\left(X_{ij}-X_j\right)^2}{N-1}}}{X_j}, \quad (1)$$

where N = the number of times the fish was aged;
X_{ij} = the ith age reading for fish j; and
X_j = the mean age for fish j.

Then, we averaged the CVs for individual fish to obtain the mean CV across all aged fish, resulting in a mean CV of 9.4% between the 3 age estimates of the primary age reader and a mean CV of 12.1% between the age estimates of the primary and secondary readers. For 36% and 27% of samples, respectively, the 3 readings by the primary reader and the estimates by both readers yielded the same age. An age discrepancy of ≤2 years was found between the estimates by the primary reader for 96% of samples and between readings by the 2 readers for 87% of samples. Importantly, between-reader deviations in age estimates were randomly distributed, as indicated by a nonsignificant result from Bowker's test of symmetry (P=0.17, Suppl. Fig. 2 [online only]).

Because the 296 Atlantic sturgeon for which age was estimated represent a nonrandom, length-stratified subset of all individuals caught over time (n=3544), the age distribution was corrected for over- and underrepresentation of size classes relative to the total catch (Chih, 2009). The full sample of all captured fish and the subset of 296 samples used in age and growth analysis were binned into 5-cm-TL size classes, and the relative frequency of each size class was used to compute its weighting factor (proportion of full sample/proportion of subset) (Fig. 2). This factor was then used as a statistical weight for each aged individual in its corresponding size class. The aggregation of Atlantic sturgeon in Long Island Sound and the Connecticut River cannot be considered a population (mixed stock plus a few, if any, adults); therefore, we refrained from estimating the growth coefficient and asymptotic length with a population-based growth model. However, we visually compared our length-at-age data to a robust growth model compiled from published studies on age and growth of Atlantic sturgeon (Dunton et al., 2016).

For the subset of Atlantic sturgeon with longitudinal annuli measurements (n=166), we first ascertained that TL and fin spine size (radius at capture [R_C]) were linearly related (TL=11.3+19.7×R_C; coefficient of determination=0.70, P<0.001). Because that was the case, we then proceeded to estimate length at age of individuals with a commonly used, proportional back-calculation method (the "biological intercept" method; Campana, 1990):

$$TL_i = TL_c + \frac{\left(R_i - R_c\right)\left(TL_c - TL_0\right)}{R_c - R_0}, \quad (2)$$

where TL_i = the fish TL at the ith annulus;
TL_c = the fish TL at capture;
R_i = the spine radius at the ith annulus;
R_0 = the spine radius (set to 0); and
TL_0 = the fish TL at the biological intercept (0.7 cm TL; Bain, 1997).

We then examined these data for the selective disappearance of fast or slow growth phenotypes from the aggregation with increasing age, using linear regressions of age at catch versus back-calculated TL at different previous ages.

Telemetry data: habitat utilization

Members of the DEEP staff used approved methods (Damon-Randall et al., 2010; Kahn and Mohead, 2010) to surgically implant acoustic transmitters (V7–V16 tags, InnovaSea Systems Inc., Boston, MA) in Atlantic sturgeon caught within the study area from 2014 through 2021 (Suppl. Table 1) (online only). Up to 35 subadult and adult Atlantic sturgeon were tagged per year, resulting in a total of 114 acoustic tags deployed by the DEEP since 2014. However, 84% of all tag deployments occurred in 2019–2021 (Suppl. Table 1) (online only); hence, data from only these 3 years were analyzed in our study for movement patterns and drivers. The DEEP also maintained several arrays of acoustic receivers (VR2W-69 kHz, VR2Tx, VR2AR monitoring receivers, InnovaSea Systems Inc.) in eastern Long Island Sound and the Connecticut River (Fig. 1). The array in the sound consisted of sub-arrays at Long Sand Shoal, Eastern Gate, and Falkner Island. The array in the river included up to 45 receivers placed linearly from the estuary to the Holyoke Dam (rkm 3–135). However, Atlantic sturgeon were detected only until rkm 52 (at Wilcox Island), and receivers were consistently deployed up to this point during the study period (Fig. 1). Receivers had a nominal detection radius of 1000 m to ensure coverage of the entire width of the Connecticut River (200–900 m). Receivers were retrieved monthly to download data and were immediately redeployed at consistent locations (±100 m).

Raw data for acoustic detections of tagged fish were compiled and analyzed by using the glatos package (vers. 0.4.0; Binder et al., 2018) in R (vers. 4.1.2; R Core Team, 2021). False detections (0.6%–1.0% of all detections) of Atlantic sturgeon were defined as those with an interval of >1 h between consecutive detections of any individual at any given receiver (Simpfendorfer et al., 2015). Data from 1 tag was excluded from analysis because the continuous detection of the fish with this tag over multiple years by a single receiver indicates that the fish either expelled the tag or expired near the receiver. Other extracted data were total number of detections, number of detecting receivers, and the date of first and last detection in the Connecticut River per year. As an additional step, we plotted the date of detection against its location (river kilometer) for each individual and visually inspected the derived abacus plots for plausibility and overall patterns (Suppl. Fig. 3) (online only). Finally, we used the recommended procedure in the glatos package to condense the millions of discrete detections into a series of year-, receiver-, and fish-specific "events," with a new event created in the following

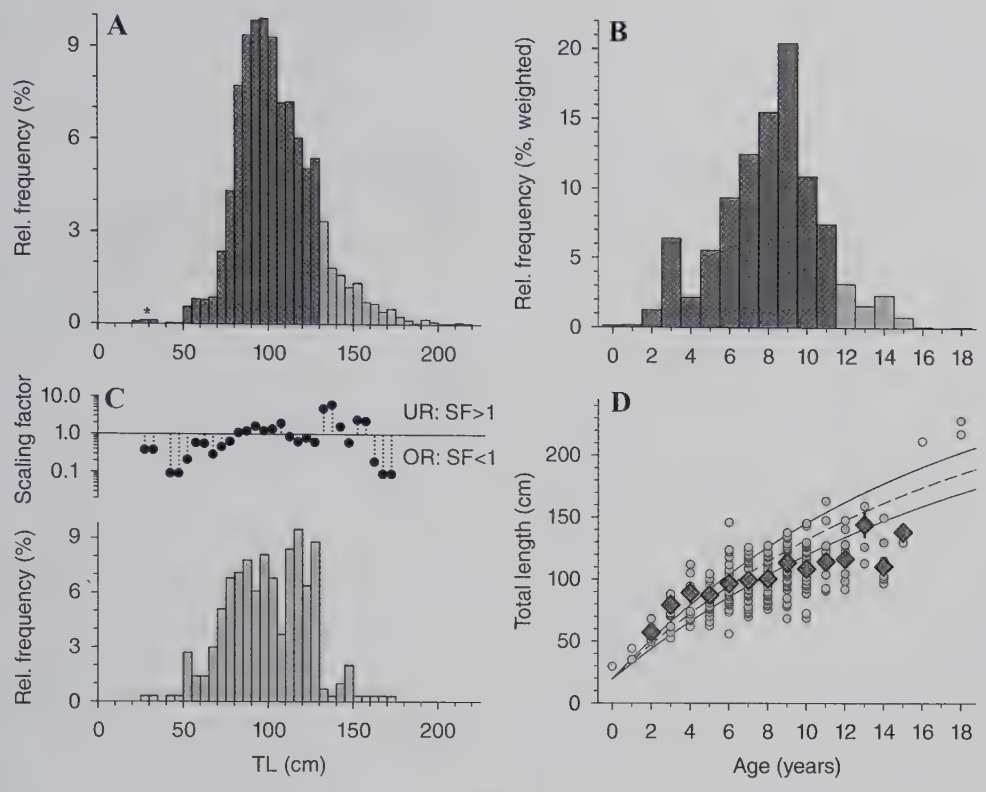

Figure 2

Length and age of the seasonal aggregation of Atlantic sturgeon (*Acipenser oxyrinchus*) in eastern Long Island Sound and the Connecticut River between 1988 and 2021. (**A**) Relative length distribution by size class (interval: 5 cm in total length [TL]) for all Atlantic sturgeon caught in the study period (number of samples [*n*]=3544), and (**B**) relative weighted age distribution based on analysis of sections of pectoral-fin spines from a subset of those fish (*n*=296). The asterisk in panel A denotes likely pre-migratory juveniles (20–35 cm TL). The light gray bars in panels A and B indicate distribution of adults, defined as those with sizes and ages greater than 130 cm TL and 12 years. (**C**) Relative length distribution of aged fish (*n*=296) (bottom graph) and statistical scaling factors (SF, black circles in top graph) derived for each size class, depending on whether age analysis overrepresented (OR) or underrepresented (UR) a given size class relative to the distribution for all captured fish in panel A. (**D**) Age–length relationship of Atlantic sturgeon (*n*=296). Circles represent age estimates for individuals, and diamonds represent weighted means for fish at ages 2–15. For the purpose of comparison, the dashed line and solid lines indicate the growth curve and 95% confidence interval from the model for Atlantic sturgeon compiled by Dunton et al. (2016).

manner: 1) every 6 h (approximately 0.5 of a tidal cycle) for fish "heard" consecutively at the same receiver, 2) if >6 h elapsed between consecutive detections on the same receiver, or 3) if a fish was detected at a new receiver. Using the start and end time of each event, we then calculated its duration and then summed up all event durations per year, receiver, and fish.

To broadly characterize habitat utilization by Atlantic sturgeon, we grouped DEEP receivers into 3 categories by habitat (Fig. 1): Long Island Sound (all sub-arrays) and the estuary (rkm 3–19) and upper section (≥rkm 22) of the Connecticut River. Distinguishing occupancy of the brackish estuarine waters of the lower section from that of the freshwater upper section of the Connecticut River was important because Atlantic sturgeon are anadromous and may migrate into freshwater for spawning. We delineated the 2 sections of the river following Meade (1966) and using long-term average salinity data from 2 monitoring stations of the U.S. Geological Survey (USGS) at Old Lyme and Essex (Connecticut water conditions, data available from website). For each fish and year, we aggregated the total time detected at receivers of each category and expressed it as the proportion of the overall time detected for each individual fish (Long Island Sound+estuary+upper section=100%). For each year, we also computed a weighted average of the number of days spent in each area, with the weight proportional to the total number of days detected for each individual. To visualize spatiotemporal clusters of occurrence of Atlantic sturgeon in the river, we computed kernel densities of aggregated detections per year and plotted them against

date and river kilometer by using the R package ggplot2, vers. 3.3.5 (Wickham, 2016). We also extracted the annual dates of first and last detection in the Connecticut River for every fish (i.e., in both the estuary and upper section), but for computing averages, the tagging year was excluded to avoid bias in the mean date of first detection.

We hypothesized that larger Atlantic sturgeon 1) went farther upstream or 2) spent more time in the freshwater upper portion of the Connecticut River, which would support the notion that they utilized the upper section as spawning habitat. To test these hypotheses, we first adjusted the TL of each individual from the year of tagging to each year of detection (2019, 2020, and 2021) by applying a von Bertalanffy growth function using the values for growth coefficient, asymptotic maximum length, and theoretical age at which length is zero published by Dunton et al. (2016). For each fish and year, we then extracted the maximum river kilometer and the number of days spent in the upper section of the river, followed by year-specific and overall bivariate Pearson correlation analyses between TL at detection and 1) number of days in the upper section or 2) max river kilometer.

To analyze potential environmental cues for seasonal movement of Atlantic sturgeon into the Connecticut River, we used USGS data (USGS Current Water Data for Connecticut, available from website) to extract daily discharge volume for the Connecticut River (in cubic meters per second) from the nearest station in Thompsonville (USGS gauging station 01184000, at rkm 106). With this approach, we assumed that upriver flow patterns were also predictive of flow conditions farther downstream. Daily bottom temperatures (in degrees Celsius) were extracted and then averaged from 3 USGS gauging stations: Middle Haddam (01193050, at rkm 25), Essex (01194750, at rkm 9), and Old Lyme (01194796, at rkm 5) stations. For better visualization, we used nonparametric locally estimated scatterplot smoothing (20% bandwidth) on all daily values. River temperature and flow conditions both followed a strong seasonal pattern and were negatively correlated to each other (correlation coefficient [r]=–0.55, P<0.001, n=624). Hence, we first computed overall weekly averages (for the period 2019–2021) and then subtracted them from the annual weekly averages to obtain weekly temperature and discharge anomalies. These anomalies were then correlated to similarly derived weekly anomalies of the percentage of Atlantic sturgeon in the Connecticut River (estuary and upper section) relative to the total number of fish detected in a given year.

Given the migratory nature of Atlantic sturgeon (Waldman et al., 2013), some detections were likely of fish with acoustic tags implanted by research groups other than the DEEP. We therefore queried the databases of the Mid-Atlantic Telemetry Observation System (available from website) and the Atlantic Cooperative Telemetry Network (available from website) to determine which research institution implanted these tags and where the tagging was done. We then extracted summary statistics for these detections pooled over all 3 years, including the total number of detections by region and institution and the number of detected fish (n=114), for the entire study area and for only the upper section of the Connecticut River.

Results

Atlantic sturgeon caught since 1988 in Long Island Sound and the Connecticut River (n=3544) ranged in size from 21 to 218 cm TL, with a mean of 105.1 cm TL (standard deviation [SD] 23.4) (Fig. 2A). Juveniles (<50 cm TL) made up 0.4% (n=13) of Atlantic sturgeon collected in 1988–2021. The vast majority (86.6%, n=3087) of all the captured fish were subadults (50–130 cm TL), and 13% (n=444) of them were adults (>130 cm TL). Ages ranged from 0 to 18 years with a weighted mean of 8.1 years (SD 2.7) and a median of 8 years (n=296). In our study, 92% of the Atlantic sturgeon for which pectoral-fin spines were analyzed were 11 years or younger (Fig. 2B). Back-calculated TLs at ages 2–6 declined with increasing age at capture (linear regression: all P≤0.003; Fig. 3), indicating that faster growing individuals selectively disappeared from the aggregation in Long Island Sound and the Connecticut River.

Between 2019 and 2021, acoustic receivers in our study area logged 1.38 million detections of a total of 85 unique Atlantic sturgeon tagged by the DEEP (mean: 8463 detections/fish; range: 2–30,384 detections/fish). At the time of tagging, fish ranged in size from 52.5 to 164.5 cm TL (mean: 109.6 cm), with 20% of them >130 cm TL. Tagging efforts continued throughout the study period; as a result, the number of detected Atlantic sturgeon more than doubled and annual detections quadrupled from 2019 to 2021 (Table 1, Fig. 4). Of all Atlantic sturgeon tagged in a given year, over 85% were redetected in the subsequent year or years. A total of 22 specimens were detected in all 3 years. We found that fish spent on average 2–3 months, maximally 4–6 months, in the study area (Fig. 1; Table 1). Once in Long Island Sound, over 90% of fish also entered the Connecticut River (estuary and upper section); only a small fraction remained exclusively in Long Island Sound each year (2%–8%, Fig. 4). The first fish entered the river between early March and early May, but it took from 2 weeks to 3 months for 50% of the fish detected in a given year to enter the river at least once (Table 1). Most fish utilized the Connecticut River, and 31%–57% of fish remained within the estuary (Fig. 4). Of the fewer Atlantic sturgeon that proceeded farther upstream and utilized the upper section of the river, half stayed there for fewer than 7 d, but 11 individuals in 2021 stayed 37–97 d. No Atlantic sturgeon were detected at receivers beyond rkm 52 in our 3-year study period. By 3–7 October, 50% of fish had exited the Connecticut River, and the last fish exited the river between 28 October and 29 November (Table 1).

Kernel density distributions similarly indicate substantial use of the estuary of the Connecticut River and a generally diminishing occupancy of areas farther upriver (Fig. 5). The densities of detections in Long Island Sound and the estuary at rkm 8–10 were high between late spring and the end of fall in all 3 years (Fig. 5). However,

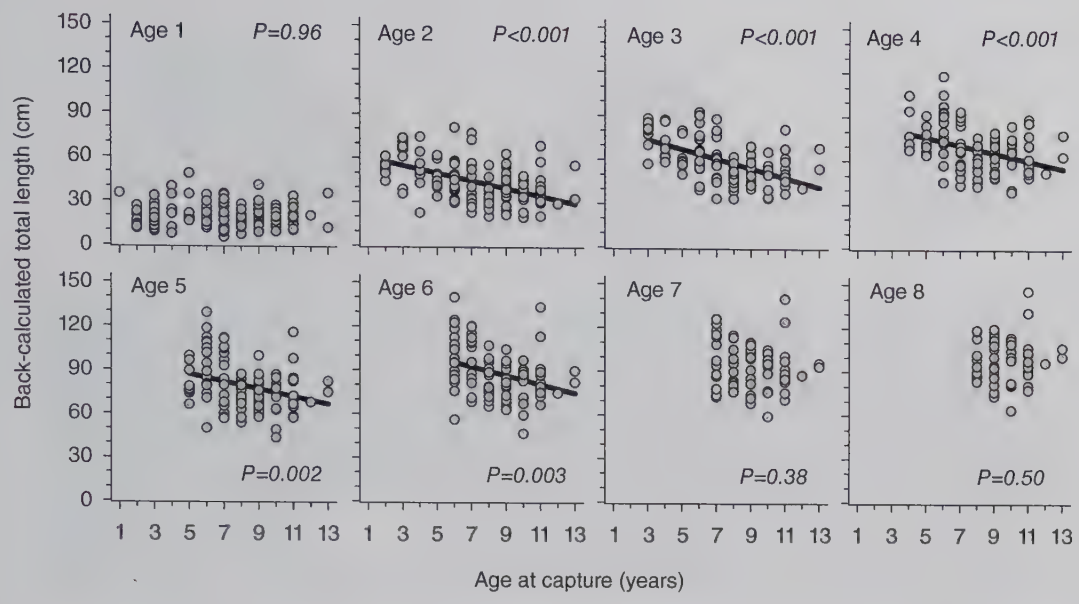

Figure 3

Relationship of back-calculated total lengths at ages 1–8 to ages at capture for Atlantic sturgeon (*Acipenser oxyrinchus*) caught from 1988 through 2021 in Long Island Sound and the Connecticut River. The thick lines in panels indicate the significant fits from linear regression. The 2 oldest individuals, with estimated ages of 16 and 18 years, were collected as mortalities and omitted from the dataset.

Table 1

Summary statistics from telemetry data collected for tagged Atlantic sturgeon (*Acipenser oxyrinchus*) during 2019–2021 in the study area of Long Island Sound and the Connecticut River. The array of acoustic receivers in the sound consisted of 3 sub-arrays at Long Sand Shoal, Eastern Gate, and Falkner Island. A receiver array was deployed in each of 2 areas in the Connecticut River: the brackish estuary (river kilometer [rkm] 3–19) and the freshwater upper section (rkm 22–52).

Statistic	2019	2020	2021
Total number of fish detections	190,380	432,703	756,311
Total number of fish detected	30	61	72
Number of fish detected in previous years[1]	6	23	57
Days spent in study area Mean[2] | Maximum	80 | 122	77 | 120	83 | 170
Date first fish entered the river	10 May	31 March	11 March
Date 50% of fish had once entered the river[1]	25 May	9 July	19 June
Date 50% of fish exited the river	7 Oct.	3 Oct.	3 Oct.
Date last fish exited the river	10 Nov.	29 Nov.	28 Oct.
% fish detected only in the sound	3	2	8
% fish in sound and estuary (not upper river)	57	31	56
% fish in upper river			
– at least 1 d	43	66	35
– at least 14 d	13	28	17
– at least 30 d	0	18	7

[1] The number of fish detected in all 3 years is 22.
[2] Includes only fish tagged in prior years.

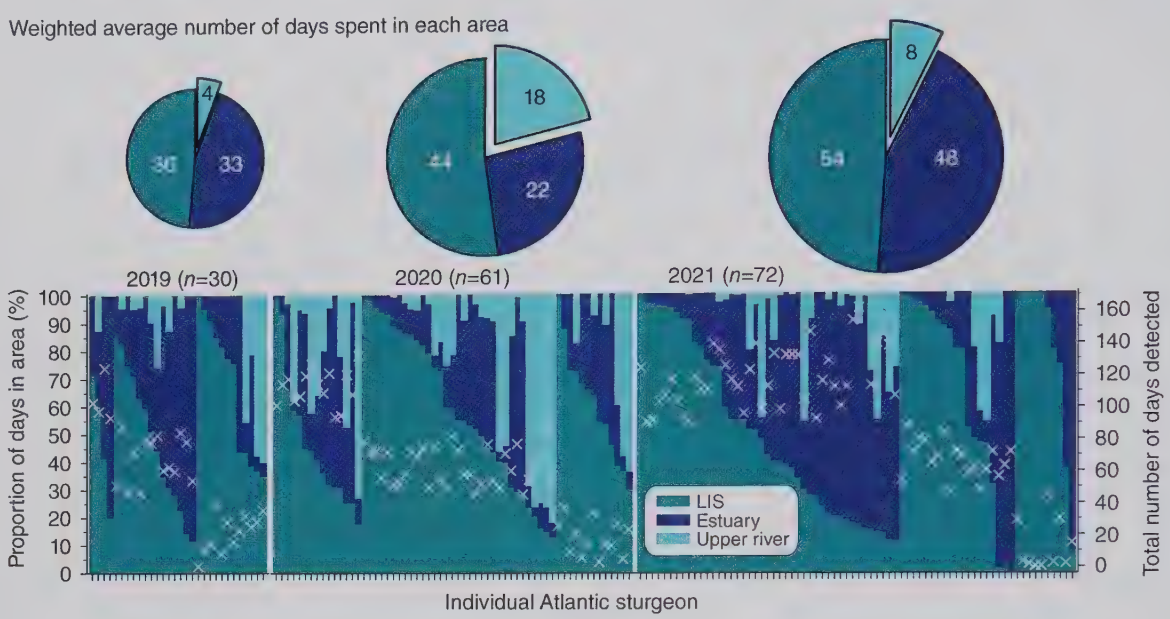

Figure 4

Overview of occupancy patterns of tagged Atlantic sturgeon (*Acipenser oxyrinchus*) in Long Island Sound (LIS) and the Connecticut River during 2019–2021, based on telemetry data. Pie charts depict a weighted average of the number of days that Atlantic sturgeon spent in each of 3 areas in each year: LIS (dark teal) and the estuary (dark blue) and upper section of the Connecticut River (cyan). In the bottom panels, the proportion of days each Atlantic sturgeon spent in each of the 3 areas in each year (colored columns) and the total number of days each individual was detected in the study area (white crosses) are represented. These numbers of days were used to weight the averages shown in the pie charts. n=number of fish detected in the given year.

in 2021, the highest relative density of detections was in the river mouth and Long Island Sound, unlike in 2019 and 2020, when relative densities were higher in the lower river (rkm 8–10) (Fig. 5). Intriguingly, although upstream detections were generally low, an area of increased densities occurred in August and September at rkm 47 (near Portland) in 2020. Of all the Atlantic sturgeon detected each year, 33% (2019), 30% (2020), and 10% (2021) visited rkm 47 for at least 1 d. Occupancy of the upper section of the Connecticut River by Atlantic sturgeon was independent of fish size: TL and the number of days spent in this section or the maximum upriver distance at which a fish was detected were statistically unrelated (Fig. 6; Pearson correlation: all $P \geq 0.06$).

The occurrence of Atlantic sturgeon in the Connecticut River (estuary and upper section) generally coincided with warm river temperatures (>21°C) and low river discharge (<500 m^3/s) (Fig. 7, top panels). The temperature pattern was season dependent. Atlantic sturgeon did not enter the Connecticut River in spring until river temperatures had at least exceeded approximately 20°C, and in fall occupancy of Atlantic sturgeon in the Connecticut River and temperature declined concomitantly (Fig. 7, bottom panels). Weekly temperature and discharge anomalies in the Connecticut River were negatively correlated to each other (Pearson correlation: r=–0.69, P<0.001, n=98), but neither category of anomalies was statistically related to the anomalies in occupancy of the river by Atlantic sturgeon (Pearson correlation: all P>0.18). Therefore, beyond coinciding with the general seasonal pattern, neither temperature nor river discharge further affected occupancy of the river by Atlantic sturgeon. However, in 2021, events of unusually high precipitation in summertime were associated with dips in river occupancy, followed by apparent reentry (Fig. 7, top-right panel).

Our database query returned an additional 324,764 detections of Atlantic sturgeon in our study area during 2019–2021 (Suppl. Table 2) (online only); these detections were for 114 individuals tagged by research groups other than the DEEP. Most individuals (n=67) were and most detections (n=263,920; mean: 3939 detections/fish) were for fish tagged in 2015–2018 by researchers from Stony Brook University in marine waters off the Rockaway Peninsula in New York (mean TL: 102.8 cm; TL range: 71–232 cm; 5% >130 cm TL; Suppl. Table 2 [online only]). Most other detected individuals (n=46) were tagged by various institutions inside and outside of the Chesapeake Bay region. Notably, only 6 fish not tagged by the DEEP (5%, all tagged in New York) proceeded farther into the upper section of the Connecticut River (Suppl. Table 2) (online only).

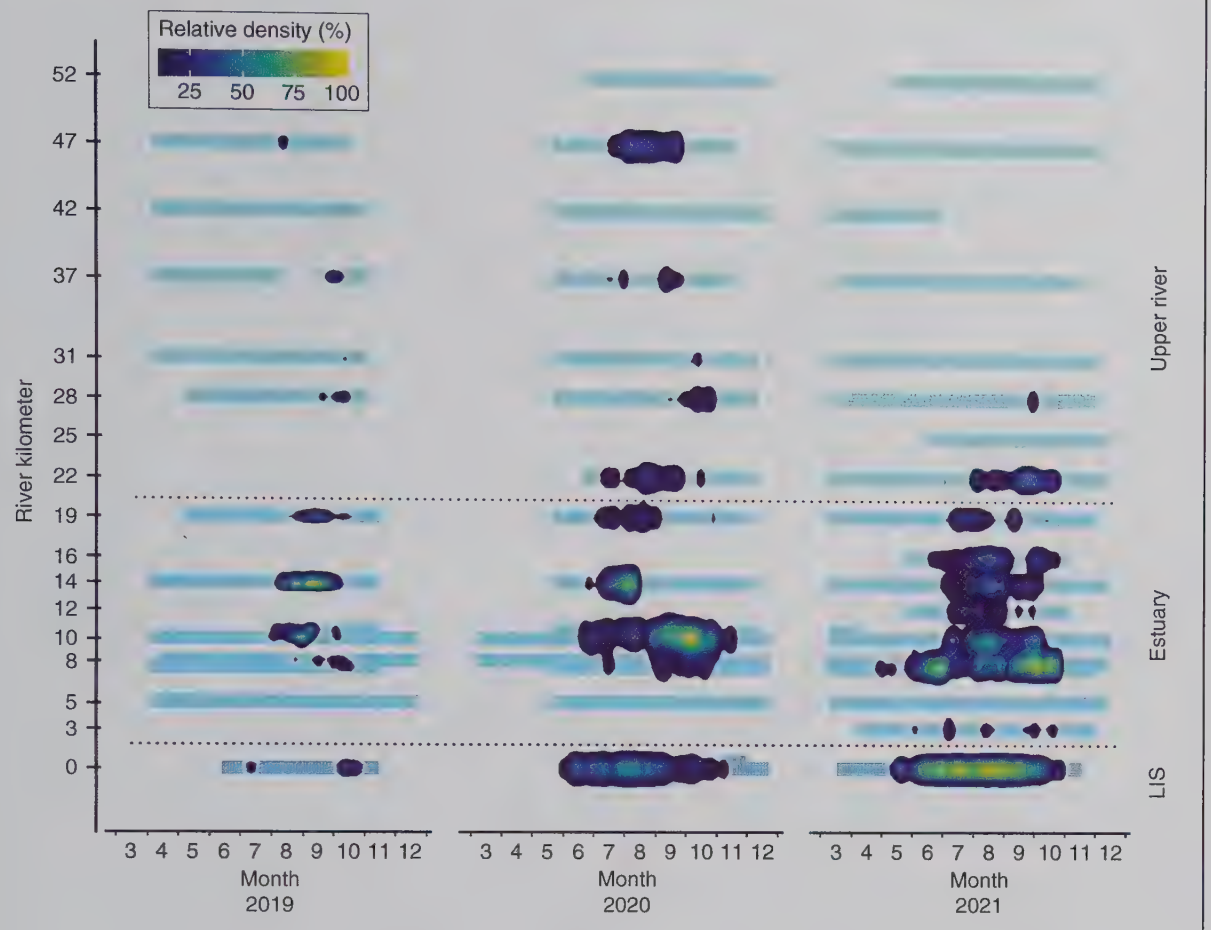

Figure 5

Spatiotemporal occupancy patterns of tagged Atlantic sturgeon (*Acipenser oxyrinchus*) in 2019–2021 in Long Island Sound (LIS) and the Connecticut River, based on telemetry data. Colored contours indicate kernel density distributions of all detections of Atlantic sturgeon relative to the total number of detections in each year. The blue horizontal bars depict the months of deployment during each year for each receiver (identified by the river kilometer of their location). Telemetry data were collected from 3 separate acoustic receiver arrays in LIS and the estuary and upper section of the Connecticut River.

Discussion

We analyzed archived pectoral-fin spines of Atlantic sturgeon and recent telemetry records to better characterize a seasonal aggregation of Atlantic sturgeon in eastern Long Island Sound and the Connecticut River. This aggregation consisted mostly of subadult, fast-growing individuals smaller than 130 cm TL and younger than 12 years; individuals we regarded as mature were rare. This relative lack of large adults was not surprising because the spawning population in the Connecticut River likely was extirpated many decades ago, and other contemporary aggregations of Atlantic sturgeon in the region have similarly truncated age structures. In a study in the New York Bight, for example, over 700 Atlantic sturgeon were assigned ages between 2 and 35 years, but only 4 specimens were older than 21 years, and the age distribution similarly consisted mostly of subadults (85% younger than 12 years) (Dunton et al., 2016).

Older individuals (≥7 years) were smaller than expected for their age, given predictions from the growth model that is currently the most robust for Atlantic sturgeon (Dunton et al., 2016; Fig. 2C). This observation is corroborated by the pattern in the lengths at age back-calculated from annuli widths in sections of pectoral-fin spines, a pattern that indicates a consistent decline in lengths at ages 2–6 with increasing age at capture. Such an apparent change in growth phenotype with age at capture, known as Lee's phenomenon (Lee, 1912; Ricker, 1969), could have a number of explanations that are not mutually exclusive, from general life history trade-offs between growth and longevity (Gerking, 1957; Ricker, 1975) to size-selective mortality (Carlander, 1945) or size-selective migration patterns (Stanley, 1980). Life history trade-offs appear unlikely to

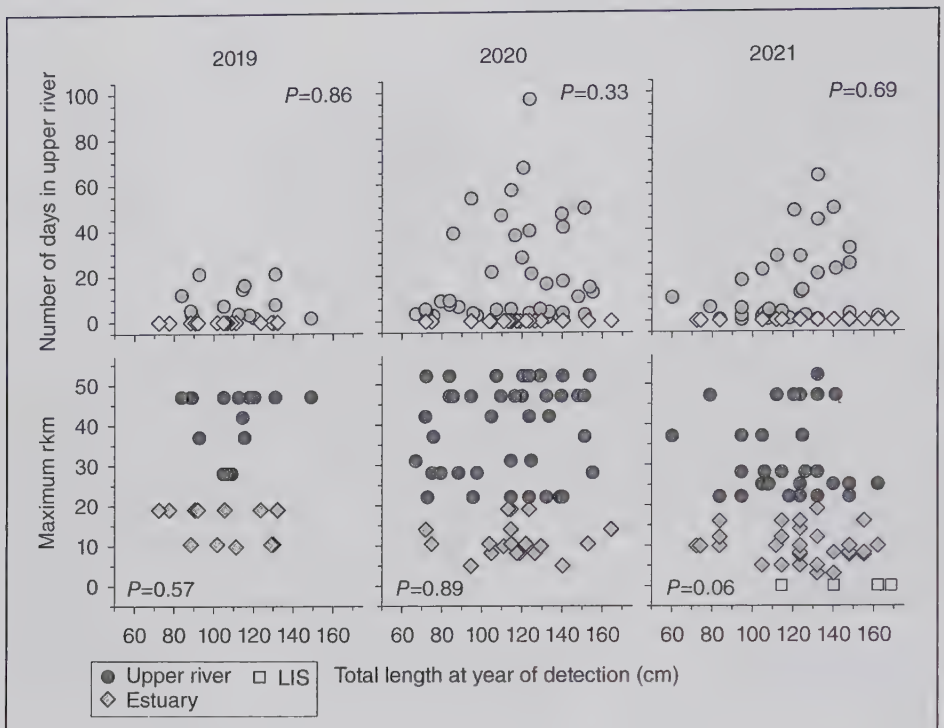

Figure 6

Occupancy of the Connecticut River by Atlantic sturgeon (*Acipenser oxyrinchus*) in relation to their size during 2019–2021. In the top panels, the number of days spent in the upper section of the river in relation to total length at the year of detection by an acoustic receiver is provided for tagged individuals. White diamonds indicate fish that spent 0 d in the upper river. In the bottom panels, the maximum river kilometer (rkm) at which each individual was detected in relation to total length at the year of detection is represented. Symbols indicate the habitat area where fish were detected: the freshwater upper section and brackish estuary of the Connecticut River and Long Island Sound (LIS). All metrics were length independent (Pearson correlation: $P \geq 0.06$).

have had an effect on growth in our study because the aggregation of Atlantic sturgeon that we focused on consisted predominantly of subadults.

There is some evidence for size-selective fishing mortality strengthening Lee's phenomenon in shovelnose sturgeon (*Scaphirhynchus platorynchus*), a freshwater sturgeon species from the upper Missouri River (Koch et al., 2009), but Atlantic sturgeon have now been protected from exploitation for over 2 decades (i.e., longer than the life of the oldest specimens in our sample). Although accidental catches of Atlantic sturgeon still occur and likely are a hindrance to the recovery of this species (Stein et al., 2004), it is doubtful that bycatch mortality could be size selective enough to cause the observed pattern. A more probable explanation therefore might be that larger, faster growing Atlantic sturgeon selectively disappear from the aggregation in Long Island Sound and the Connecticut River not because they die but because they already left to migrate back to their natal rivers.

Still, our interpretations remain speculative because of a few compounding sources of uncertainty. First, aging of Atlantic sturgeon and using measurements of annuli widths from fin spine sections are notoriously difficult, are less precise than desirable (i.e., CV >5%), and are poorly validated. However, potential underestimation of ages is largely a concern for older, adult Atlantic sturgeon, not in subadults that were the vast majority of Atlantic sturgeon included in this study. Second, we lacked information about the sex ratio and spatial origin of the aggregation of Atlantic sturgeon in our study area, and both sex and origin are known to affect overall growth patterns. For example, female Atlantic sturgeon grow more slowly and to larger maximum sizes than males (Van Eenennaam et al., 1996; Stevenson and Secor, 1999; Stewart et al., 2015), and Atlantic sturgeon from northern latitudes (>38°N) grow slower than fish originating from more southern systems (Smith, 1985; Dunton et al., 2016). Hence, potential changes in sex ratio or origin over time could confound the observed changes in growth.

Gear selectivity might have played a role, too, given that the majority of Atlantic sturgeon in this study were caught with gill nets (15–18-cm stretched mesh) that we suspect selected against the largest fish (>180 cm TL; Suppl. Fig. 4 [online only]). However, we found that Lee's phenomenon

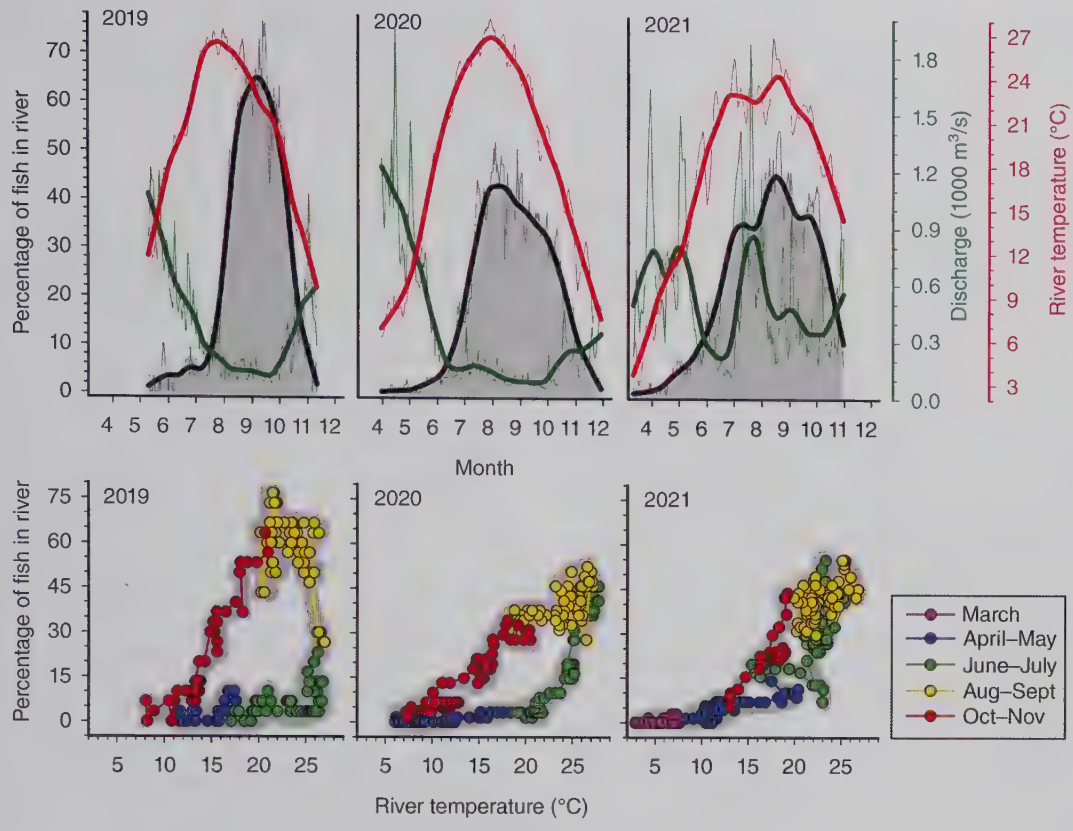

Figure 7

Seasonal occurrence of Atlantic sturgeon (*Acipenser oxyrinchus*) in the Connecticut River in relation to river discharge (green lines) and temperature (red lines) in 2019–2021. In the top panels, thin lines depict daily values, and thick lines represent values from locally estimated scatterplot smoothing (20% bandwidth). Black lines and gray shading indicate the percentage of fish present in the monitored part of the river (from North Cove in the estuary up to river kilometer 52 at Wilcox Island) relative to all fish detected in each year. In the bottom panels, the relationship between temperature and the percentage of fish present in the river in each year is represented, by month or pair of months. The gray area around the colored points in each panel was added to highlight the overall seasonal progression of the temperature–occupancy relationships.

remained detectable, even when we restricted the dataset to fish <100 cm TL (i.e., well below the presumed selectivity), indicating that this pattern was not just a sampling artifact. To better characterize the aggregation of Atlantic sturgeon in our study area and elucidate reasons for its growth changes over time, future studies should include sampling with larger mesh sizes and determination of the sex and origin of specimens (Waldman et al., 2013).

Analysis of the telemetry records revealed several intriguing patterns, aided by the dataset size (about 1.4 million detections of Atlantic sturgeon over 3 years) and the design of the receiver arrays that allowed inference of seasonal occupancy of Atlantic sturgeon in eastern Long Island Sound and both the estuary and upper section of the Connecticut River. Overall, Long Island Sound and the Connecticut River clearly provide important seasonal habitats for Atlantic sturgeon, supporting the emergent view that natal and non-natal rivers fulfill critical ontogenetic habitat requirements for Atlantic sturgeon (White et al., 2024). Despite the expected large variability between years, months, and individuals, we found that this aggregation of Atlantic sturgeon typically utilizes the study area between spring and fall. However, individual fish stayed there for only 2–3 months on average, either because movements within Long Island Sound took fish beyond the receiver arrays or because their stay was a transient part of a coastal migration (Dunton et al., 2010; Kazyak et al., 2021). During winter, Atlantic sturgeon largely emigrate out of Long Island Sound and the Connecticut River, likely to seek warmer waters (>9°C) on the continental shelf of the Northwest Atlantic Ocean (Rothermel et al., 2020).

Movement of Atlantic sturgeon into the estuary and upper section of the Connecticut River resembled the seasonal cycle of temperatures in the river, with peak temperature and peak occupancy co-occurring around late summer. However, the onset of the ingress into the Connecticut

River in spring and summer appears to be driven more by a temperature threshold (20°C–25°C). Episodes of high discharge negatively affected occurrence of Atlantic sturgeon in the Connecticut River, likely because of the preference of Atlantic sturgeon for energetically more favorable conditions of low flow. This response to changes in discharge volume is consistent with the selective tidal transport behavior of green sturgeon (*Acipenser medirostris*) in San Francisco Bay (Kelly et al., 2020) and the synchronization of upriver movements with flood tides by Atlantic sturgeon in the Hudson River (Dovel and Berggren, 1983). Climate change is predicted to increase extreme weather events; therefore, extreme rainfall and discharge events, such as those observed in July 2021 (when flow peaked for the year at 1855 m^3/s; USGS Current Water Data for Connecticut), are likely to become more frequent (Runkle et al., 2022). In a recent assessment, diadromous fish and benthic invertebrates were found to be highly vulnerable to climate change and decadal variability (Hare et al., 2016), due in part to such changes in discharge patterns. Given the complex effect of river discharge on the distribution of Atlantic sturgeon in this study, increased frequency of flooding in the summer could disrupt utilization of the Connecticut River by this species.

The density of acoustic detections of tagged fish in the study area indicate that Atlantic sturgeon spent most of their time within Long Island Sound and the brackish estuary of the Connecticut River. We interpret this pattern in where fish spent their time as related to feeding behavior, given that estuaries are particularly rich in prey organisms for Atlantic sturgeon, such as benthic mollusks, polychaetes, arthropods, and in rare cases even fish (Johnson et al., 1997; Haley, 1999; Guilbard et al., 2007; McLean et al., 2013; Novak et al., 2017). Specifically for the estuary of the Connecticut River, Savoy (2007) found that Atlantic sturgeon preyed almost exclusively on polychaetes. The area is also a known summer feeding ground for shortnose sturgeon (*Acipenser brevirostrum*), the only other native sturgeon species in the area (Savoy and Benway, 2004).

A considerable proportion of individuals (35%–66%) each year proceeded farther upriver from the estuary into freshwater for periods ranging from a single day to a few weeks. These fish were no larger or smaller than those remaining farther downstream. Most fish made fast, linear movements far into the upper section of the Connecticut River, as has previously been observed for Atlantic sturgeon in Minas Bay (an inlet of Bay of Fundy in Canada), with these movements interpreted as extensive searching for or movement between food patches (McLean et al., 2013). We suspect that migrating Atlantic sturgeon were searching for alternative prey sources in the upper section of the Connecticut River, perhaps driven by intra- or interspecific seasonal competition for benthic prey in the estuary of the river (Savoy and Benway, 2004).

Interspecific competition with shortnose sturgeon may influence movements of Atlantic sturgeon. Shortnose sturgeon are generally more common in freshwater areas, and Atlantic sturgeon are often concentrated in deeper, more saline waters of the estuary (Haley, 1999). However, the distributions and, therefore, the prey of both species likely overlap. A previous analysis for the estuary of the Connecticut River revealed that shortnose sturgeon mostly eat amphipods and polychaetes (Savoy and Benway, 2004) and Atlantic sturgeon almost exclusively prey on polychaetes there (Savoy, 2007). Given that shortnose sturgeon migrate to the estuarine portion of the river in late spring to late summer (Benway, 2002; Buckley and Kynard, 1985), the 2 sturgeon species are likely to occupy the same area and share a common, primary food source. Such overlap may engender exploitative competition and prompt Atlantic sturgeon to explore potential new foraging grounds in the upper portion of the Connecticut River. There, shortnose sturgeon are known to prey on mayflies (Ephemeroptera), midges (Chironomidae), and freshwater clams (*Pisidium* spp.), but comparable diet data for Atlantic sturgeon are lacking (Savoy and Benway, 2004).

The seasonal use of freshwater habitat by anadromous Atlantic sturgeon is more commonly associated with spawning behavior, and Atlantic sturgeon historically spawned in the Connecticut River before spawning runs ceased likely many decades ago (Van Eenennaam et al., 1996). Intriguingly, in 2019 and particularly in 2020, we discerned a hotspot of seasonal occupancy near the receiver at Portland (rkm 47), which is sufficiently upstream from the historic salt-wedge maximum (rkm 26) (Meade, 1966) and features deep sections (>10 m) with cobble or gravel substrate that Atlantic sturgeon prefer for spawning (Smith and Clugston, 1997; Bain et al., 2000; Hatin et al., 2002). However, most fish that swam upriver were subadults. Although the largest individuals in each year (141–154 cm) were technically adults, only males or Atlantic sturgeon from southern populations (the Carolina and South Atlantic DPSs) have been found to be already mature at this size (Smith et al., 1984; Van Eenennaam et al., 1996).

Moreover, the timing of these freshwater excursions was inconsistent with known spring spawning runs of Atlantic sturgeon in other northern rivers. In the Hudson River, most Atlantic sturgeon are already spent from early to mid-June (Van Eenennaam et al., 1996), and it has been reported from another study that Atlantic sturgeon move into freshwater from the end of May to mid-July (Breece et al., 2021). In the Saint John River (in New Brunswick, Canada), estimated spawning dates for Atlantic sturgeon are in early July, on the basis of larval growth models (Taylor and Litvak, 2017). Atlantic sturgeon in the Savannah River in Georgia initiate their spring runs from February to March (Vine et al., 2019). In contrast, the Atlantic sturgeon in our study arrived at the Portland area in mid- to late August (Suppl. Table 3) (online only), too late for a spring spawning run as expected for Atlantic sturgeon of the New York Bight DPS. Only southern populations of Atlantic sturgeon make additional spawning runs in fall (Smith et al., 1984; Collins et al., 2000; Ingram and Peterson, 2016). In light of all evidence, we therefore believe that feeding-related explorations are the most parsimonious reason for Atlantic sturgeon to make freshwater excursions as we observed them in this study. This

assertion does not exclude the possibility of rare, ephemeral spawning events by Atlantic sturgeon that continue to elude detection in the upper section of the Connecticut River (Coleman et al., 2024).

Conclusions

Long Island Sound and the Connecticut River serve as much-used habitat for a dynamic, seasonal aggregation of mostly subadult Atlantic sturgeon with ecologically intriguing age and growth patterns. Many of the tagged Atlantic sturgeon returned to this area year after year (DEEP[4]), indicating that the area is an important feeding ground. Although Atlantic sturgeon are known to utilize estuaries to feed (Haley, 1999; Dunton et al., 2010; McLean et al., 2013), we found that juveniles and subadults also commonly spent time and energy to travel upriver into freshwater habitats—a behavior that had previously been associated only with spawning. The Connecticut River is likely not the only system where non-natal juvenile and subadult fish utilize freshwater; therefore, future studies should continue exploration of the importance of upriver areas for juvenile and subadult Atlantic sturgeon in other rivers on the East Coast of the United States.

Given that Atlantic sturgeon from all 5 DPSs likely contribute to the aggregation in Long Island Sound and the Connecticut River (Waldman et al., 2013), its conservation and restoration in the face of anthropogenic change could positively affect other Atlantic sturgeon stocks. This is especially true for smaller stocks like those in the James and Delaware Rivers, which are not as robust as the Hudson River stock but still contribute 6%–12% of the fish in the aggregation in the Connecticut River (Waldman et al., 2013). Continued survey and research efforts are clearly warranted to improve understanding of the growth, movements, and genetic makeup of this aggregation of Atlantic sturgeon, and this work should include targeting of large individuals (>130 cm TL) and further investigations of subadult use of the upriver environments.

Resumen

El esturión del Atlántico (*Acipenser oxyrinchus*) se agrega estacionalmente en la Sonda de Long Island y el río Connecticut, pero aún no se conoce lo suficiente de la estructura de tallas y edades ni del uso del río. Analizamos todos los datos de longitud disponibles de monitoreos (1988–2021: número de muestras [*n*]=3544), estimamos la edad a partir de secciones de las espinas de las aletas pectorales (*n*=296) y medimos la anchura de los anillos para realizar un análisis retrospectivo de la talla a la edad (*n*=166). Los peces tuvieron entre 21 y 218 cm de longitud total ([LT], media: 105.2 cm LT), pero el 87% de ellos medían entre 50 y 130 cm LT. Las edades variaron entre 0 y 18 años (media: 8.1 años), estimándose que el 92% de todos los individuos eran menores de 12 años. La anchura de los anillos indicó que los peces de crecimiento más rápido desaparecieron selectivamente de la zona de estudio a lo largo del tiempo. Para revelar los patrones de movimiento, particularmente para la parte superior el río Connecticut (agua dulce), analizamos 3 años (2019–2021) de detecciones acústicas de 85 individuos. Estos peces ocurrieron en el área de estudio de marzo a noviembre, pero permanecieron en promedio solo 54–91 d. La mayoría de los peces que entraron en las estaciones receptoras en la Sonda de Long Island también se desplazaron al río, pero utilizaron principalmente su estuario salobre inferior. Una gran proporción de individuos (35%–66%) realizó incursiones río arriba hacia el agua dulce, coincidiendo con el bajo caudal y las temperaturas cálidas del río a finales del verano. Por lo tanto, tanto las porciones salobres como de agua dulce del río Connecticut sirven como importantes hábitats estacionales de alimentación para el esturión del Atlántico ≤130 cm TL.

Acknowledgments

We thank all seasonal and other DEEP employees that participated in data collection, in particular D. Pacileo and R. St. Amand. We gratefully acknowledge the permission of D. Fox, I. Park, C. Stence, K. Dunton, M. Balazik, and E. Hilton to report data from tags deployed on Atlantic sturgeon detected in Long Island Sound and the Connecticut River. The constructive feedback of 3 anonymous reviewers greatly helped improve earlier versions of this manuscript. This study was funded by a grant from Connecticut Sea Grant (project R/LR-29) awarded to H. Baumann, T. Savoy, and J. Benway, a NOAA Species Recovery Grant (NA18NMF4720090), and DEEP.

Literature cited

ASMFC (Atlantic States Marine Fisheries Commission).
2017. 2017 Atlantic sturgeon benchmark stock assessment and peer review report, 456 p. ASMFC, Arlington, VA. [Available from website.]

ASSRT (Atlantic Sturgeon Status Review Team).
2007. Status review of Atlantic sturgeon (*Acipenser oxyrinchus oxyrinchus*), 174 p. Report to NOAA, National Marine Fisheries Service, Northeast Regional Office. Natl. Mar. Fish. Serv., NOAA, Gloucester, MA. [Available from website.]

Bain, M. B.
1997. Atlantic and shortnose sturgeons of the Hudson River: common and divergent life history attributes. Environ. Biol. Fishes 48:347–358.

Bain, M., N. Haley, D. Peterson, J. R. Waldman, and K. Arend.
2000. Harvest and habitats of Atlantic sturgeon *Acipenser oxyrinchus* Mitchill, 1815 in the Hudson River estuary: lessons for sturgeon conservation. Bol. Inst. Esp. Oceanogr. 16(1–4):43–53.

[4] DEEP (Connecticut Department of Energy and Environmental Protection). 2025. Unpubl. data. DEEP, 79 Elm St., Hartford, CT 06106.

Balazik, M. T., S. P. McIninch, G. C. Garman, and R. J. Latour.
2012. Age and growth of Atlantic sturgeon in the James River, Virginia, 1997–2011. Trans. Am. Fish. Soc. 141: 1074–1080.

Baremore, I. E., and J. D. Rosati.
2014. A validated, minimally deleterious method for aging sturgeon. Fish. Bull. 112:274–282.

Baumann, H., S. J. Sutherland, and R. S. McBride.
2013. Longitudinal length back-calculations from otoliths and scales differ systematically in haddock. Trans. Am. Fish. Soc. 142:184–192.

Benway, J. M.
2002. Shortnose sturgeon (*Acipenser brevirostrum*) food habits in the Connecticut River. M.S. thesis, 43 p. South. Conn. State Univ., New Haven, CT.

Binder, T., T. Hayden, and C. Holbrook.
2018. An introduction to R for analyzing acoustic telemetry data, vers. 2.0, 98 p. Great Lakes Acoust. Telem. Obs. System, Great Lakes Fish. Commission, Ann Arbor, MI. [Available from website.]

Breece, M. W., A. L. Higgs, and D. A. Fox.
2021. Spawning intervals, timing, and riverine habitat use of adult Atlantic sturgeon in the Hudson River. Trans. Am. Fish. Soc. 150:528–537.

Buckley, J., and B. Kynard.
1985. Yearly movements of shortnose sturgeons in the Connecticut River. Trans. Am. Fish. Soc. 114:813–820.

Campana, S. E.
1990. How reliable are growth back-calculations based on otoliths? Can. J. Fish. Aquat. Sci. 47:2219–2227.

Carlander, K. D.
1945. Age, growth, sexual maturity, and population fluctuations of the yellow pike-perch, *Stizostedion vitreum vitreum* (Mitchill), with reference to the commercial fisheries, Lake of the Woods, Minnesota. Trans. Am. Fish. Soc. 73: 90–107.

Chih, C.-P.
2009. The effects of otolith sampling methods on the precision of growth curves. N. Am. J. Fish. Manag. 29: 1519–1528.

Coleman, N., D. Fox, A. Horne, N. J. Hostetter, J. Madsen, M. O'Brien, I. Park, C. Stence, and D. Secor.
2024. Spawning run estimates and phenology for an extremely small population of Atlantic sturgeon in the Marshyhope Creek–Nanticoke River system, Chesapeake Bay. Mar. Coast. Fish. 16:e10292.

Collins, M. R., T. I. J. Smith, W. C. Post, and O. Pashuk.
2000. Habitat utilization and biological characteristics of adult Atlantic sturgeon in two South Carolina rivers. Trans. Am. Fish. Soc. 129:982–988.

Damon-Randall, K., R. Bohl, S. Bolden, D. Fox, C. Hager, B. Hickson, E. Hilton, J. Mohler, E. Robbins, T. Savoy, et al.
2010. Atlantic sturgeon research techniques. NOAA Tech. Memo. NMFS-NE-215, 62 p.

Dovel, W. L., and T. J. Berggren.
1983. Atlantic sturgeon of the Hudson River estuary, New York. New York Fish Game J. 30:140–172.

Dunton, K. J., A. Jordaan, K. A. McKown, D. O. Conover, and M. G. Frisk.
2010. Abundance and distribution of Atlantic sturgeon (*Acipenser oxyrinchus*) within the Northwest Atlantic Ocean, determined from five fishery-independent surveys. Fish. Bull. 108:450–465.

Dunton, K. J., A. Jordaan, D. H. Secor, C. M. Martinez, T. Kehler, K. A. Hattala, J. P. Van Eenennaam, M. T. Fisher, K. A. McKown, D. O. Conover, et al.
2016. Age and growth of Atlantic sturgeon in the New York Bight. N. Am. J. Fish. Manag. 36:62–73.

Federal Register.
2012a. Endangered and threatened wildlife and plants; final listing determinations for two distinct population segments of Atlantic sturgeon (*Acipenser oxyrinchus oxyrinchus*) in the Southeast. Fed. Regist. 77:5914–5982. [Available from website.]
2012b. Endangered and threatened wildlife and plants; threatened and endangered status for distinct population segments of Atlantic sturgeon in the Northeast Region. Fed. Regist. 77:5880–5912. [Available from website.]
2017. Endangered and threatened species; designation of critical habitat for the endangered New York Bight, Chesapeake Bay, Carolina and South Atlantic distinct population segments of Atlantic sturgeon and the threatened Gulf of Maine distinct population segment of Atlantic sturgeon. Fed. Regist. 82:39160–39274. [Available from website.]

Galligan, J. P.
1960. History of the Connecticut River sturgeon fishery. Wildl. Conserv. Bull. 6:1–6.

Gerking, S. D.
1957. Evidence of aging in natural populations of fishes. Gerontologia 1:287–305.

Guilbard, F., J. Munro, P. Dumont, D. Hatin, and R. Fortin.
2007. Feeding ecology of Atlantic sturgeon and lake sturgeon co-occurring in the St. Lawrence estuarine transition zone. Am. Fish. Soc. Symp. 56:85–104.

Haley, N. J.
1999. Habitat characteristics and resource use patterns of sympatric sturgeons in the Hudson River estuary. M.S. thesis., 124 p. Univ. Mass. Amherst, Amherst, MA.

Hare, J. A., W. E. Morrison, M. W. Nelson, M. M. Stachura, E. J. Teeters, R. B. Griffis, M. A. Alexander, J. D. Scott, L. Alade, and R. J. Bell.
2016. A vulnerability assessment of fish and invertebrates to climate change on the northeast US continental shelf. PLoS ONE 11(2):e0146756.

Hatin, D., R. Fortin, and F. Caron.
2002. Movements and aggregation areas of adult Atlantic sturgeon (*Acipenser oxyrinchus*) in the St Lawrence River estuary, Québec, Canada. J. Appl. Ichthyol. 18: 586–594.

Hilton, E. J., B. Kynard, M. Balazik, A. Horodysky, and C. Dillman.
2016. Review of the biology, fisheries, and conservation status of the Atlantic sturgeon (*Acipenser oxyrinchus oxyrinchus* Mitchill, 1815). J. Appl. Ichthyol. 32(Suppl. 1): 30–66.

Ingram, E. C., and D. L. Peterson.
2016. Annual spawning migrations of adult Atlantic sturgeon in the Altamaha River, Georgia. Mar. Coast. Fish. 8: 595–606.

Ingram, E. C., R. M. Cerrato, K. J. Dunton, and M. G Frisk.
2019. Endangered Atlantic sturgeon in the New York Wind Energy Area: implications of future development in an offshore wind energy site. Sci. Rep. 9:12432.

Johnson, J. H., D. S. Dropkin, B. E. Warkentine, J. W. Rachlin, and W. D. Andrews.
1997. Food habits of Atlantic sturgeon off the central New Jersey coast. Trans. Am. Fish. Soc. 126:166–170.

Kahn, J., and M. Mohead.
2010. A protocol for use of shortnose, Atlantic, Gulf, and green sturgeons. NOAA Tech. Memo. NMFS-OPR-45, 62 p.

Kazyak, D. C., S. L. White, B. A. Lubinski, R. Johnson, and M. Eackles.
2021. Stock composition of Atlantic sturgeon (*Acipenser oxyrinchus oxyrinchus*) encountered in marine and estuarine environments on the U.S. Atlantic Coast. Conserv. Genet. 22:767–781.

Kehler, T., J. A. Sweka, J. Mohler, A. Higgs, and G. Kenney.
2018. Age and growth of juvenile Atlantic sturgeon in the lower Hudson River. N. Am. J. Fish. Manag. 38:84–95.

Kelly, J. T., S. E. Lankford, J. J. Cech Jr., and A. P. Klimley.
2020. Estimating the energetic savings for green sturgeon moving by selective tidal stream transport. Environ. Biol. Fishes 103:455–463.

Koch, J. D., M. C. Quist, C. L. Pierce, K. A. Hansen, and M. J. Steuck.
2009. Effects of commercial harvest on shovelnose sturgeon populations in the upper Mississippi River. N. Am. J. Fish. Manag. 29:84–100.

Koppelman, L. E., P. K. Weyl, M. G. Gross, and D. S. Davies.
1976. The urban sea: Long Island Sound, 223 p. Praeger Publ., New York.

Lee, R. M.
1912. An investigation into the methods of growth determination in fishes by means of scales. ICES J. Mar. Sci. s1(63):3–34.

McLean, M. F., M. J. Dadswell, and M. J. W. Stokesbury.
2013. Feeding ecology of Atlantic sturgeon, *Acipenser oxyrinchus oxyrinchus* Mitchill, 1815 on the infauna of intertidal mudflats of Minas Basin, Bay of Fundy. J. Appl. Ichthyol. 29:503–509.

Meade, R. H.
1966. Salinity variations in the Connecticut River. Water Resources Res. 2:567–579.

Moser, M. L., M. Bain, M. R. Collins, N. Haley, B. Kynard, J. C. O'Herron II, G. Rogers, and T. S. Squiers.
2000. A protocol for use of shortnose and Atlantic sturgeons. NOAA Tech. Memo. NMFS-OPR-18, 18 p.

Novak, A. J., A. E. Carlson, C. R. Wheeler, G. S. Wippelhauser, and J. A. Sulikowski.
2017. Critical foraging habitat of Atlantic sturgeon based on feeding habits, prey distribution, and movement patterns in the Saco River estuary, Maine. Trans. Am. Fish. Soc. 146:308–317.

Pikitch, E. K., P. Doukakis, L. Lauck, P. Chakrabarty, and D. L. Erickson.
2005. Status, trends and management of sturgeon and paddlefish fisheries. Fish Fish. 6:233–265.

R Core Team.
2021. R: a language and environment for statistical computing. R Foundation for Statistical Computing, Vienna, Austria. [Available from website, accessed November 2021.]

Ricker, W. E.
1969. Effects of size-selective mortality and sampling bias on estimates of growth, mortality, production, and yield. J. Fish. Res. Board Can. 26:479–541.
1975. Computation and interpretation of biological statistics of fish populations. Bull. Fish. Res. Board Can. 191, 382 p.

Rothermel, E. R., M. T. Balazik, J. E. Best, M. W. Breece, D. A. Fox, B. I. Gahagan, D. E. Haulsee, A. L. Higgs, M. H. P. O'Brien, M. J. Oliver, et al.
2020. Comparative migration ecology of striped bass and Atlantic sturgeon in the US Southern mid-Atlantic bight flyway. PLoS ONE 15(6):e0234442.

Runkle, J., K. E. Kunkel, S. M. Champion, D. R. Easterling, B. C. Stewart, R. Frankson, W. Sweet, and J. Spaccio.
2022. Connecticut State climate summary 2022. NOAA Tech. Rep. NESDIS 150-CT, 6 p.

Savoy, T.
2007. Prey eaten by Atlantic sturgeon in Connecticut waters. Am. Fish. Soc. Symp. 56:157–165.

Savoy, T., and D. Pacileo.
2003. Movements and important habitats of subadult Atlantic sturgeon in Connecticut waters. Trans. Am. Fish. Soc. 132:1–8.

Savoy, T., and J. Benway.
2004. Food habits of shortnose sturgeon collected in the lower Connecticut River from 2000 through 2002. Am. Fish. Soc. Monogr. 9:353–360.

Savoy, T., L. Maceda, N. K. Roy, D. Peterson, and I. Wirgin.
2017. Evidence of natural reproduction of Atlantic sturgeon in the Connecticut River from unlikely sources. PLoS ONE 12(4):e0175085.

Secor, D. H.
2002. Atlantic Sturgeon fisheries and stock abundances during the late nineteenth century. Am. Fish. Soc. Symp. 28:89–100.

Simpfendorfer, C. A., C. Huveneers, A. Steckenreuter, K. Tattersall, X. Hoenner, R. Harcourt, and M. R. Heupel.
2015. Ghosts in the data: false detections in VEMCO pulse position modulation acoustic telemetry monitoring equipment. Animal Biotelem. 3:55.

Smith, T. I. J.
1985. The fishery, biology, and management of Atlantic sturgeon, *Acipenser oxyrhynchus*, in North America. Environ. Biol. Fishes 14:61–72.

Smith, T. I. J., and J. P. Clugston.
1997. Status and management of Atlantic sturgeon, *Acipenser oxyrinchus*, in North America. Environ. Biol. Fishes 48:335–346.

Smith, T. I. J., D. E. Marchette, and G. F. Ulrich.
1984. The Atlantic sturgeon fishery in South Carolina. N. Am. J. Fish. Manag. 4:164–176.

Stanley, C. A.
1980. Lee's phenomenon in the western subspecies of the Australian salmon, *Arripis trutta esper*. Aust. J. Mar. Freshw. Res. 31:13–19.

Stein, A. B., K. D. Friedland, and M. Sutherland.
2004. Atlantic sturgeon marine bycatch and mortality on the continental shelf of the Northeast United States. N. Am. J. Fish. Manag. 24:171–183.

Stevenson, J. T., and D. H. Secor.
1999. Age determination and growth of Hudson River Atlantic sturgeon, *Acipenser oxyrinchus*. Fish. Bull. 97: 153–166.

Stewart, N. D., M. J. Dadswell, P. Leblanc, R. G. Bradford, C. Ceapa, and M. J. W. Stokesbury.
2015. Age and growth of Atlantic sturgeon from the Saint John River, New Brunswick, Canada. N. Am. J. Fish. Manag. 35:364–371.

Sunde, L. A.
1961. Growth and reproduction of the lake sturgeon (*Acipenser fulvescens* Rafinesque) of the Nelson River in Manitoba. M.S. thesis, 93 p. Univ. British Columbia, Vancouver, Canada. [Available from website.]

Taylor, A. D., and M. K. Litvak.
2017. Timing and location of spawning based on larval capture and ultrasonic telemetry of Atlantic sturgeon in the Saint John River, New Brunswick. Trans. Am. Fish. Soc. 146:283–290.

Van Eenennaam, J. P., S. I. Doroshov, G. P. Moberg, J. G. Watson, D. S. Moore, and J. Linares.
1996. Reproductive conditions of the Atlantic sturgeon (*Acipenser oxyrinchus*) in the Hudson River. Estuaries 19:769–777.

Vine, J. R., S. C. Holbrook, W. C. Post, and B. K. Peoples.
2019. Identifying environmental cues for Atlantic sturgeon and shortnose sturgeon spawning migrations in the Savannah River. Trans. Am. Fish. Soc. 148:671–681.

Waldman, J. R., T. King, T. Savoy, L. Maceda, C. Grunwald, and I. Wirgin.
2013. Stock origins of subadult and adult Atlantic sturgeon, *Acipenser oxyrinchus*, in a non-natal estuary, Long Island Sound. Estuar. Coasts 36:257–267.

Waldman, J., S. E. Alter, D. Peterson, L. Maceda, N. Roy, and I. Wirgin.
2019. Contemporary and historical effective population sizes of Atlantic sturgeon *Acipenser oxyrinchus oxyrinchus*. Conserv. Genet. 20:167–184.

White, S., M. Breece, D. Fox, D. Kazyak, A. Higgs, I. Park, C. Busch, B. Lubinski, R. Johnson, and A. Welsh.
2024. Spatiotemporal patterns in habitat use of natal and non-natal adult Atlantic sturgeon in two spawning rivers. Animal Biotelem. 12:9.

Wickham, H.
2016. Data analysis. *In* ggplot2: elegant graphics for data analysis, 2nd ed., p. 189–201. Springer, New York.

Fishery Bulletin

Guidelines for authors

Contributions published in *Fishery Bulletin* describe original research in marine fishery science, fishery engineering and economics, and marine environmental and ecological sciences (including modeling). Preference will be given to manuscripts that examine processes and underlying patterns. Descriptive reports, surveys, and observational papers may occasionally be published but should appeal to an audience outside the locale in which the study was conducted.

Although all contributions are subject to peer review, responsibility for the contents of papers rests upon the authors and not on the editor or publisher. *Submission of an article implies that the article is original and is not being considered for publication elsewhere.*

All submissions are subject to a double-blind review to remove the identity of author and reviewer during the review process.

Plagiarism and double publication are considered serious breaches of publication ethics. To verify the originality of the research in papers and to identify possible previous publication, manuscripts may be screened with plagiarism-detection software.

Manuscripts must be written in English; authors whose native language is not English are strongly advised to have their manuscripts checked by English-speaking colleagues before submission.

Artificial intelligence (AI), machine learning, or similar algorithmic tools should not be used to write or generate scientific content, including text, tables, and figures, for manuscripts submitted to *Fishery Bulletin*. Although some authors may use such tools to improve the readability or syntax of their manuscript, it must be done with extreme caution, and authors must review and edit the result. If such a tool is used, authors must declare the name of the tool, where it was used, and the purpose for which it was used in an "Artificial intelligence declaration" section after the "Acknowledgments" section. Authors remain accountable for all elements of their manuscript and should state that they take full responsibility for the content of their manuscript in the AI declaration.

Once a paper has been accepted for publication, online publication takes approximately 2 weeks.

There is no cost for publication in *Fishery Bulletin*.

Types of manuscripts accepted by the journal

Articles generally range from 20 to 30 double-spaced typed pages (12-point font) and describe an original contribution to fisheries science, engineering, or economics. Tables and figures are not included in this page count, but the number of figures should not exceed 1 figure for every 4 pages of text. Articles contain the following divisions: abstract, introduction, methods, results, discussion, and conclusions.

Notes are generally less than 10 double-spaced typed pages (12-point font), including the Literature cited section. Like articles, notes describe an original contribution to fisheries science. They follow a format similar to that for articles: abstract, introduction, methods, results, and discussion, but the results and discussion sections may be combined and a conclusions section should not be included. They should include no more than 2 figures or tables (2 of each would be too many). They are distinguished from full articles in that they report a noteworthy new observation or discovery—such as the first report of a new species, a unique finding, condition, or event that expands our knowledge of fisheries science, engineering, or economics—and do not require a lengthy discussion. Manuscripts on range extensions will not be considered.

Companion articles should be submitted together and are published together as a scientific contribution. Both articles should address a closely related topic and may be articles that result from a workshop or conference.

Review articles published under the banner "A Marine Fisheries Review" are papers of exceptional quality that continue the traditions of our sister journal *Marine Fisheries Review* inside the pages of *Fishery Bulletin* (*Marine Fisheries Review* has suspended publication). Review articles should address a timely topic that is relevant to aspects of fisheries science and marine biology. They should include an abstract, but the format of an article, per se, will be up to its author. Please contact the scientific editor to discuss your ideas regarding a potential review article before embarking on such a project.

Perspective essays generally are less than 5 double-spaced typed pages (12-point font) and provide clarification of misused terms or misunderstood topics in fisheries science. Essays are accepted at the discretion of the scientific editor. Opinion pieces on policy will not be considered. They should include an abstract and a list of the literature cited, but no other sections should divide the article. Please contact the scientific editor to discuss your idea before making a submission.

Preparation of manuscript

Title page should include authors' full names, affiliations, mailing addresses, and the senior author's email address.

Abstract should be limited to 200 words (one-half typed page), state the main scope of the research, and emphasize the authors' conclusions and relevant findings. Do not review the methods of the study or list the contents of the paper. Because abstracts are circulated by abstracting agencies, it is important that they represent the research clearly and concisely.

General text must be typed in 12-point Times New Roman font throughout. A brief introduction should convey the

broad significance of the paper; the remainder of the paper should be divided into the following sections: Materials and methods, Results, Discussion, Conclusions, and Acknowledgments. Headings within each section must be short, reflect a logical sequence, and follow the rules of subdivision (i.e., there can be no subdivision without at least 2 subheadings). The entire text should be intelligible to interdisciplinary readers; therefore, all acronyms, abbreviations, and technical terms should be written out in full and defined the first time they are mentioned. Abbreviations should be used sparingly because they are not carried over to indexing databases and slow readability for those readers outside a discipline. They should never be used for the main subject (e.g., species or method) of a paper.

For general style, follow the U.S. Government Publishing Office *Style Manual* (2016, available at website) and *The CSE Manual: Scientific Style and Format for Authors, Editors, and Publishers* (2024, 9th ed.) published by the Council of Science Editors. For scientific nomenclature, use the current edition of the American Fisheries Society's (AFS) *Common and Scientific Names of Fishes from the United States, Canada, and Mexico* and its companion volumes (*Crustaceans, Mollusks, Cnidaria and Ctenophora*, and *World Fishes Important to North Americans*). For species not found in the previously mentioned AFS publications and for more recent changes in nomenclature, use the Integrated Taxonomic Information System (ITIS, available at website), or, secondarily, the California Academy of Sciences *Catalog of Fishes* (available at website) for species names not included in ITIS. Common (vernacular) names of species should be lowercase. Citations must be given for the identification of specimens. For example, "Fish species were identified according to Collette and Klein-MacPhee (2002); sponges were identified according to Stone et al. (2011)."

Dates should be written as follows: 11 January 2025. Measurements should be expressed in metric units, for example, "58 metric tons (t);" if other units of measurement are used, please make this fact explicit to the reader. Use numerals, not words, to express whole and decimal numbers in the general text, tables, and figure captions (except at the beginning of a sentence). For example, "We considered 3 hypotheses. We collected 7 samples in this location." Use American spelling. Refrain from using the shorthand slash (/), an ambiguous symbol, in the general text.

Cite all software, special equipment, and chemical solutions used in the study within parentheses in the general text, including the version number, company name, and the city and state (or nation) of the company headquarters, for example, "SAS, vers. 9.4 (SAS Institute Inc., Cary, NC)."

Word usage and grammar that may be useful are the following:

- *Aging*
  For our journal, the word *aging* is used to mean both age determination and the aging process (senescence). Authors should make clear which meaning is intended where ambiguity may arise.

- *Fish and fishes*
  The plural of the word *fish* (a collective noun that implies individuals without regard to species) is *fish*.
  Example: The *fish* were collected by trawl net.
  Example: The numbers of *fish* collected that season were less than the numbers from previous years.

  The plural for *fish species* is *fishes* (a contrived plural used by taxonomists to mean several or more *fish species*) or one can use *fish species* (which is preferred in this journal for clarity across disciplines).
  Example: The *fishes* of Puget Sound [biodiversity is implied] or
  Example: The *fish species* of Puget Sound [preferred plural for clarity across disciplines].

- *Crab and crabs, squid and squids, etc.*
  The plural of the word *crab* (i.e., many individuals without regard to species) is *crab*.
  Example: The crab were sorted by weight.
  Example: Many red king *crab* were dying [Many individuals of one species of crab.]

  The plural of *crab species* is *crabs* (a word used by taxonomists) or *crab species* (the latter is preferred in this journal for clarity).
  Example: These *crabs* were selected for treatment. [Different crab species are implied.]
  Example: These *crab species* were selected for treatment. [Preferred word choice for clarity.]
  Example: Snow *crabs* are found throughout the North Pacific Ocean and Bering Sea. [There are 2 species of snow crab; therefore the word *crabs* can be used here.]
  Example: *Two species* of snow *crab* are found throughout the North Pacific Ocean and Bering Sea. [Preferred usage for clarity.]
  Example: Three crabs were selected for treatment. [3 species of crab are implied.]
  Example: Three crab species were selected for treatment. [Preferred word choice for clarity.]

- We use *fisherman* and *fishermen*, not *fisher* and *fishers*, in this journal. One can always use crew member, vessel operator, and angler (the latter for recreational fishing).

- *The definite article with common names of species*
  When the singular common name of a species represents the entire class or group to which it belongs, use the definite article.
  Example: Only one species of the genus *Salmo* is found in the Atlantic Ocean—*the* Atlantic salmon (*Salmo salar*).
  Example: The sonic emissions of *the* bottlenose dolphin are complex.

  For plural common names, this rule does not apply.
  Example: Chinook salmon are found throughout the Pacific Ocean.
  Example: Bottlenose dolphins are found in temperate and tropical waters.

- *Sex*
  For the meaning of male and female, use the word *sex*, not *gender*. Do not write, "fish were sexed." Write, "sex was determined."

- *Participles*
  As adjectives, participles must modify a specific noun or pronoun.
  Example: Using mark-recapture methods, these scientists determined the size of the population. [Correct. The participle *using* modifies the word *scientists*.]
  Example: These scientists, based on the collected data, concluded that the mortality rate of these fish had increased. [Incorrect. The scientists were not based on the collected data.]
  Example: These scientists concluded, on the basis of collected data, that the mortality rate of these fish had increased. [Correct. The offending participle has been eliminated and an adverbial phrase modifies the verb *concluded*.]

Equations and mathematical symbols should be set from a standard mathematical program (MathType or Equation Editor). Equations formatted in LaTex are not acceptable. For mathematical symbols in the general text (α, χ^2, π, $\pm$, etc.), use the symbols provided by the MS Word program and italicize all variables, except those variables represented by Greek letters and the superscript and subscript parts of variables and expressions. Do not use photo mode when creating these symbols in the general text, and do not cut and paste equations, letters, or symbols from a different software program.

Number equations (if there are more than one) for future reference by scientists; place the number within parentheses at the end of the first line of the equation.

Literature cited section comprises published works and those accepted for publication (in press) in peer-reviewed journals. Follow the name and year system for citation format in this section (i.e., citations should be listed alphabetically by the authors' last names, and then by year if there is more than one citation by the same author. A list of abbreviations for citing journal titles can be found on our website.

Authors are responsible for the accuracy and completeness of all citations. Avoid the use of multiple citations when a single citation sufficiently supports a statement; cite the work that first reported the information that supports a statement, not all of the subsequent works. Literature citation format: Authors (last name, followed by initials for first name and, if given, middle name of first author; then list names of additional authors with initials before last names). Year. Title of article. Abbreviated title of the journal in which it was published. Always include either the range of page numbers (for a journal article) or a total number of pages (for a book or other type of publication). List a sequence of citations in the general text chronologically, for example, "(Smith, 1932; Green, 1998; Smith and Jones, 2015)."

Acknowledgments should be no more than 6 lines of text. Only those who have contributed in an outstanding way should be acknowledged by name. For recognition of other persons or groups, use a general term, such as *crew*, *observers*, or *research coordinators*, and do not include names with these terms.

Digital object identifier (doi) code ensures that a publication has a permanent location online. A doi link (which may include a doi code) should be included at the end of citations of published literature. Authors are responsible for submitting accurate doi links. Faulty links will be deleted at the page-proof stage.

Footnotes are used for all documents that have not been formally peer reviewed and for observations and personal communications, but these types of references should be cited sparingly in manuscripts submitted to the journal.

All reference documents, administrative reports, internal reports, progress reports, project reports, contract reports, personal observations, personal communications, unpublished data, manuscripts in review, and council meeting notes are footnoted in 10-point font and placed at the bottom of the page on which they are first cited. Footnote format is the same as that for formal literature citations. A link to the online source (e.g., [Available from http://www... , accessed July 2024.]), or the mailing address of the agency or organization holding the document, should be provided so that readers may obtain a copy of the document.

Tables are often overused in scientific papers; it is seldom necessary to present all the data associated with a study. Tables should not be excessive in size and must be cited in numerical order in the text. Headings should be short but ample enough to allow the table to be intelligible on its own.

All abbreviations and unusual symbols must be explained in the table legend. Other incidental comments may be footnoted with numeral footnote markers. Use asterisks only to indicate significance in statistical data. Do not put a table legend on a page separate from the table; place the legend above the table. *Do not submit tables in photo mode.*

- Note probability with a capital, italic *P*.
- Provide a zero before all decimal points for values less than one (e.g., 0.07).
- Round all values to 2 decimal points.
- Use a comma in numbers of 5 digits or more (e.g., 13,000 but 3000).

Figures must be cited in numerical order in the text. Graphics should aid in the comprehension of the text, but they should be limited to presenting patterns rather than raw data. The number of figures should not exceed 1 figure for every 4 pages of text.

Figure legends should explain all symbols and abbreviations seen in the figure and should be double spaced on a separate page at the end of the manuscript.

Line art and halftone figures should be saved at resolutions >600 dots per inch (dpi) and >300 dpi, respectively. Color is allowed in figures to show morphological differences among species (for species identification), to show stain reactions, to show gradations (such as those of temperature and salinity within maps), and to distinguish between numerous lines and symbols in graphs. Figures approved for color should be saved in CMYK format.

All figures must be submitted as PDF, TIFF, or EPS files.

- Capitalize only the first letter of the first word and proper nouns in all labels within figures.
- Do not use overly large font sizes for labels in maps and for axis labels in graphs.
- Use the same point size for all labels, except for panel labels (e.g., **A**), which should be slightly larger than other labels (e.g., 11 point versus 8 point).
- Use a sans serif font for all labels. Panel labels (e.g., **A**), however, should be in Times New Roman font.
- Do not use bold fonts or bold lines in figures. Do not use italic fonts. Exceptions include use of italic fonts for labels of bodies of water in maps and a bold font for panel labels (e.g., **A**).
- Do not place outline rules around graphs.
- Do not include vertical and horizontal lines in the background of graphs. Ticks for values on the *x*-axis and *y*-axis will suffice.
- Place a north arrow and label degrees latitude and longitude (e.g., 170°E) in all maps. If scale of map requires more than degrees, use degrees minutes, not decimal degrees.
- Place panel labels (e.g., **A**, **B**, and **C**) within the upper-left area of each graph or photo in a multi-panel figure, from left to right, then top to bottom. If the letter is not visible against a dark background, put a white box behind it. Do not use white labels.
- Avoid placing labels vertically or diagonally. *Y*-axis labels can be vertical. Words in horizontal labels can be stacked vertically to fit.
- Use symbols, shading, or patterns (not clip art) in maps and graphs.
- For scale bars in maps, use kilometers. Use the label *km* or *kilometers* (lowercased).

Supplementary materials that are considered essential, but are too large or impractical for inclusion in a paper (e.g., metadata, figures, tables, videos, and websites), may be provided with an article. These materials are subject to the editorial standards of the journal. A URL to the supplementary material and a brief explanation for including such material should be sent at the time of initial submission of the paper to the journal.

- **Metadata, figures, and tables** should be submitted in standard digital format (MS Word or PDF file) and should be cited in the general text, for example, as "... was determined (Suppl. Table 3, Suppl. Fig. 1)."
- **Websites** should be cited with a URL in the general text.
- **Videos** must not be larger than 30 MB to allow a swift technical response for viewing the video. Authors should consider whether a short video uniquely captures what text alone cannot capture for the understanding of a process or behavior under examination in the article. Supply an online link to the location of the video.

Copyright law does not apply to *Fishery Bulletin*, which falls within the public domain. However, if an author reproduces any part of an article from *Fishery Bulletin*, reference to source is considered correct form (e.g., Source: Fish. Bull. 117:105).

Failure to follow these guidelines and failure to correspond with editors in a timely manner will delay publication of a manuscript.

Submission of manuscript

Submit a manuscript online at the ScholarOne Manuscripts website for *Fishery Bulletin*. Commerce Department authors must provide proof of internal clearance of their manuscripts with either a completed and signed NOAA Form 25-700 or a copy of the clearance email from the Research Publication Tracking System. For further details on electronic submission, please contact the associate editor, Cara Mayo, at

cara.mayo@noaa.gov.

When requested, the text and tables should be submitted in MS Word format. Each figure should be sent as a separate PDF, TIFF, or EPS file. Send a copy of a figure in the original software if conversion to any of these formats yields a degraded version of the figure.

Questions? If you have questions regarding these guidelines, please contact the managing editor, Kathryn Dennis, at

kathryn.dennis@noaa.gov.

Questions regarding manuscripts under review should be addressed to Associate Editor Cara Mayo.

Fishery Bulletin

Subscription form

Superintendent of Documents **Publications** Order Form

*5178

☐ YES, please send me the following publications:

____ Subscriptions to *Fishery Bulletin*
for $32.00 per year ($44.80 foreign)

The total cost of my order is $ _____ . Prices include regular domestic postage and handling and are subject to change.

_____
(Company or Personal Name) (Please type or print)

_____
(Additional address/attention line)

_____
(Street address)

_____
(City, State, ZIP Code)

_____
(Daytime phone including area code)

_____
(Purchase Order No.)

Charge your order. IT'S EASY!

Please Choose Method of Payment:

☐ Check payable to the Superintendent of Documents
☐ GPO Deposit Account ☐☐☐☐☐☐☐–☐
☐ VISA or MasterCard Account
☐☐☐☐☐☐☐☐☐☐☐☐☐☐☐☐
☐☐☐☐ (Credit card expiration date)

To fax your orders (202) 512-2104

_____
(Authorizing Signature)

Mail to: Superintendent of Documents
P.O. Box 979050, St. Louis, Missouri 63197
Tel. no. (U.S. callers): 866-512-1800
Tel. no. (International callers): 1-202-512-1800

Thank you for your order!

Also available online at
https://bookstore.gpo.gov/products/fishery-bulletin
email: ContactCenter@gpo.gov